Ebb Shoal Water Depth at Hornafjörður Tidal Inlet with Respect to Sediment Transport

Bjarki Ómarsson

EBB SHOAL WATER DEPTH AT HORNAFJÖRÐUR TIDAL INLET WITH RESPECT TO SEDIMENT TRANSPORT

Bjarki Ómarsson

30 ECTS thesis submitted in partial fulfillment of a
Magister Scientiarum degree in Civil Engineering

Advisors
Sigurður M. Garðarsson
Sigurður Sigurðarson

Faculty Representative
Helgi G. Gunnarsson

Faculty of Civil and Environmental Engineering
School of Engineering and Natural Sciences
University of Iceland
Reykjavik, May 2015

Ebb Shoal Water Depth at Hornafjörður Tidal Inlet with Respect to Sediment Transport
Tidal Inlet
30 ECTS thesis submitted in partial fulfillment of a M.Sc. degree in Civil Engineering

Abstract

The ebb shoal at the Hornafjörður tidal inlet poses a navigational problem due to limited water depth. Furthermore there has been a relative land rise of 13 mm/year for the past 17 years. Considerable sediment transport occurs on the ebb shoal, called Grynnslin, and in the area close to it. Sediment transport is one of the main factors that influence the ebb shoal water depth. Ships navigating over the ebb shoal face the dangers of shallow water depth and often get damaged. Economical losses that stem from fishing ships not being able to unload their catch is estimated 4.5 million ISK per year, which then has a multiplication effects into the society at Hornafjörður. Classification of the tidal inlet showed it to be "Mixed Energy (wave dominated)" where both tidal and wave forces are strong. The wave effects on the ebb shoal are significant. The results from offshore wave sediment transport calculations show that west and east of the tidal inlet the sediment transport capacity is considerably larger than on the ebb shoal itself, indicating that there are some sheltering effects on the ebb shoal and with the areas on either side acting as a sediment buffer zone. If these buffer zones would be increased in size, then regular dredging could be a realistic choice since the sediment transport on the ebb shoal would decrease.

Útdráttur

Við Hornafjarðarós eru grynnsli sem eiga það til að hindra siglingar um ósinn vegna of lítillar dýptar. Í ofanálag þá er landris á svæðinu sem er í meðaltali 13 mm/ár fyrir síðustu 17 ár. Töluverður sandburður á sér stað á svæðinu sem veldur breytilegri dýpt yfir Grynnslin eins og þau eru jafnan kölluð. Þessi dýpt er oft ekki nægileg og þá eiga skip á hættu að verða fyrir skemmdum þegar siglt er yfir Grynnslin. Efnahagslegt tjón vegna þess að skip þurfi að landa annars staðar o.fl. nemur 4.5 milljónum króna á ári, sem hefur þá bein áhrif á samfélagið í Hornafirði. Flokkun á ósnum sýndi að hann sé ölduríkjandi en þó með sterka sjávarfallakrafta. Hafaldan hefur verulegt áhrif á Grynnslin sjálf. Niðurstöður sýndu að vestan og austan megin við ósinn var sandburðurinn vegna öldu töluvert meiri en á Grynnslunum sjálfum, sem gefur til kynna að þeim er skýlt að hluta frá sandburði þar sem sandurinn safnast saman sitthvorum megin við Grynnslin. Ef þessi svæði væru stækkuð, þá væru reglulegar sanddælingar á Grynnslunum raunhæfur kostur því sandburðurinn myndi minnka töluvert.

Contents

Contents

List of Figures

List of Tables

LIST OF TABLES

xvi

Glossary

The main symbols are listed below. All parameters are in SI units.

A	=	Tidal inlet throat area
a	=	Amplitude of near-bed wave orbital motion
α	=	The angle between wave fronts and coastline
β	=	Bed slope
c	=	Wave celerity
c_b	=	Sediment concentration
D	=	Water depth
D_B	=	Water depth at breaker line
D_s	=	Directional spreading
d_{50}	=	Mean grain diameter
d_c	=	Closure depth
δ_w	=	Wave boundary layer thickness
f	=	Frequency
f_0	=	Base frequency
f_w	=	Friction factor
g	=	Acceleration of gravity
γ	=	Wave breaking ratio
H_b	=	Wave height at breaker line
H_{rms}	=	Mean square root of wave height
H_s	=	Significant wave height
$H_{s,12h}$	=	Non-breaking significant wave height that is exceeded 12 hours per year
$\overline{H}$	=	Mean wave height
$\overline{H}_s$	=	Mean offshore significant wave height
$\overline{H}_{s,1yr}$	=	Mean annual significant wave height
h_C	=	Maximum depth of tidal inlet channel
h_{cr}	=	Minimum depth over crest of the ebb shoal
h_E	=	Maximum depth of ebb shoal
θ	=	Shields number
θ'	=	Shields parameter determined for a plane bed
θ_c	=	Critical Shields number
k	=	Wave number
k_r	=	Bed roughness
K_L	=	Wave length definition factor

L	=	Wave length
L_0	=	Deep water wave length
λ_l	=	Linear concentration
M_{tot}	=	Total volume of sediments transported through an inlet per year
ω	=	Wave frequency
$\hat{Q}$	=	Peak tidal discharge
Q_b	=	Bed load sediment transport
Q_s	=	Suspended load sediment transport
Q_t	=	Total sediment transport
P	=	Tidal prism
p	=	Probability of all particles of a layer moving
R^2	=	Linear regression coefficient
R_f	=	Relative river strength
R_t	=	Mean tidal range
R_{TW}	=	Relative tide strength
ρ	=	Density of seawater
ρ_s	=	Density of sediment
s	=	Relative density of sediment
T	=	Wave period
T_p	=	Peak wave period
T_s	=	Wave period associated with $H_{s,12h}$
T_z	=	Zero up-crossing wave period
τ_b	=	Maximum bed shear stress
U	=	Instantaneous flow velocity at $y = \delta_w$
U_b	=	Maximum wave induced velocity outside the wave boundary layer
U_f	=	Wave friction velocity
V_E	=	Ebb shoal volume
Φ_B	=	Dimensionless bed load transport
X_B	=	Distance from breaker line to coast
x	=	Directional standard deviation
y	=	Distance from seabed

Acknowledgments

I would like to thank my advisor, Mr. Sigurður Sigurðarson, for his guidance and immense support. His good understanding on the topic has been of great value throughout the course of the project. I truly appreciate the opportunity to take part in the ongoing research at Hornafjörður tidal inlet. My advisor, Dr. Sigurður Magnús Garðarsson, gets my thanks for his guidance and support.

Mr. Gísli Viggósson and Mr. Vignir Júlíusson get my thanks for their invaluable knowledge about Hornafjörður tidal inlet and its history.

The engineers at IRCA (Siglingasvið Vegagerðarinnar) Ingunn Erna Jónsdóttir and Pétur Ingi Sveinbjörnsson get my thanks for their help with the DHI programs *MIKE21 SW* and *Litdrift*.

My thanks to Prof. Hans Hanson and Prof. Magnus Larson at Lund University for a good discussion and their proposals about the project.

My gratitude to the Icelandic Road and Coastal Administration (IRCA) for the use of their facilities and documents related to the project.

Finally, I would like to thank my family for their understanding, encouragement and great support throughout the study.

1 Introduction

1.1 General Introduction

The Hornafjörður tidal inlet is located on the south-east coast of Iceland. Inside the inlet there is the fishing village Höfn which is dependent on the fishing industry. Therefore navigation of fishing ships through the inlet is vital for Höfn. The tidal prism, which is defined as the volume of water flowing through an estuary between mean high tide and mean low tide, is around 64 million m^3. The maximum mean velocity over the tidal entrance cross section is approximately 2 m/s. The tidal inlet is dependent on the wave action and tidal flow. The flow is controlled by the tidal elevation in the area, the size of the basin inside of the inlet and the shape and size of grains on the seabed.

The tidal flow forms shoals on both sides of the inlet. At the inlet throat there is an ebb jetty (í. straumband) which is sustained by large tidal flow. The shoals are formed where the tidal flow decreases and sand grains settle on the seabed. This is consistent with the schematic figure of a standard tidal inlet (see Fig. 1.1). The ebb shoal that forms outside the tidal inlet at Hornafjörður is called Grynnslin and it can, along with wave action, delay or hinder ships from navigating through the inlet.

The tidal inlet at Hornafjörður has two basins, Hornafjörður and Skarðsfjörður, that contribute to the flow through the inlet (see Fig. 1.2). A part of the run-off from Vatnajökull, which is the largest glacier in Iceland, flows into the Hornafjörður basin. It has been estimated that the fresh water is less than 3% of the magnitude that goes into the basins at any time and is therefore insignificant to the flow through the inlet.

The inlet is narrow, it bends and curves, has limited depth and lies partially open to the sea. The material at the seabed is sand, gravel, large gravel and hard rock. The tidal currents at the inlet are strong and so are the offshore waves.
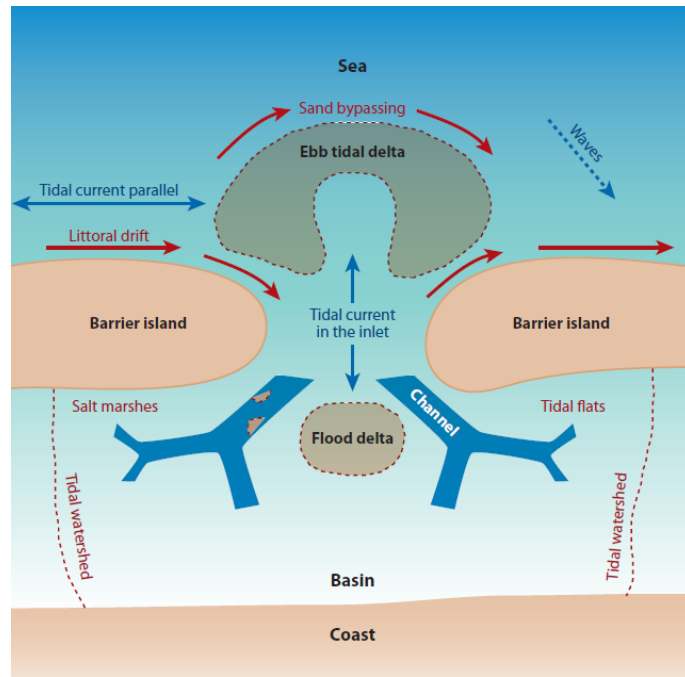
Figure 1.1: Schematic figure of an idealized tidal inlet system, showing the different geo-
morphologic elements and the dominant physical processes and phenomena (de Swart
and Zimmerman, 2009)

.
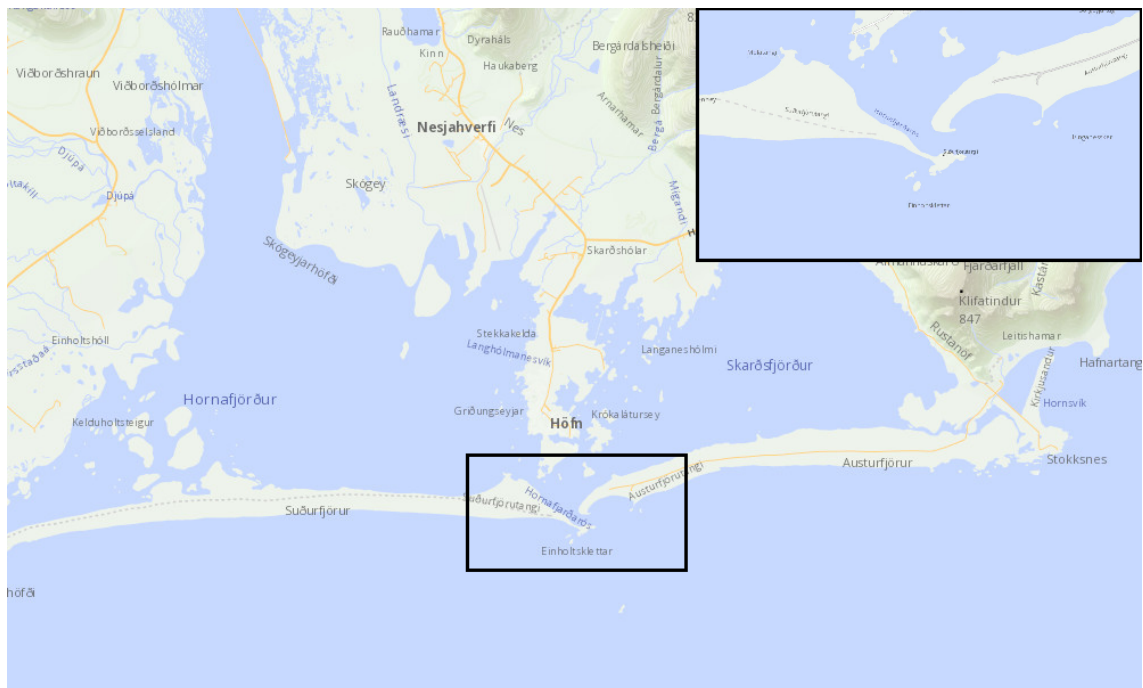
Figure 1.2: Overview of the tidal inlet at Hornafjörður (já.is, 2015).

1.2 Background

On the 10th of September in 2014 an open meeting was held at Höfn, attended by members of the town and harbour council, representatives from the fishing industry, locals interested in the subject as well as members of the Icelandic parliament. The speakers were Gísli Viggósson, former civil engineer at the Icelandic Maritime Administration (IMA) and now retired, Sandra Rán Ásgrímsdóttir engineer at Vegagerðin (Icelandic Road and Coastal Administration), Sigurður Sigurðarson civil engineer at Vegagerðin and Ásgeir Gunnarsson fishing manager (í. útgerðarstjóri) at Skinney-Þinganes, the main fishing company at Höfn.

Gísli has worked on projects concerning Hornafjörður for the past decades and has therefore a good insight into the problems that the tidal inlet poses. He gave a wide overview over the historical development, the research and actions taken to stabilize the inlet.

In the years 1978-80 and 1989-90 were dramatic changes in weather (í. umhleypingar) and in both cases the tidal inlet got filled up, i.e. sediments settled in the inlet channel in great magnitude. This halted ship traffic through the inlet. Figure 1.3 shows how the tidal inlet looked in the spring of 1990. A new channel formed between Hvanney and the South Barrier and the East Barrier lengthened into the inlet. Subsequently, measures were taken to stabilise the tidal inlet. That was done in three parts. Firstly, a shore protection was established on the South Barrier connecting the barrier and Hvanney (in 1991) (see Fig. 1.4). Secondly, after extensive numerical and hydraulic model testing a curved jetty was constructed on the tip of the East Barrier to prevent it from lengthening into the inlet (in 1995) (see Fig. 1.4). Lastly, a jetty was constructed east of the inlet connecting to the Þinganessker to hinder or slow sediment transport from east (in 2001) (see Fig. 1.4). The tidal inlet has stayed reasonably stable since these constructions were made and has not filled up again but the ebb shoal depth still varies.

The presentation by Sandra was based on her work with with Sigurður and Gísli. She performed an extensive research on Grynnslin which included bathymetric surveys, sediment transport modelling and wave action measurements and modelling.

In continuation of Sandra's presentation Sigurður went in detail over the bathymetric surveys and their meaning. He presented also some ideas on how the problem could be addressed, i.e. with variations of breakwaters or jetties extending from each side of the inlet out into deeper waters. But in his opinion most of those suggestions would only be temporary and result in movement of the shoal further out.

Lastly Ásgeir spoke and he gave perspective on how the tidal inlet effects the industry and therefore the society of Hornafjörður. Skinney-Þinganes has eight ships and for six of them the shoal depth on Grynnslin is a hindering factor. Estimated yearly loss of income because ships have had to unload in other harbours due to small shoal depth is estimated

Figure 1.3: The tidal inlet at Hornafjörður in the spring of 1990. A new inlet has started to form at the South Barrier and the East Barrier is lengthening into the inlet (Arnason, 2015).

Figure 1.4: Overview of the tidal inlet and completed constructions at the South Barrier, East Barrier and Þinganessker (Arnason, 2015).

about 4.5 million ISK. This loss has multiplication effects into the society at Hornafjörður, which is mainly loss of work in fish processing and shipping. In order to be competitively comparable with other large fishing towns the number of ships have to be increased and

improved. That is difficult because special made ships are expensive and return only a small profit when resold. So understandably this is a heated discussion for the people of Hornafjörður.

1.2.1 Recent Research

Many new studies have been made concerning the tidal inlet at Hornafjörður. Land rise measurements and bathymetric surveys have been done at Hornafjörður for the past years, as well as sediment transport estimates.

Relative Sea Level Changes

Several geological factors contribute to the relative sea level changes at Hornafjörður. The glacial isostatic rebound due to retreating of Vatnajökull glacier is the dominant one. Other factors such as general sea level rise due to polar glacier melt, tectonic movements and weight effects (í. þyngdaráhrif) have less effects, because they approximately cancel each other out.

Measurements from a GPS station at Höfn shows that for the past 17 years Hornafjörður has risen 13 mm/year on average. In the first half of the period the rise was 10 mm/year, in the second half of the period it was 15 mm/year and for the last quarter of the period it was 17 mm/year (Jóhannesson and Ófeigsson, 2014).

The land rise for the past 17 years has been steadily accelerating. However the measurement period of 17 years is really short with regard to land rise and therefore it is hard to accurately estimate long term land rise. It might as well start to suddenly drop again or stay steady. But with these projections; estimated land rise at Hornafjörður for the the period 1997-2050 could be between 0.7 and 1.0 m. The upper limits of this estimate has great uncertainty.

With the rising of the land or lowering of the sea level it is foreseen that the tidal prism will decrease. A numerical tidal flow model from Vatnaskil Consulting Engineers was used to predict the decrease in tidal prism. The model took into account the bathymetry and measurements of the tidal cycle (í. sjávarfallasveifla) with tidal amplitude of around 1.7 m. This was run through the current model for the present bathymetry on the one hand and for a 0.5 and 1.0 m land rise on the other. The tidal prism is then calculated by integrating the current curve.

For a 0.5 and 1.0 m relative land rise it was found that the tidal prism will decrease about 35% and 66% respectively (Gunnarsson and Pálmarsson, 2014). The uncertainty lies in

areas with water depth between 1 to 2 m, which emerges out of the sea for 1 m land rise. These areas had older bathymetry data applied to them because they were the only ones available.

Bathymetric Survey

In 1978 and 1979 two height systems were established based on tidal measurements in the inlet entrance, one was for the harbour area and the other for the sea outside the inlet. Bathymetric surveys were based on the height system for the entrance but from 2005 it was changed so they would be based on the height system in the harbour. So the most recent bathymetry surveys, such as those that are used in this thesis, do not show the actual depth. The minimum navigational water depth could be between 70 to 80 cm less than in the published bathymetric surveys (Tryggvason, 2015).

Bathymetric surveys of the ebb shoal through the years have been irregular, with only one measurement in the period from 1900 to 1998. But since then the bathymetric surveys have become more regular and from 2009 the water depth at Grynnslin has been measured every 2 to 3 months.

At the ebb shoal or Grynnslin strong tidal currents and offshore waves control the sediment transport. Therefore the water depth at Grynnslin is constantly changing. Dominant wave direction is from south-west, but every 10 to 15 years or so, waves from south-east become dominant and transport sediments towards west. The water depth at Grynnslin is usually between 7 to 7.5 m chart datum (CD) and is often considerd as 7.3 m.

Sediment Transport

According to PIANC (2014) classification of coastal profiles, the Hornafjörður tidal inlet and the coast on either side of it is classified as a *Exposed Littoral Dune or Cliff Coast*. It is characterised by a wide sandy beach and a wide shore-face with up to three bars; the coast can consist of dunes or cliffs and the geology is dominated by semi-hard material such as glacial till or sandstone.

On those type of coastal profiles the annual gross littoral or alongshore sediment transport ranges from 50 thousand m^3/year up to more than 1 million m^3/year with the littoral zone ranging from 300 m up to more than 1,000 m.

A sediment transport numerical model (Asgrímsdóttir et al., 2014) was run for the years 2000-2012 with a program developed by DHI (The Danish Hydrology Institute) called *Litdrift*. The program has several inputs such as wave action, mean grain size, fall velocity

and more. The program was run for the profiles shown in Figure 1.5 which span from a location at 85 km west of Hornafjörður tidal inlet to a location 6 km east of it.
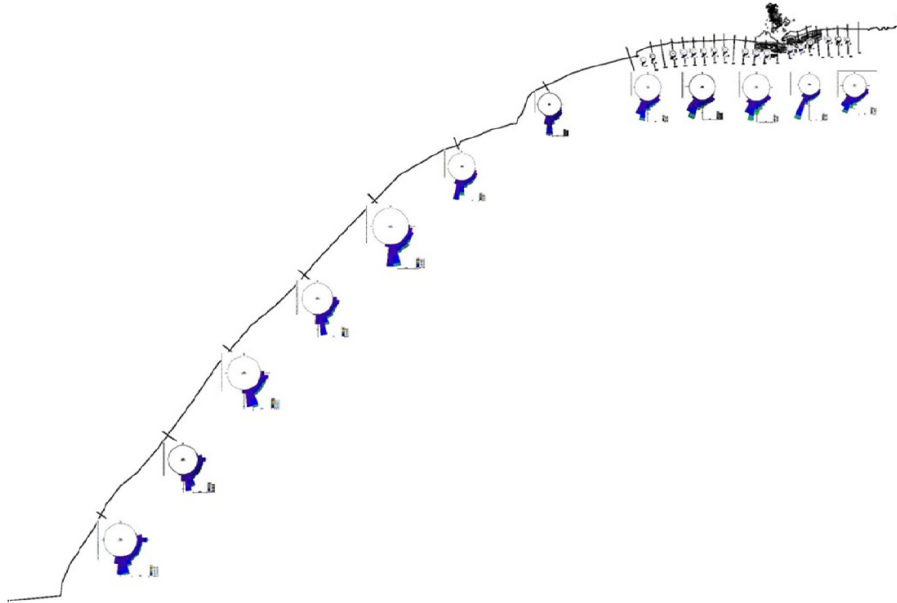
Figure 1.5: Location of the sediment transport profiles (Asgrímsdóttir et al., 2014).

The results are shown in Table 1.1. These results are compared to the results that were found in Section 3.3.2 which focuses on a area closer to the tidal inlet and has profiles every 500 m, spanning from a location 4 km west of the tidal inlet to a location 2 km east of it (see Fig. 3.20). The transport values in Table 1.1 would imply quite a lot of local variation in shoreline evolution since the gradients are so large.

Table 1.1: *Net sediment transport results from* Litdrift *model for 2000-2012 (Asgrímsdóttir et al., 2014).*

	Coast Orientation	Net sedim. tr.
Profiles	[°]	[$\times 10^3$ m^3]
85000W	123	-1726
75000W	124	-1205
65000W	128	-1202
55000W	129	-138
45000W	135	-1716
35000W	157	-1102
25000W	146	-1417
15000W	171	-446
14000W	170	-732
13000W	173	-443
12000W	176	-401
11000W	179	-128
10000W	179	-287
9000W	182	-80
8000W	182	-65
7000W	182	-218
6000W	184	-206
5000W	184	-299
4000W	183	-92
3000W	181	-141
2000W	180	244
1000W	179	59
0	162	-332
1000E	174	-94
2000E	178	-532
3000E	184	-224
4000E	183	-94
5000E	182	-204
6000E	182	134

Sediment samples were taken in 1979 and 1990 (see Fig. 1.6). Sample 5 was taken east of Þinganessker at 8 m water depth where the mean grain size, d_{50}, was found to be 0.24 mm. Sample 6 between Þinganessker and the tidal inlet showed a rather course material with mean grain size about 3.5 mm. Sample 7 was taken south-east of Hvanney and showed mean grain size to be about 0.2 mm. Samples 5 to 7 show the grain sizes that were found at the ebb shoal in 1979.
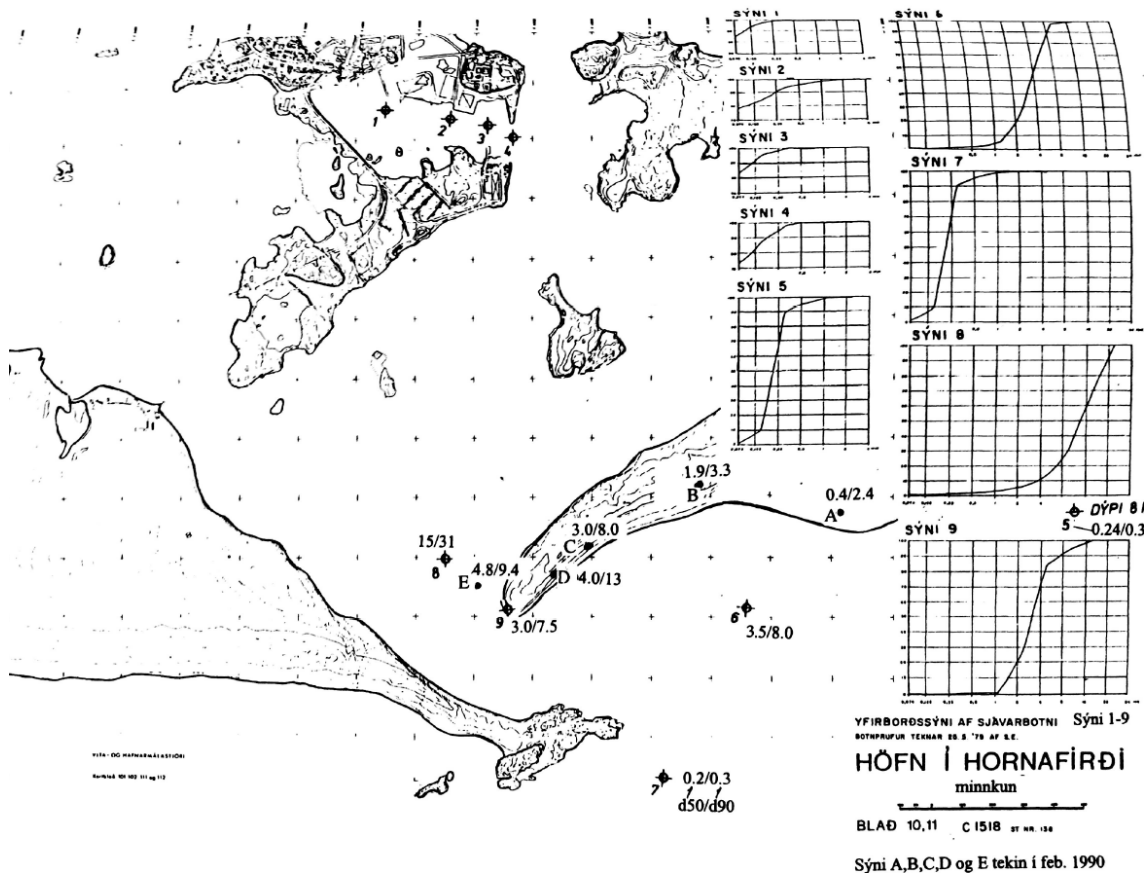
Figure 1.6: Material at seabed, spatial information and grain size (Viggósson and Sigurðarson, 2000).

1.2.2 Meeting at Lund University

The author had a meeting with two professors at Lund University on 21st of November 2014. Professor Hans Hanson and professor Magnus Larson work at the Water Resources department of Lund University and have great knowledge in this area.

The status of the thesis was presented to them and they were asked a simple question: "How can the depth at the ebb shoal be increased?". Their answer was in return also simple: "Reduce the sediment transport towards the ebb shoal". There are no magic solutions or short cuts to influence the ebb shoal depth and the most efficient solution is to try to hinder the sediment transport somehow. They proposed a construction of a jetty from Hvanney towards south-west connecting to Einholtsklettar, since the main wave action and therefore sediment transport is from that direction, and perhaps connecting to the reefs. This would trap considerable amount of sediment which then would have to be dredged yearly. The jetty would have to be long enough to trap the yearly sediment

transport at that location. Figure 1.7 shows somewhat how their proposal would look like.
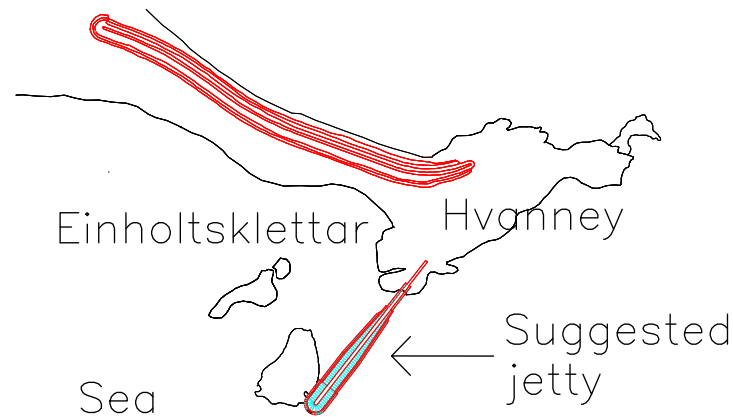
Figure 1.7: Proposal by the professors at Lund University, a jetty from Hvanney towards south-west.

1.3 Objectives

The main objective of this thesis is to estimate the sediment transport at the ebb shoal. Sediment transport is one of the major factors influencing the ebb shoal water depth. The focus is on sediment transport but at the same time the goal is also to try to answer the question: What effects will the relative land rise have on the sediment transport and water depth on the ebb shoal? Future decisions regarding the ebb shoal all depend on the sediment transport, therefore knowing the sediment transport at the ebb shoal is of great importance. The objective is to estimate how much that sediment transport is, both from the tidal flow and from wave action.

1.4 Literature Review

The three main parts of the thesis are classification of tidal inlet, calculations regarding the ebb shoal and model sediment transport calculations.

A classification of a tidal inlet has proven helpful in understanding the tidal inlet better. An accurate way to classify a tidal inlet is by looking at its shape (de Vriend et al., 1999). The method of Hayes (1979) is a simple method using only the mean wave height and mean tidal range for the classification but it is the most used method for classifying a tidal inlet besides shape classification. A more recent method by Nielsen et al. (2014) has been

used for tidal inlets in Australia and has given good results but as it is quite recent it has not been used much elsewhere.

The water depth at the ebb shoal is important for navigation over the ebb shoal therefore an attempt was made to estimate it with three empirical equations from (Buonaiuto and Kraus, 2003) which are based on results from tidal inlets located in the United States. These equations are dependent on the wave height and tidal prism, so an equation by Walton and Adams (1976) calculating the volume of the ebb shoal which uses also the tidal prism can be related. The empirical equation used by Walton and Adams (1976) is based on numerous tidal inlets in the United States and is slightly altered by Kraus (2010).

The sediment transport model by DHI (*MIKE21 SW* and *Litdrift*) uses the latest sediment transport theories which have proven successful. The version of the model that is used is from 2011. It includes theories from (Fredsøe et al., 1985), (Deigaard et al., 1986), (Zyserman and Fredsøe, 1994), (Swart, 1974) and many others.

For the past year the Icelandic Roand and Coastal Administration (IRCA) conducted a large study, see (Asgrímsdóttir et al., 2014), about the Hornafjörður tidal inlet which covers to some extent nearly every aspect of consideration for the problems that the tidal inlet poses. This thesis is based on and in continuation of that work but with focus on water depth on the ebb shoal and the sediment transport there.

2 Methods

2.1 Classification of Tidal Inlets

One tidal inlet can be significantly different from another and the natural forces can act differently on an individual tidal inlet considering e.g. how it is shaped, geographical location and so on. Classification of the tidal inlets can shed some light on this and the forces that are at work.

The three largest factors that contribute to the water exchange through a tidal inlet are tides, waves and river flow. The tides are regular while the waves and river flow are more episodic. At a first glance it can be said that the tides are the main driver in shaping of an inlet. Studies have indeed shown that there is a correlation between inlet throat area A and volume P of the tidal prism (O'Brien, 1969). Despite that however, the shaping of tidal inlets is in general said to be the result of all three factors. The question is how to quantify their relative strength for a definitive classification. Due to the severe wave climate in the waters around Iceland, a coastline open to offshore waves is commonly classified as wave dominated.

2.1.1 Shape Classification

One method of tidal classification is to classify it by shape and condition and even though it is a bit primitive it is often rather accurate. Figure 2.1 depicts various forms and shape of tidal inlets that can be used for the shape classification.

Fresh water flow at Hornafjörður tidal inlet is small compared to the tidal flow and therefore the tidal inlet is not expected to be river dominated. The two largest factors in consideration for the classification are the tidal flow and waves and thus the tidal inlet is expected to be either wave or tide dominated.

Figures 2.1a and 2.1b show a common wave dominated tidal inlet, with low tidal energy in Fig. 2.1a and high tidal energy in Fig. 2.1b. The basin in Fig. 2.1b is larger than in Fig. 2.1a due to larger tidal energy. Figure 2.1c shows a common tide dominated tidal inlet in

the shape of a *v*.
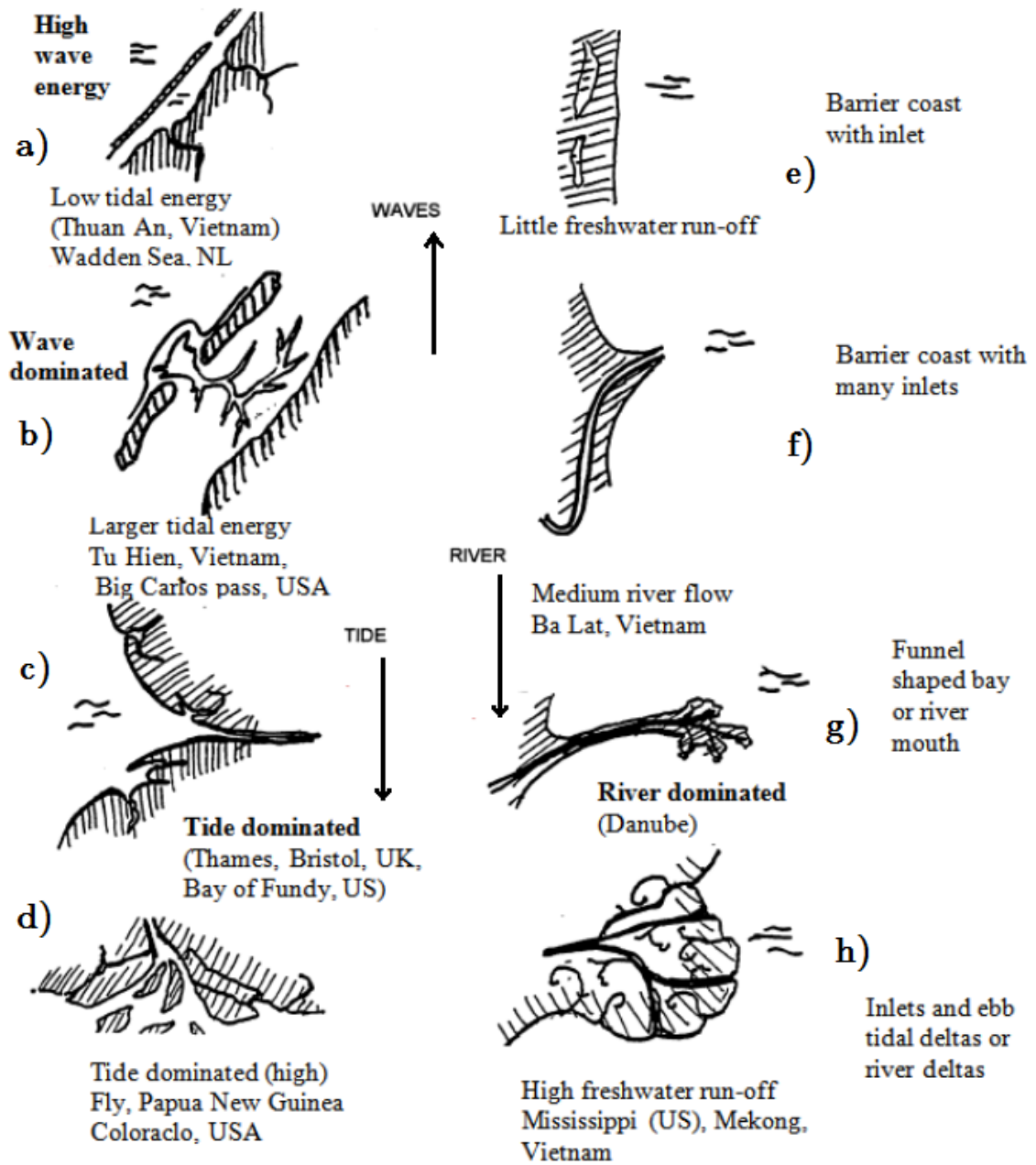
Figure 2.1: Classification of tidal inlet shapes based on influence of waves, tide and river flow (de Vriend et al., 1999).

2.1.2 Hayes Classification

The classification by Hayes (1979) uses the relative strength of waves versus tides in terms of mean wave height $\overline{H}$ and mean tidal range R_t (see Fig. 2.2). The mean tidal range established for Hornafjörður in 1979 was $R_t = 1.98$ m and recent analysis from Tryggvason (2015) confirms that.
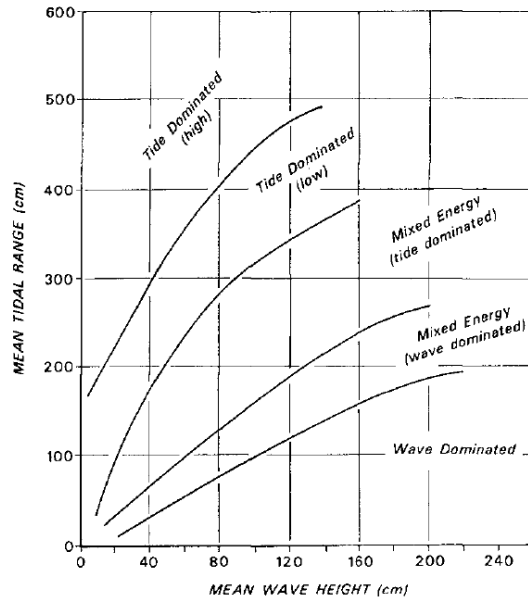
Figure 2.2: Hayes classification graph (Hayes, 1979).

Since there were no actual real data available for the wave height at the tidal inlet, a time series from the wave program *MIKE21 SW* was used to find the mean wave height. Hindcast data from the European Centre for Medium-Range Weather Forecasts (ECMWF) were used in the wave program. It included the wave height every 6 hours during the period from 2000 to 2012.

In this thesis the term *mean wave height* that Hayes uses is taken as the *mean significant wave height* but as the terminology for *significant wave height* was unclear until recent years the term *mean wave height* was often used. It was also unclear whether the wave height to be used should be on the ebb shoals themselves or offshore, so both cases were considered with ebb shoal wave height found from three locations on the ebb shoal P1, P2 and P3 (see Fig. 2.3) and the offshore wave height from a wave buoy located south of Hvanneyjarsker reefs on 32 m depth.
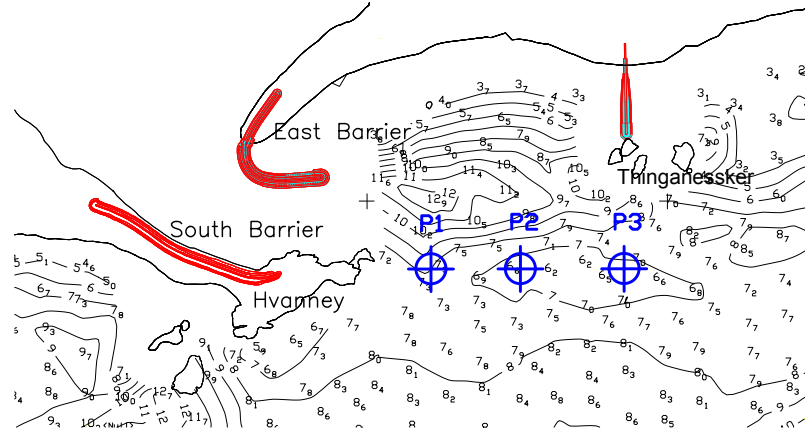
Figure 2.3: Location of points P1, P2 and P3 marked with blue crosses.

2.1.3 Nielsen & Thuy Classification

A recent research done by Nielsen et al. (2014) considers the balance between tides and waves in shaping of tidal inlets and it shows that the peak tidal discharge $\hat{Q}$ (m^3/s) is better suited to represent tidal strength, rather than the tidal prism P (m^3) which is often used instead. The dimensionless relative tidal strength is,

$$R_{TW} = \frac{\hat{Q}}{\sqrt{g\overline{H}_s^5}}, \tag{2.1}$$

where $\overline{H_s}$ is the mean offshore significant wave height and g is acceleration of gravity. Similarly the dimensionless relative river strength is defined as,

$$R_f = \frac{Q_f}{\sqrt{g\overline{H}_s^5}}, \tag{2.2}$$

where Q_f is the fresh water discharge.

Nielsen et al. (2014) classified 180 estuaries from the south-east coast of Australia with this method and found limiting value between tide and wave dominance to be around $R_{TW} = 75$ (see Fig. 2.4).
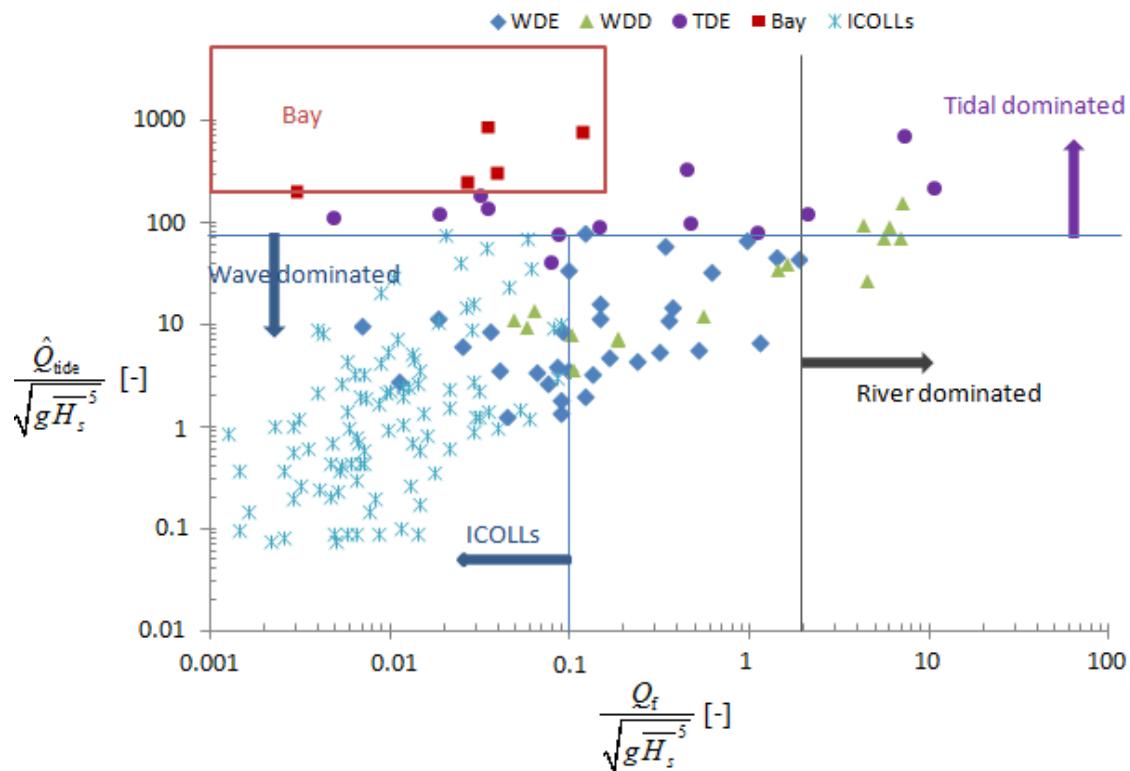
Figure 2.4: Classification of 180 estuaries in Australia (Nielsen et al., 2014).

2.2 The Ebb Shoal

Because of the variable nature of the ebb shoal the water depth is constantly changing. Thorough examination of the ebb shoal was needed to understand how and when the sediment on the ebb shoal moves and in consequence how the water depth is affected. Bathymetric surveys were used for that examination as well as equations that have proven successful in estimating ebb shoal water depth.

2.2.1 Bathymetric Surveys

From the year 2009 to 2014 around 15 bathymetric were made on the ebb shoal. Those bathymetric surveys are all shown in Appendix A along with 10 various bathymetric difference planes.

What is most interesting is the period from the fall of 2013 to late summer of 2014. The massive sediment transport that happened then has not been noticed before since regular

bathymetric surveys were begun.

In the fall of 2005 around 55 to 65 thousand m^3 of sediment was dredged close to inlet channel and was thought as a navigational channel for ships to sail safely over the ebb shoal. The bathymetric survey in March 2006, the first survey after the dredging, showed that most of the sediment had returned and no trace of the channel was to be seen. This shows somewhat the large capacity of what the sediment transport can be at the ebb shoal.

2.2.2 Seasonal Variations

It was noted by a local pilot at Höfn, Vignir Júlíusson, who has been surveying the bathymetry at Grynnslin regularly, that he thought the depth at the ebb shoal changed significantly depending on whether it was summer or winter. An attempt was made to prove this because it would e.g. be easier to argue for the best time to implement construction of jetties or sediment dredging actions.

The bathymetric surveys date from 1998 to 2014 and they are 48 in total, but sometimes they are only performed once or twice per year. Obviously there are fewer surveys during the wintertime than at summertime. The focus was on the three points, P1, P2 and P3 (see Fig. 2.3) on the ebb shoal.

For the purpose of analysing the seasonal variation, MATLAB toolboxes and graphical presentations were used. The Matlab function *pburg* returns the power spectral density (PSD) estimate of a discrete-time signal and the function *autocorr* returns the sample autocorrelation function (ACF) of the univariate, stochastic time series with confidence bounds.

2.2.3 Water Depth on Ebb Shoals

From studies of tidal inlets, mainly conducted in the U.S., equations have been formulated that describe the depth at a tidal inlet ebb shoal. They estimate the water depth on the ebb shoal with regards to wave height and tidal prism and so they could be useful in this thesis.

Floyd (1968) gives a relationship between maximum depth of the channel h_C at inlet entrance and the maximum depth of the ebb shoal, h_E, as,

$$h_E = 0.5 \, h_C. \tag{2.3}$$

Buonaiuto and Kraus (2003) determined a predictive expression of the minimum water depth over the crest h_{Cr} of the ebb shoal. They used analysis of 18 inlets from around the

coast of the United States. These equations are,

$$h_{Cr1} = 0.27 + 3.6\overline{H}_{s,1yr},$$
$$h_{Cr2} = 0.0063P^{0.35},$$
$$h_{Cr3} = -0.066 + 0.046(\overline{H}_{s,1yr}P)^{1/4}, \tag{2.4}$$

where $\overline{H}_{s,1yr}$ is the yearly offshore significant wave height and P is the tidal tidal prism in m^3 which is defined as the volume of water leaving an estuary between mean high tide and mean low tide.

The equations in Eq. (2.4) have respective linear regression coefficients, $R^2 = 0.81$, 0.83 and 0.87, for the data which the three equations were based on. Note that the depth over the crest, h_{Cr}, is measured with respect to mean lower low water, since waves influence the seabed mostly at this lower tide level.

The equations in (2.4) use different mechanisms for the ebb shoal water depth but the third part of Eq. (2.4) uses both the wave height and tidal prism which was of interest here because it was estimated that the tidal prism will decrease with rising land. Figure 2.5 shows how much, depicting the relationship between h_{Cr3} and $(H_sP)^{1/4}$.
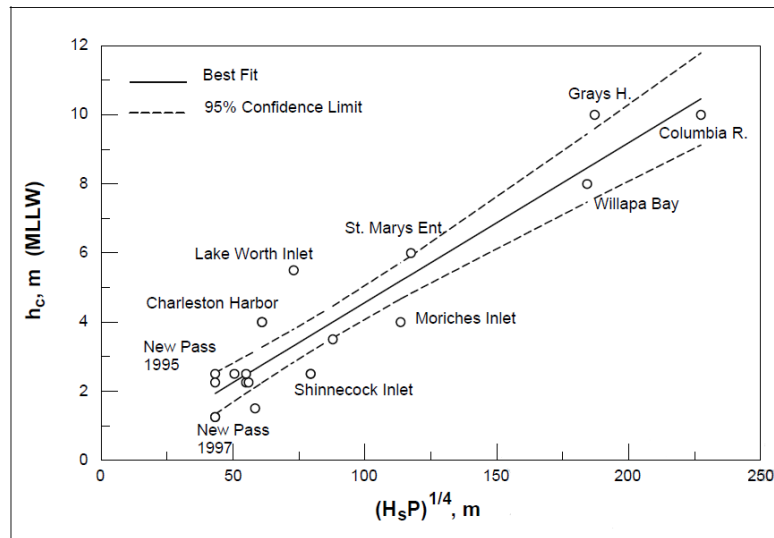
Figure 2.5: *Minimum depth over crest of an ebb shoal, h_{Cr3}, vs. $(H_sP)^{1/4}$. Some of the inlets used for the analysis by Kraus (2010) are marked with their names (Kraus, 2010).*

2.2.4 Volume of Sand in the Ebb Shoal

Walton and Adams (1976) give the ebb shoal volume as a function of the tidal prism of the backbarrier system (see Fig. 2.6). Hence the result of the land rise, which is decrease in tidal prism, can be related to the ebb shoal volume. The equation given by Walton and Adams (1976) is

$$V_E = C_E P^{1.23}, \tag{2.5}$$

where V_E is the ebb-shoal volume in m^3, $C_E = 2.21 \times 10^{-2}$ and P is the tidal prism in m^3.

There are small differences in the data Walton and Adams (1976) tabulated and what their plots show. However Kraus (2010) corrects that with Fig. 2.6 and that results in slightly altered constants of Eq. (2.5), which now becomes,

$$V_E = C_E P^{1.1673}, \tag{2.6}$$

with $C_E = 2.121 \times 10^{-2}$.
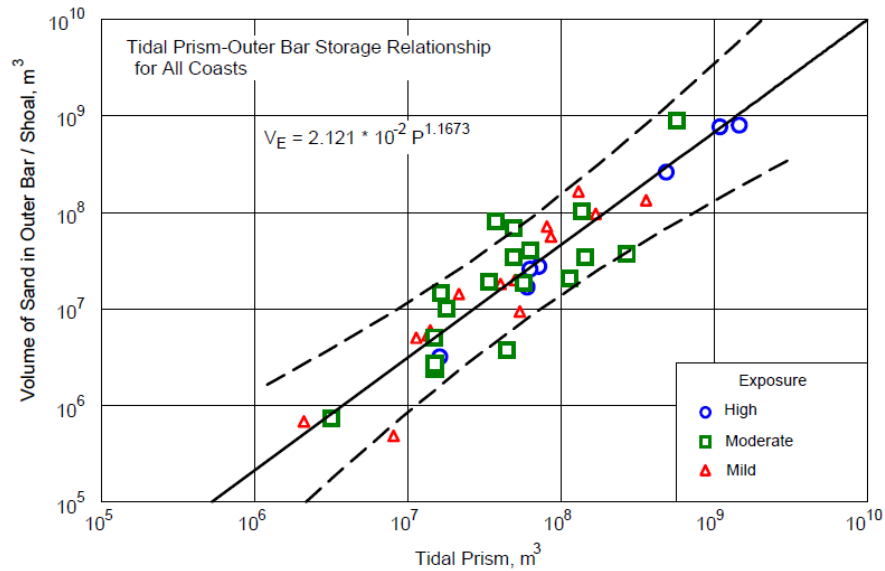
Figure 2.6: Volume of ebb tidal shoal as function of tidal prism (Kraus, 2010).

2.3 Sediment Transport Model

Bruun et al. (1991) concluded in their studies that the sediment transport in front of the Hornafjörður tidal inlet was something around a couple hundred thousand cubic meters in each direction, but with governing eastward direction. They put forward a ratio that is

practical to evaluate the inlet stability with respect to sediment transport,

$$P/M_{tot}. \tag{2.7}$$

The ratio takes into account the tidal prism, P, and volume of sediments transported through the inlet per year, M_{tot}, i.e. whether some part of the sediments is left in the inlet, transported offshore or into the lagoon. The ratio for Hornafjörður tidal inlet was estimated from experience based on other inlets and found to be of order 200. By assuming the tidal prism to be $P \approx 60 \times 10^6$ m^3 Bruun et al. (1991) found the volume of sediment transported to the inlet to be $M_{tot} = 300$ thousand m^3/year. However, the sediment transport comes to the inlet irregularly, e.g. one storm can transport up to 1/3 of the sediments.

Programs from DHI, *MIKE21 SW* and *Litdrift*, were used to perform littoral drift or alongshore sediment transport calculations. *MIKE21 SW* calculates wave parameters which were then used as part of the input for *Litdrift*. The output from *Litdrift* gives the littoral drift/alongshore sediment transport.

2.3.1 Spectral Wave Modelling

MIKE21 SW is a spectral wind-wave model developed by DHI and it simulates the growth, decay and transformation of wind-generated waves and swells in offshore and coastal areas.

Refraction

The wave transformation depends greatly on the bathymetry of the area in consideration. If a wave comes at an angle towards a coast it refracts as it gets near to it with regard to water depth. The angle between the wave fronts and the coastline, α, is given by Snell's law as,

$$\sin \alpha = \frac{\sin(\alpha')L}{L'}, \tag{2.8}$$

where L is the wave length and $'$ denotes reference point in the profile.

The wave length L is calculated explicitly in each point. The expression used is defined by the factor,

$$K_L = \frac{\omega^2 D}{g}, \tag{2.9}$$

where ω is the wave frequency, D is the water depth and g is the acceleration of gravity.

If $K_L > 1.0$, the following expression is applied (Fenton and McKee, 1991),

$$L_0 = \frac{g}{2\pi} \cdot T^2, \qquad (2.10)$$

$$L = L_0 \left(\tanh \left(\left(\frac{2\pi D}{L_0} \right)^{0.75} \right) \right)^{2/3}, \qquad (2.11)$$

where T is the wave period and L_0 is the deep water wave length.

If $K_L < 1.0$, the following expression is applied (Wu and Thornton, 1986),

$$L = \frac{2\pi D}{\sqrt{K_L} \cdot \left(1 + \frac{K_L}{6} \cdot (1 + \frac{K_L}{5}) \right)}, \qquad (2.12)$$

where K_L is found from Eq. (2.9).

Shoaling

In case of unbroken waves the wave height is determined by the conservation of energy flux along wave orthogonal.

$$H^2 \cdot c(1+G) \cdot \cos\alpha \approx \text{constant} \qquad (2.13)$$

$$G = \frac{2kD}{\sinh(2kD)} \qquad (2.14)$$

where $c = L/T$ is the celerity of the wave and $k = 2\pi/L$ is the wave number.

Breaking

As a criterion for wave breaking, a maximum of the ratio between the wave height and the water depth is introduced,

$$\gamma = \frac{H}{D}, \ \gamma_{max} = 0.8. \qquad (2.15)$$

For broken waves, γ is a function of the distance from the breaker line, X_b, and water depth at breaker line, D_B (see (Andersen and Fredsøe, 1983) and (Deigaard et al., 1986)),

$$\gamma = 0.5 + 0.3 \exp\left(-0.11 \frac{X_B}{D_B} \right). \qquad (2.16)$$

2.3.2 Alongshore Sediment Transport Modelling

The *Litdrift* models covers the description of alongshore current and sediment transport also called littoral drift. The model assumes that the beach is uniform in either direction from a reference profile, which should be located perpendicularly to coast, and has arbitrary coastal profile.

Sediment transport is often categorized into three parts; bed load transport, suspended load transport and sheet flow. The bed load is defined as,

> *"The part of the total load that is in more or less continuous contact with the bed during the transport."*

The suspended load is defined as,

> *"The part of the total load that is moving without continuous contact with the bed as a result of the agitation of fluid turbulence."* (Fredsøe and Deigaard, 1992)

The sheet flow occurs when a thin layer of the bed liquidizes under strong waves and or strong current force. Generally the total sediment is given as,

$$Q_t = Q_b + Q_s, \tag{2.17}$$

where Q_b and Q_s are sediment transports due to bed load and suspended load respectively.

Boundary Layer, Friction Factor and Bed Roughness

The boundary layer for a rough turbulent case can be determined from the ratio between the amplitude in the near bed orbital motion and the bed roughness, a/k_r where lower limit of a/k_r is 2.

Jonsson and Carlsen (1976) give the explicit approximation for calculating the wave boundary layer thickness, δ_w, as,

$$\delta_w/k_r = 0.072 \left(\frac{a}{k_r}\right)^{3/4}. \tag{2.18}$$

The boundary layer thickness is defined as the moment when the free stream velocity is maximum. The variation of δ_w with time is neglected.

The wave friction factor, f_w, is defined by,

$$U_f^2 = \frac{\tau_b}{\rho} = \frac{1}{2} f_w U_b^2, \tag{2.19}$$

where U_f is the wave friction velocity, τ_b is the maximum bead shear stress and U_b is the maximum wave induced velocity outside the wave boundary layer.

The friction factor, f_w, is a function of a/k_r. In (Jonsson and Carlsen, 1976) it is given with the following expression,

$$\frac{1}{4\sqrt{f_w}} + \log_{10}\left(\frac{1}{4\sqrt{f_w}}\right) = -0.08 + \log_{10}\left(\frac{a}{k_r}\right). \tag{2.20}$$

But for practical calculations it is more convenient to use the following approximation given by Swart (1974),

$$f_w = \exp\left(5.213 \cdot \left(\frac{a}{k_r}\right)^{-0.194} - 5.977\right). \tag{2.21}$$

The variation in the bed shear stress is found by assuming that the instantaneous bed shear stress can be found by use of the wave friction factor,

$$\frac{\tau}{\rho} = \frac{1}{2} f_w U^2, \tag{2.22}$$

where U is the instantaneous flow velocity at $y = \delta_w$ and y is the distance from sea bed.

Bed Load Transport

Bed load sediment transport is dependent on the bed shear stress from the flow velocity. The Shields number is a non-dimensional bed shear stress which is used to calculate the initiation of motion in a fluid flow and is described as,

$$\theta = \frac{\tau_b}{\rho g(s-1)d_{50}} \ , \ s = \frac{\rho_s}{\rho}, \tag{2.23}$$

where ρ is the density of seawater, ρ_s is the density of sediment, s is the relative density of the sediment and d_{50} is the mean grain diameter. The default value of the relative density in the transport model is $s = 2.65$.

The critical Shields number, θ_c, is the number for which sediments start to move, any Shields number lower than that does not result in bed load transport. It often varies between 0.04 to 0.06 but in the sediment transport model it is set at default as 0.045. The bed load transport can be calculated as,

$$Q_b = \Phi_b \sqrt{g(s-1)d_{50}^3}, \tag{2.24}$$

where the dimensionless bed load transport, Φ, is given by (Engelund and Fredsøe, 1976) as,

$$\Phi_b = 5p(\sqrt{\theta'} - 0.7\sqrt{\theta_c}), \tag{2.25}$$

where p is found by Eq. (2.28) and θ' is found by Eq. (2.27).

Suspended Load Transport

The suspended sediment transport is calculated as the product of the instantaneous flow velocities, U, and the instantaneous sediment concentration, c_b, with,

$$Q_s = \frac{1}{T} \int_0^T \int_{2d_{50}}^D (U c_b) dz dt. \qquad (2.26)$$

The time integration of the diffusion equation for suspended sediment is repeated until a periodic solution is obtained.

Once the variation of the friction velocity U_f over the wave period has been determined by the boundary layer module over flat bed, the following property may be derived for every time step (Engelund and Fredsøe, 1976),

$$\theta' = \frac{U_f^2}{(s-1)g d_{50}}. \qquad (2.27)$$

The deterministic description of the sediment concentration is given by Eq. (2.28)-(2.30),

$$p = \left[1 + \left(\frac{\frac{\pi}{6}\beta}{\theta' - \theta_c} \right)^4 \right]^{-0.25}, \qquad (2.28)$$

$$\lambda_l = \sqrt{\frac{\theta' - \theta_c - \frac{\pi}{6}\beta p}{0.027 s \theta'}}, \qquad (2.29)$$

$$c_b = \frac{0.65}{(1 + 1/\lambda_l)^3}, \qquad (2.30)$$

where θ' is the Shield's parameter determined for a plane bed, p is the probability of all particles of a layer moving, β is the bed slope, λ_l is the linear concentration and c_b is the sediment concentration. Equation (2.31) is an empirical description of the sediment concentration (Zyserman and Fredsøe, 1994), c_b. This equation was used in the sediment transport model.

$$c_b = \frac{0.331(\theta' - \theta_c)^{1.75}}{1 + 0.720(\theta' - \theta_c)^{1.75}} \qquad (2.31)$$

All the methods and theories discussed in Sections 2.3.1 and 2.3.2 are used in *MIKE21 SW* and *Litdrift*.

2.3.3 Model Input and Output

Wave Modelling with MIKE21 SW

Wave height, wave direction and wind force are parameters obtained from wave hindcast from the European Centre for Medium-Range Weather Forecast (ECMWF) for every 12 hours at three chosen boundary locations far offshore at (63.5°N, 16.5°W), (63.5°N, 15.0°W) and (64.0°N, 14.0°W) (see Fig. 2.7). The parameters from these three points is applied to the whole boundary.

The mean water level was obtained from MOGT which is an Icelandic weather observatory (MOGT, 2015). An overview of the main parameters for *MIKE21 SW* is shown in Table 2.1.

All these parameters along with the bathymetry are the input for *MIKE21 SW*. It is crucial to have proper bathymetry measurements for accurate results. The bathymetry used was from a mix of bathymetric surveys performed by IMA (Icelandic Marine Administration) and ICG Hydrographic Department (í. Sjómælingar Íslands). The density of the measurement points is highest close to the tidal inlet but further away they are more dispersed. The ebb shoal water depth is constantly changing but for the sediment transport calculations the water depth on the ebb shoal was between 6.3 and 6.5 m.

The model was run for the period from September 2013 to August 2014 or exactly one year. The output is the significant wave height, peak wave period, mean wave direction and directional standard deviation for every time step inside the boundary of the calculation area.
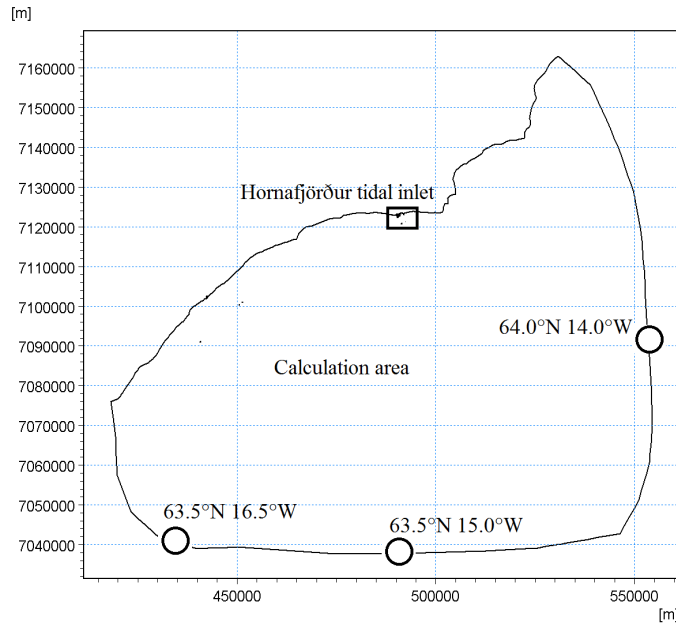
Figure 2.7: Overview of the calculation area. Hornafjörður tidal inlet is marked with square and the location of boundary points with circles.

Table 2.1: Overview of inputs for MIKE21 SW.

Wave Parameters	Value
Wave height	From ECMWF
Wave period	From ECMWF
Wave direction	From ECMWF
Wind force	From ECMWF
Wave breaking constant	$H_b = 0.8$ D
Mean water level	From MOGT
Current	No current
Ice	No ice
Diffraction	Soothing factor = 1
Fetch	Jonswap formula

Sediment Transport Modelling with Litdrift

A so called wave climate file was created from the output from *MIKE21 SW* which was then read into *Litdrift*. The wave climate file includes information about many parameters, e.g. wave height, wave period, directional standard deviation and reference depth from *MIKE21 SW*. These parameters were changed slightly in the *Litdrift* wave climate file.

2 Methods

The wave height is changed to root mean square value of wave height with

$$H_{rms} = \frac{H_s}{\sqrt{2}} \tag{2.32}$$

and the wave period is changed to the mean zero up-crossing wave period with

$$T_z = \frac{T_p}{1.3}, \tag{2.33}$$

where T_p is the peak wave period. Directional spreading was calculated from the directional standard deviation according to DHI as

$$D_s = -0.0002x^2 - 0.0092x + 1.0628, \tag{2.34}$$

where x is the directional standard deviation. All this information is taken from a location of a reference depth which is then applied for the whole profile in question. The reference depth was chosen with regard to the closure depth which is defined as the depth at which no significant alongshore or cross-shore transports takes place due to littoral processes. Hallermeier (1981) described the closure depth with the following equation

$$d_c = 2.28 \cdot H_{s,12h} - \frac{68.5}{H_{s,12h}^2 (gT_s^2)}, \tag{2.35}$$

where d_c is the predicted depth of closure, referenced to mean low water, $H_{s,12h}$ is the non-breaking significant wave height that is exceeded 12 hours per year and T_s is the associated wave period.

The sediment characteristics used in the model were

Roughness	=	0.01 m
Mean grain size	=	0.25 mm
Fall velocity	=	0.27 m/s
Geometrical spread	=	1.4

Final output from *Litdrift* were sediment transports distributions towards west and east along a profile.

3 Results and Discussion

3.1 Classification

3.1.1 Shape Classification

Hornafjörður tidal inlet, with its ebb and tidal shoal, is mostly similar to the wave dominated tidal inlet in Fig. 2.1b with large tidal energy. However the ebb jetty (í. straumband) at Hornafjörður tidal inlet lies straight towards east but not orthogonal to the coast like in Fig. 2.1b. Therefore according to the shape classification the Hornafjörður tidal inlet is wave dominated but also has strong tidal forces acting on it.

3.1.2 Hayes Classification

On the ebb shoal at points P1, P2 and P3 where the mean depth is 7.4 m, 6.9 m and 6.8 m (see Fig. 2.3), the respective mean wave heights are $\overline{H} = 1.41$ m, 1.34 m and 1.3 m. There is not much difference between them and therefore the average $\overline{H} = 1.35$ m is used for the ebb shoal wave height. The offshore mean wave height at the wave buoy was however $\overline{H} = 1.90$ m.

These parameters, with the mean tidal range $R_t = 1.98$ m, were located in the Hayes classification graph and it showed the tidal inlet to be inside the "Mixed Energy (wave dominated)" for part of the classification in both the case for ebb shoal wave height and offshore wave height (see Fig. 3.1). For the offshore wave height the classification is on the border of being inside "Wave Dominated".

Therefore as it is "Mixed Energy (wave dominated)", both wave and tidal flow is significant at the tidal inlet. The waves are though a slightly stronger force than the tidal flow.

Figure 3.1: Hornafjörður tidal inlet located on the Hayes classification graph, marked with stars (Hayes, 1979).

The coast of Iceland is commonly wave dominated and therefore this was not as definitive as was hoped for. But bearing in mind that Hayes used only selected tidal inlets from the United States in the making of his graph, it is maybe not so surprising. Tidal inlets in the United States have finer sediments than Hornafjörður tidal inlet and the maximum mean velocity over tidal entrance cross section is assumed to be on average 1 m/s, whereas in Hornafjörður it is closer to 2 m/s according to (Viggósson and Sigurðarson, 2000). This difference between the two types of tidal inlets could account for the vague classification of "Mixed Energy (wave dominated)" for Hornafjörður tidal inlet but it could also be that the tidal inlet has both strong waves and strong tidal force acting upon it.

3.1.3 Nielsen & Thuy Classification

A wave buoy of type Waverider is located 2.2 nautical miles south of the entrance, south of Hvanneyjarsker reefs at 32 m water depth ($66°26.30'$N $23°22.00'$W) and has been operating since the year 1990. Data from this buoy were used to classify the Hornafjörður tidal inlet. Measurements for the period 2000-2009 were used to find the mean offshore significant wave height, it was found to be $\overline{H}_s = 1.90$ m.

The peak tidal discharge and fresh water discharge has been measured to be $\hat{Q} = 3440 \, \text{m}^3/\text{s}$ and $Q_f = 100 \, \text{m}^3/\text{s}$ respectively. According to Eq. (2.1) and (2.2) this gives the relative tide strength as $R_{TW} = 222$ and relative river or fresh water strength as $R_f = 6.4$. Figure 3.2 shows that the Hornafjörður tidal inlet is tidal dominated. This is contradictory to former classifications, shape and Hayes classification.
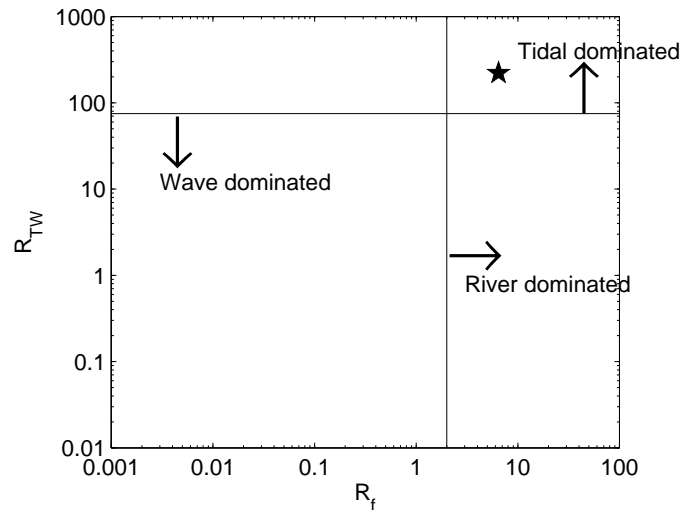
Figure 3.2: Classification of Hornafjörður tidal inlet by the Nielsen & Thuy method, marked with a star.

It is not clear why this method shows the tidal inlet to be tidal dominated when the expected results for Hornafjörður tidal inlet was wave dominated. According to the two former classifications the tidal inlet is wave dominated but with large tidal force also acting upon it.

This method, by Nielsen & Thuy, possibly accounts more for the tidal forces which are perhaps smaller, in the Australian tidal inlets used to formulate this classification, than in the Hornafjörður tidal inlet. Also Fig. 2.4 has very few points in the tidal dominated range. Other reasons, such as sediment type difference between Australia and Iceland and sheltering effects from Hvanneyjarsker, could also explain this contradictory classification. Icelandic sediment is mostly basalt, with sharp edges and large shear stress, while sediment in Australia is finer and is more easily transported than the basalt sediment.

Figure 3.3 shows the significant wave height at the ebb shoal and offshore. South of Hvanneyjarsker, the wave height is shown to be between 3.2 and 3.6 m (orange) but at the ebb shoal it is shown to be between 2.4 and 3.2 m (yellow/green). This indicates that the sheltering effects from Hvanneyjarsker reefs decreases wave height at the ebb shoal. Figure 3.4 shows the ratio between the wave height on the ebb shoal and offshore to be approximately 0.8, for the common wave directions of 120-240°. Therefore the waves on the ebb shoal are approximately 20% smaller than offshore.

16.11.2013 6:00:00 Time Step 305 of 1456.
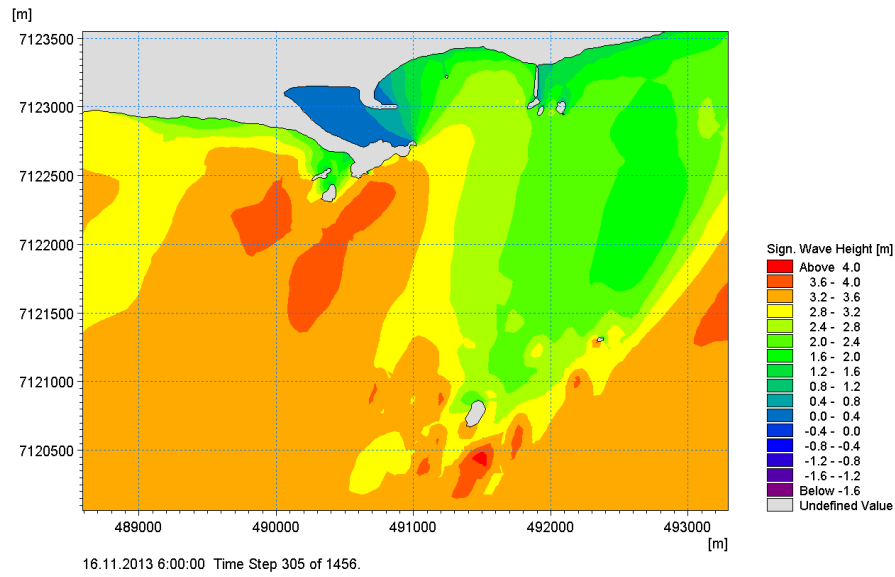
Figure 3.3: Significant wave height at the ebb shoal and offshore.
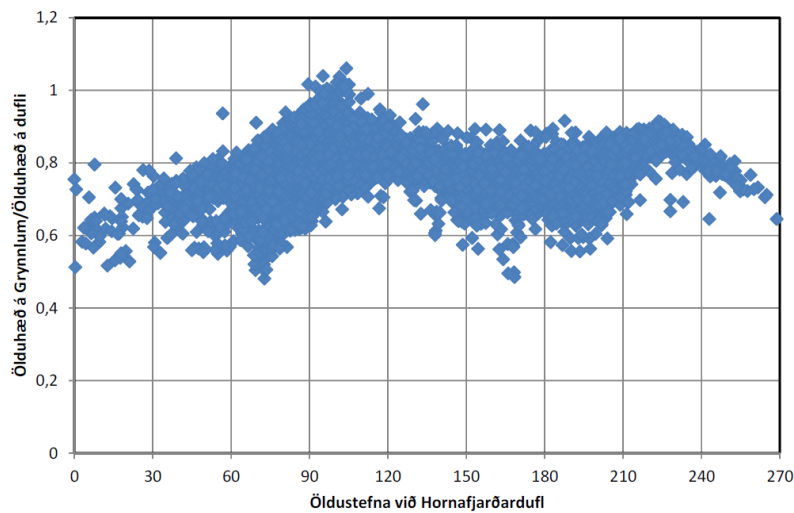
Figure 3.4: The ratio between wave heigh on ebb shoal and offshore (y-axis) plotted against wave direction (x-axis) (Asgrímsdóttir et al., 2014).

According to the classification methods above it was concluded that the Hornafjörður tidal inlet is wave dominated. However, there is also a strong tidal energy acting upon the tidal inlet and therefore there are mixed energies of waves and tidal flow, but the waves being slightly stronger of the two.

3.2 Ebb Shoal Analysis

3.2.1 Bathymetric Surveys

For the period between 2009 and 2014 there were 15 bathymetric surveys available and from those were made 10 bathymetric difference planes. For clarification purposes an overview graph of when the measurements were taken was made (see Fig 3.5).
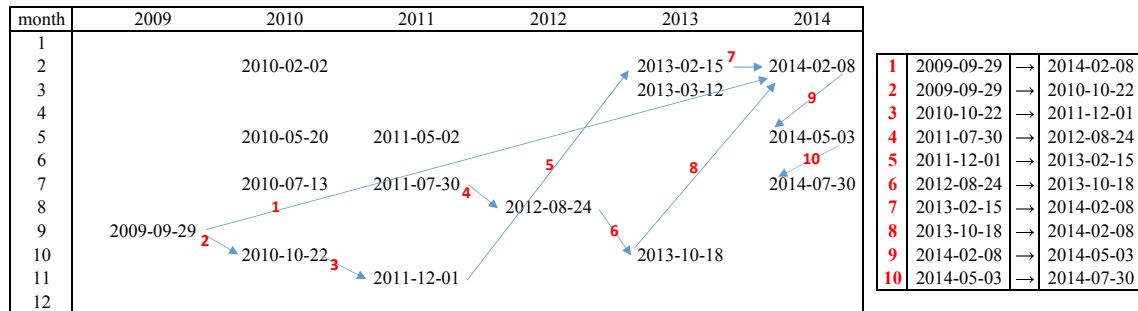
Figure 3.5: Overview over recently performed bathymetric surveys and bathymetric difference planes (red numbers).

The dredging in 2005 showed that sediment transport on the ebb shoal can be around 55 to 65 thousand m^3 in matter of a few months. However, in the period from the fall of 2013 to late summer of 2014 it was around 300 thousand m^3. This is an extreme case which has not been seen since regular bathymetric surveys began. This period is of great interest because it shows the sediment transport capacity of the tidal inlet and it is this period that is examined exclusively in the present bathymetric analysis and later in the sediment transport model.

The tidal flood surges through the tidal inlet channel and toward the sea. The direction of this ebb jetty is indicated with red arrows in the explanation figure (see Fig. 3.6). On the figure the areas close to Hvanney and Þinganessker are marked with green and orange lines and the main part of the ebb shoal is indicated within the blue curved lines. The jetties that were constructed at the South Barrier, East Barrier and Þinganessker, to stabilise the tidal inlet, are shown with red thick lines at each location.
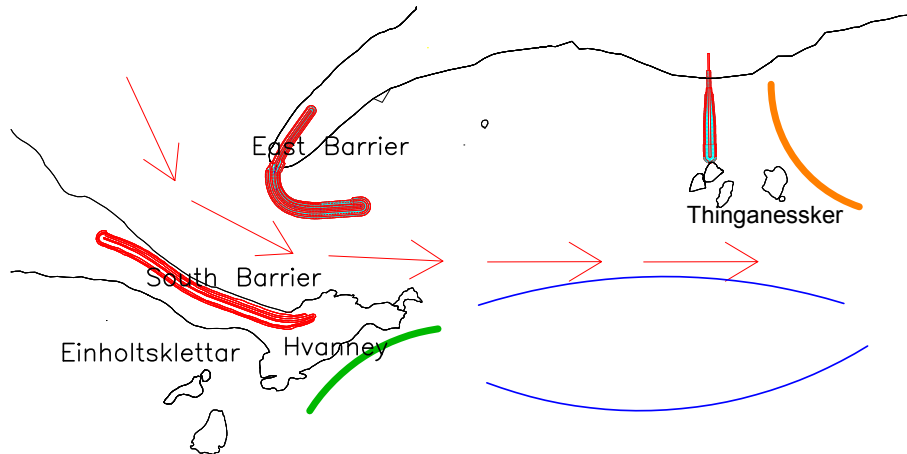
Figure 3.6: Explanation figure. Red arrows show the ebb jetty direction, blue lines indicate the location of the ebb shoal, green line indicates the area close to Hvanney and orange line indicates the area close to Þinganessker. The jetties at the South Barrier, East Barrier and Þinganessker are shown with red thick lines.

The ebb jetty (í. straumband), indicated with red arrows in Fig. 3.6, reaches the furthest to east when the weather is mild over the summertime (see Fig. 3.7). Then the waves are small and do little to counteract the tidal flow from the inlet, which transports sediment from the ebb jetty resulting in large water depth (see Fig. 3.7). The tidal inlet channel directs the tidal flow straight towards east and reaches far before it disperses or slows down. This poses a problem because even though the ebb jetty reaches far, the sediment settles where the flow force decreases, i.e. at the end of and at the sides of the flow, which is directly in front of the tidal inlet channel at the ebb shoal (blue lines in Fig. 3.6). Therefore it becomes an obstacle in the navigation route into the inlet.

In contrast to measurements taken at summer the late winter ebb jetty (see 3.8) is smaller because of larger wave heights that break up on the ebb shoal and transport sediment into the ebb jetty. In south-east storms much sediment gathers east of Þinganessker (orange line in Fig. 3.6) at winter which it does not over the summertime because then the tidal flow is stronger than the wave action and transports sediment away from the ebb jetty towards east.

(a) 2010-05-20

(b) 2010-07-13
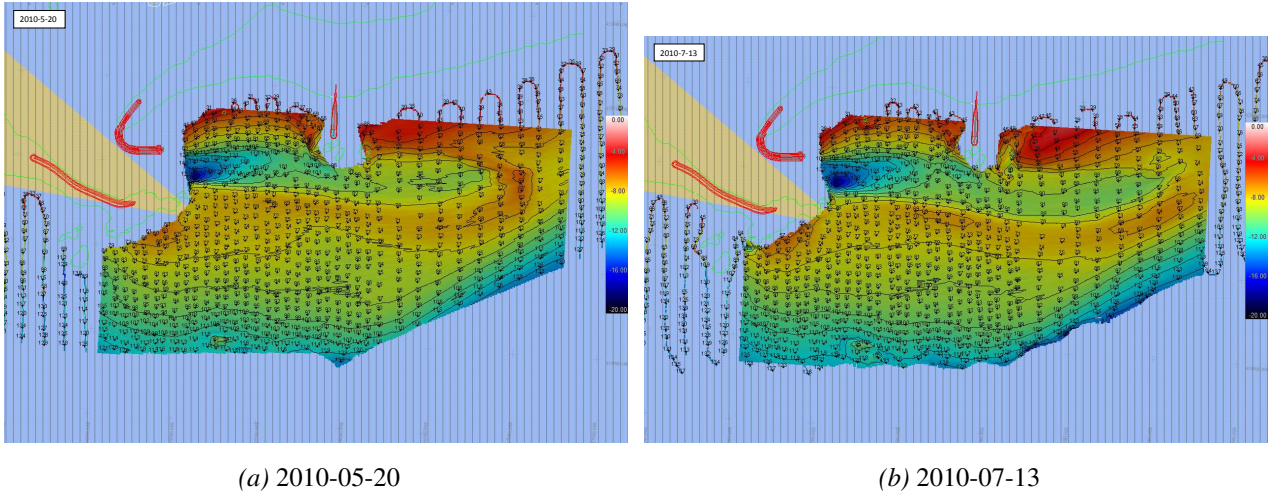
Figure 3.7: *Bathymetric surveys taken at summer. They show the same area as Fig. 3.6 with the same jetties shown with thick red lines. The color scale indicating water depth, ranges from -20 m up to 0 m with blue color showing large water depth and red showing small water depth. These surveys are shown enlarged in Appendix A.1.*

(a) 2010-02-02

(b) 2013-03-12
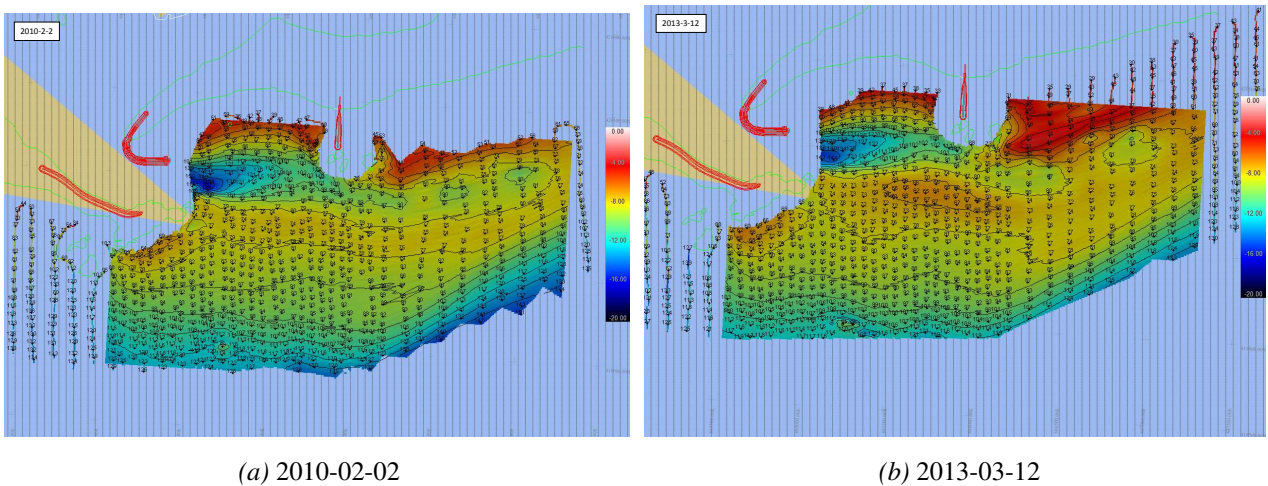
Figure 3.8: *Bathymetric surveys taken at winter. They show the same area as Fig. 3.6 with the same jetties shown with thick red lines. The color scale indicating water depth, ranges from -20 m up to 0 m with blue color showing large water depth and red showing small water depth. These surveys are shown enlarged in Appendix A.1.*

The bathymetric surveys in Fig. 3.9 were taken in October 2013, February 2014, May 2014 and July 2014. They are taken in the period when extreme sediment transfer occurs. The wave seems to be coming much from the east as can been well noticed in Fig. 3.9c and

3.9d. In the fall and winter much sediment is gathering east and south-east of Þinganessker (see Fig. 3.9a and 3.9b).

(a) 2013-10-18

(b) 2014-02-08

(c) 2014-05-03

(d) 2014-07-30
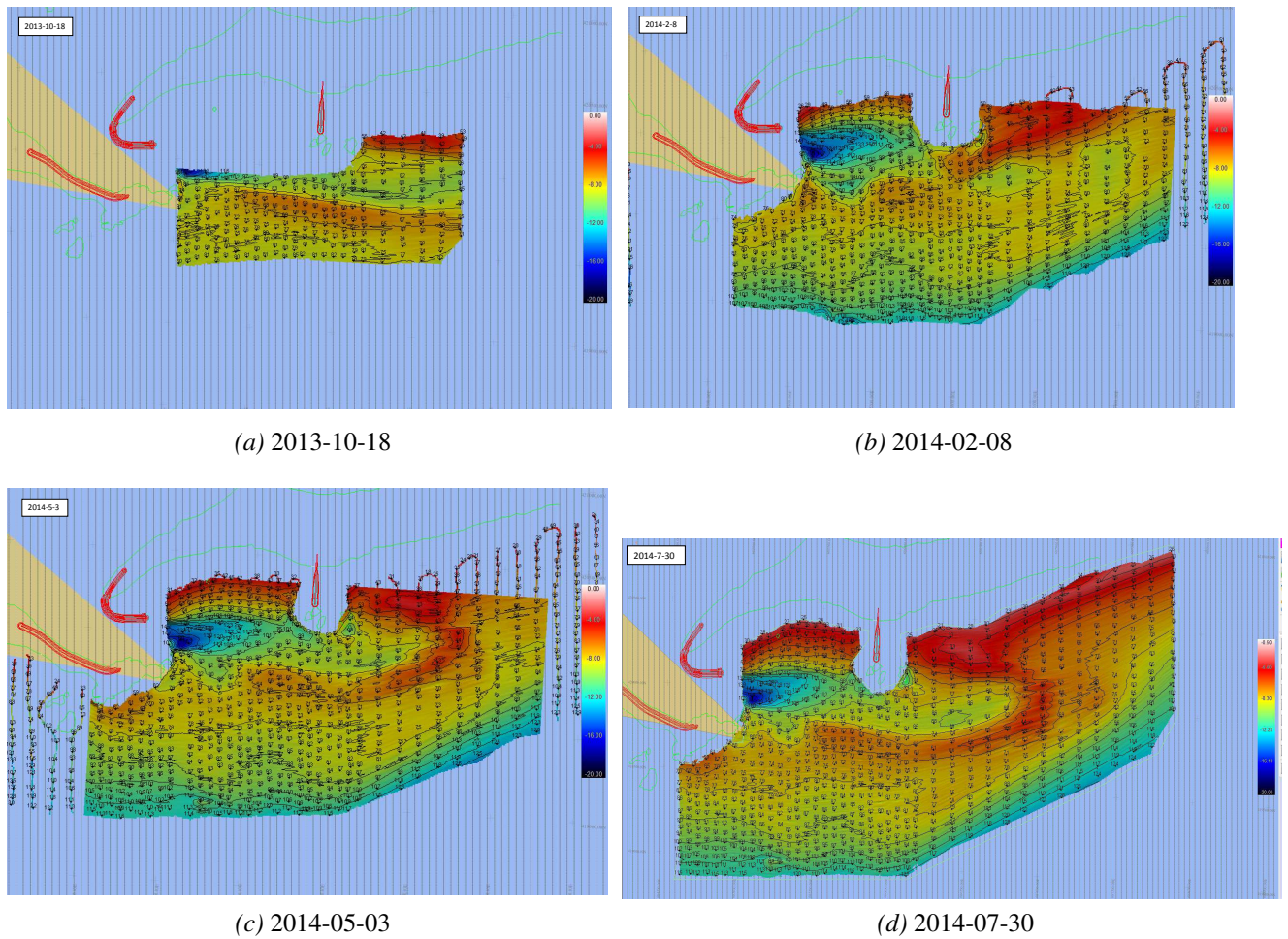
Figure 3.9: Bathymetric surveys from October 2013 to July 2014. They show the same
area as Fig. 3.6 with the same jetties shown with thick red lines. The color scale
indicating water depth, ranges from -20 m up to 0 m with blue color showing large
water depth and red showing small water depth. These surveys are shown enlarged in
Appendix A.1.

This is better depicted on the bathymetric difference planes in Fig. 3.10 where the accumulated sediment is shown in red and the eroded sediment is shown in blue. Some erosion is shown near to Hvanney and the inlet channel, opening up a safe navigation route, shown with blue in Fig. 3.10a.

The red in Fig. 3.10a, showing aggregated sediment at Þinganessker between October and February, eroded towards east from February to May as can be seen in Fig. 3.10b

where the blue erosion is similar in volume as the red aggregation in Fig. 3.10a. The red aggregation in Fig. 3.10b, which was transported from Þinganessker eroded further still in the period from May to July and can be similarly seen in Fig. 3.10c.

The red accretion in Fig. 3.10b has been estimated as 300 thousand m^3 and the blue erosion in same figure is similar in volume. In Fig. 3.10c the red accretion has been estimated about 240 thousand m^3 and the blue erosion in same figure about 200 thousand m^3.

(a) 2013-10-18 to 2014-02-08

(b) 2014-02-08 to 2014-05-03

(c) 2014-05-03 to 2014-07-30
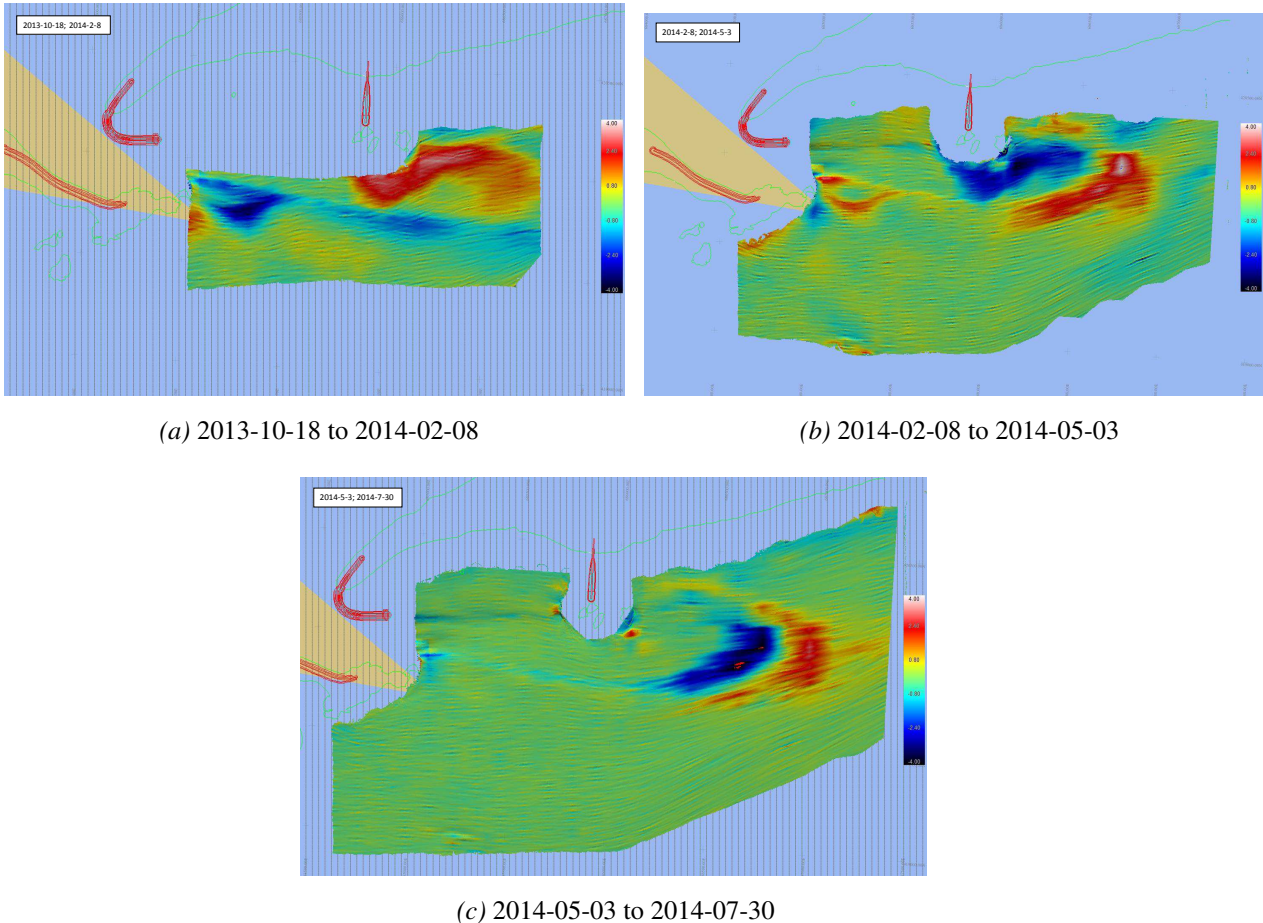
Figure 3.10: Bathymetric difference planes from October 2013 to July 2014. They show the same area as Fig. 3.6 with the same jetties shown with thick red lines. The color scale indicating difference in depth between two dates, ranges from -4 m up to 4 m with blue color showing sediment erosion and red showing sediment accretion. These surveys are shown enlarged in Appendix A.2.

This sediment transport is mostly due to the tidal flood and it shows the immense power it can wield. The sediment transport at the ebb shoal depends on the tidal flood and wave force. Over the summertime the tidal flood is strong but gets weaker during winter.

3.2.2 Seasonal Variations

The depth time series for the points P1, P2 and P3 (see Fig. 2.3) are shown in Fig. 3.11. The depth at P1 is on average larger than the depth at P2 and P3 with the average being 7.4, 6.9 and 6.8 m respectively. One reason for larger water depth in P1 could be that waves rebound from Hvanney resulting in sediments taken away from the area closest to Hvanney (orange line in Fig. 3.6). Waves are larger during winter than during summer. Hence they come periodically, which suggests that seasonal variation should be at least well recognizable in point P1 because larger waves cause more erosion.
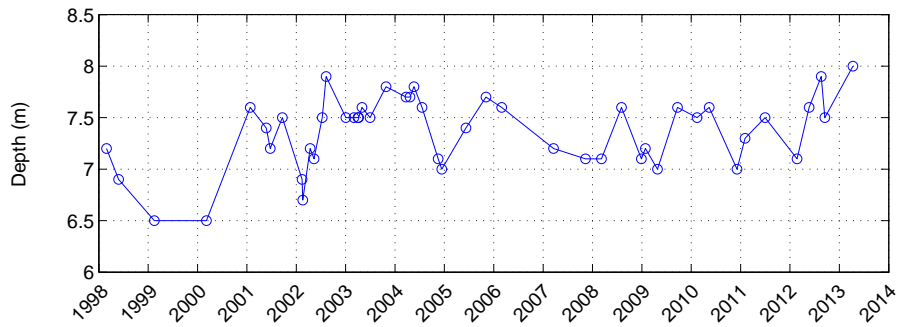
(a) P1
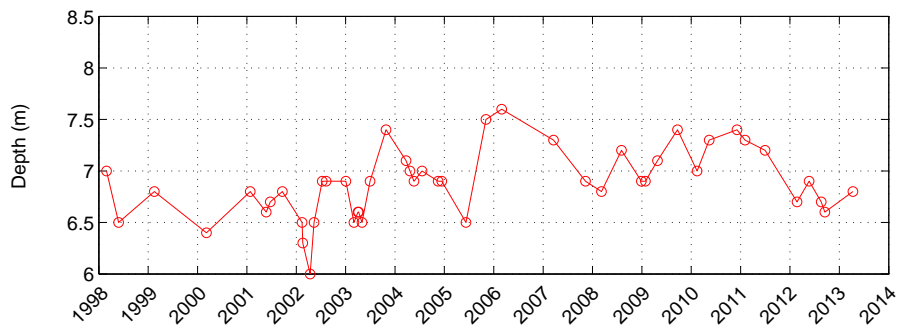
(b) P2
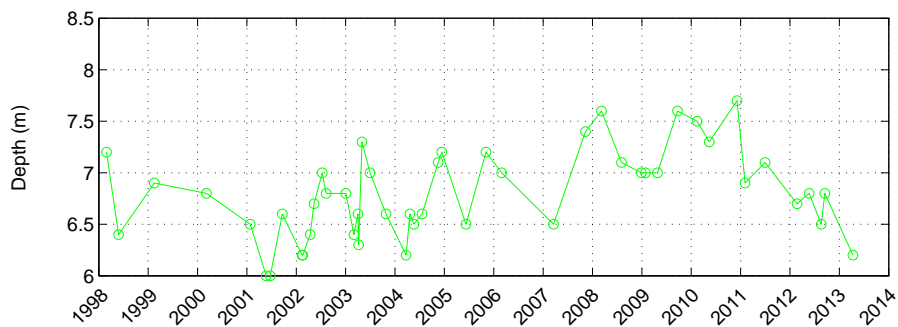
(c) P3

Figure 3.11: Timeseries of depth at points P1, P2 and P3 (see Fig. 2.3).

The the power spectral density (PSD) and the autocorrelation function (ACF) were found for the time series in Fig. 3.11, using the MATLAB functions *pburg* and *autocorr*. The results of that is shown in Fig. 3.12 with the PSD in the left column and the ACF in the right column.

The crests and trough in the PSD, which is given with *pburg*, shows where there is either upward or downward variation in water depth. The PSD uses normalized frequency with sample size 48, since there are 48 bathymetric surveys, and it can therefore be defined as,

$$\frac{f}{f_0}, \text{ where } f_0 = \frac{1}{2\pi \text{ rad}} \cdot 48 \text{ samples.} \tag{3.1}$$

In Fig. 3.12a the normalized frequency for two of the troughs are approximately 0.17 and 0.5 $\times \pi$ rad/sample. Therefore according to Eq. (3.1) this means that water depth in P1 decreases every 4 and 12 months.

This is more clearly depicted in the ACF, which is given with *autocorr*. The ACF indicates the recurrence of either water depth increase of decrease same as the PDS, where the lag can be understood as the month recurrence. In the ACF for P1 there is a decrease in lag 4 and 12 (see Fig. 3.12b). The stem in lag 4 is well within the blue confidence bounds and is essentially zero and therefore insignificant for this analysis. The stem in lag 12 however, is outside the confidence bounds and is therefore significant and indicates furthermore, decrease in water depth every 12 months. The results for points P2 and P3 are less definitive, but the ACF for point P2 (see Fig. 3.12d) seems to show an increase in water depth every 7-8 months (lag 7/8).

The PSD and AFC show the variation of the depth with a certain frequency. To better see what time of year that occurs an attempt was made to depict it by overlaying all the years and fitting a 6th order polynomial through the data points (see Fig. 3.13). In order for the polynomial to begin and end in roughly the same place, 6 months of data were added before and after.

In Fig. 3.13b and 3.13c the seasonal variation is not clear for points P2 and P3 because even though the polynomial shows a low point in a certain month the depth data can vary almost 1 m in either decrease or increase of depth. It is clearer in P1 where the data points are more dense and according to Fig. 3.13a where the water depth decreases during the summertime from May to July.

(a) PDS in P1

(b) ACF in P1

(c) PDS in P2

(d) ACF in P2

(e) PDS in P3

(f) ACF in P3
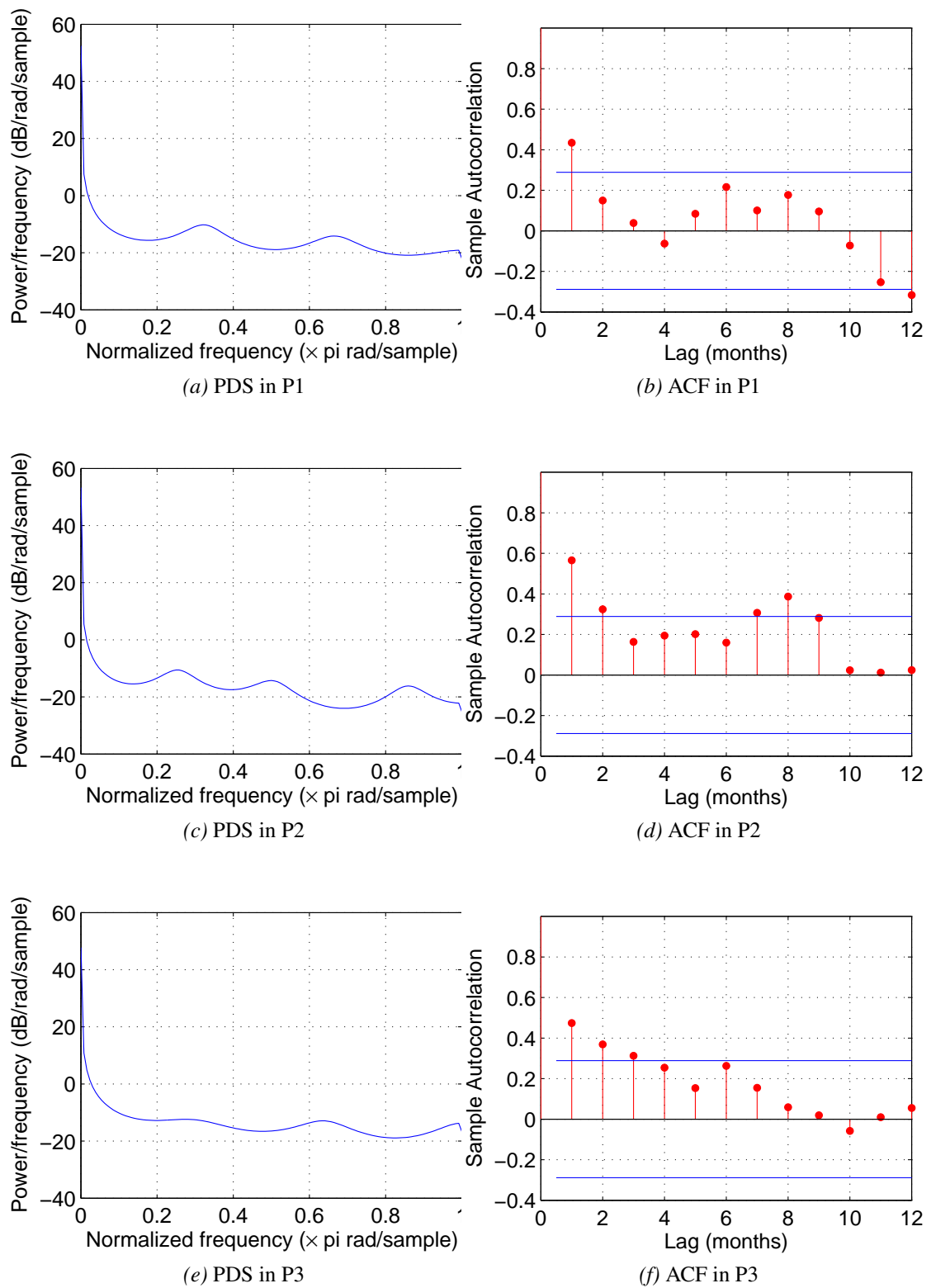
Figure 3.12: Power spectral density (PSD) and autocorrelation function (ACF) of water depth in points P1, P2 and P3 (see Fig. 2.3).

(a) P1

(b) P2

(c) P3
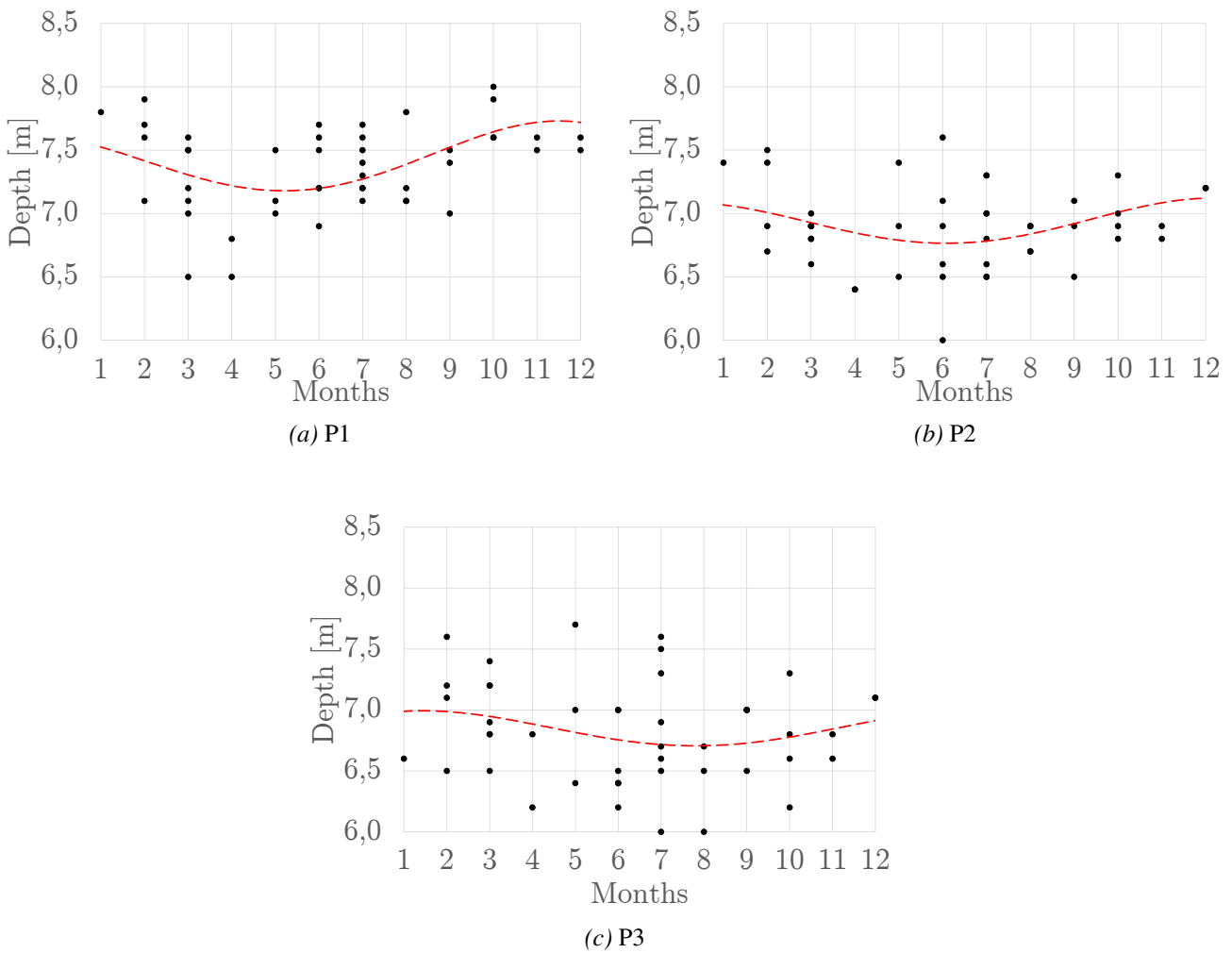
Figure 3.13: Overlay plots of water depth at P1, P2 and P3 (see Fig. 2.3). The red dotted line is a 6th order polynomial fitted to the data points.

For a time series analysis it is best if the data are continuous and regular. In this case however there are sometimes 2 to 3 months between sample measurements. In the analysis it is assumed to be every month, which was bound to skew the results somewhat. Despite that though, some seasonal variation is noticed, at least in point P1. This indicates that the wave effects were significant on the ebb shoal.

As was predicted, the water depth in P1 shows seasonal variation with decrease in water depth every 12 months. But whether that is only due to the proximity to Hvanney and seasonal variation in wave height is not known.

Comparison to the bathymetric surveys in Section 3.2.1, e.g. Fig. 3.10b and 3.10c, show

the depth at the ebb shoal is decreasing over the summertime. This is consistent with the results from the overlay plots shown in Fig. 3.13.

3.2.3 Water Depth and Volume Calculations

According to Eq. (2.3) half of the tidal inlet channel water depth can be taken as the maximum water depth of the ebb shoal. That was easily confirmed with one of the bathymetric surveys, e.g. Fig. 3.8a, which is shown enlarged in Appendix A. It shows that the depth in the channel was little under 15 m while the maximum depth on the ebb shoal was around 7.5 m. The depth at Grynnslin varies a bit but is most often considered to be between 7 to 7.5 m and the value of 7.3 m is the common assessment.

For a tidal prism, $P = 64 \times 10^6$ m^3, and average annual offshore significant wave height, $\overline{H}_{s,1yr} = 8.6$ m (Asgrímsdóttir et al., 2014), the results from Eq. (2.4) are shown in Table 3.1.

Table 3.1: Ebb shoal depth calculations.

h_{cr1} [m]	31.2
h_{cr2} [m]	3.4
h_{cr3} [m]	7.0

From the results it can be concluded that by only looking at either the wave height or tidal prism separately, as is done in the first two parts of Eq. (2.4), the results are not good. The first part gives way too large water depth and the second part too low.

Because of sheltering effects from Hvanneyjarsker the offshore significant wave height is probably overestimated but even though it were 20% less the first part of the equation would still give too large water depth. A tidal inlet in the U.S.A. with same tidal prism as in Hornafjörður tidal inlet has half the tidal flow compared to Hornafjörður tidal inlet, which may not be accounted for in the second part of the equation.

But by combining these two factors in the third part the results are close to reality. Figure 3.14 shows depth over crest, h_{cr3}, plotted against $(H_sP)^{1/4}$ and for the case of Hornafjörður tidal inlet $(H_sP)^{1/4} = 153$ and $h_{cr3} = 7.0$ m.
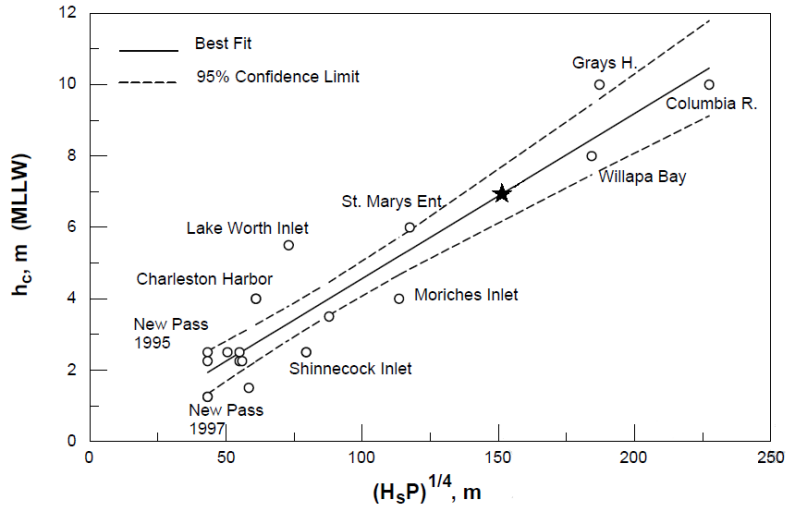
Figure 3.14: Minimum depth over crest of an ebb shoal vs. $(H_sP)^{1/4}$ (Kraus, 2010). The ebb shoal or Grynnslin is shown with a star.

For a 0.5 m an 1.0 m relative land rise there will be a respective 35% and 66% decrease in the tidal prism, P, which is based on predicted decrease in the tidal prism (see Section 1.2.1). The ebb shoal water depth was then calculated according to Eq. (2.4c) and the results are shown in Table 3.2.

Table 3.2: Ebb shoal depth calculations after land rise.

	$P_{0.5m}$	$P_{1.0m}$
h_{cr3} [m]	6.3	5.3

These calculations indicate that the water depth could decrease considerably with relative land rise or about 10% and 24% for respective 0.5 and 1.0 m relative land rise. The tidal prism value of $P = 64 \times 10^6$ m^3 is a value that was measured 20 years ago and most likely the tidal prism is smaller now. The sensitivity analysis in Table 3.3 and Fig. 3.15 shows how the ebb shoal crest depth calculations change with respect to tidal prism and wave height. The water depth is calculated largest for large wave heights and tidal prism and in contrast lowest for small wave heights and tidal prism.

Table 3.3: Sensitivity analysis of the ebb shoal crest depth, h_{Cr3}, for varying waveheight H_s and tidal prism P.

h_{Cr3}		H_s/H_{s0}									
		0.6	0.7	0.8	0.9	1.0	1.1	1.2	1.3	1.4	1.5
	1.2	6.4	6.7	6.9	7.1	7.3	7.5	7.7	7.8	8.0	8.1
	1.1	6.3	6.5	6.8	7.0	7.1	7.3	7.5	7.6	7.8	7.9
	1.0	6.1	6.4	6.6	6.8	7.0	7.1	7.3	7.5	7.6	7.7
	0.9	6.0	6.2	6.4	6.6	6.8	7.0	7.1	7.3	7.4	7.5
P/P_0	0.8	5.8	6.0	6.2	6.4	6.6	6.8	6.9	7.0	7.2	7.3
	0.7	5.6	5.8	6.0	6.2	6.4	6.5	6.7	6.8	6.9	7.1
	0.6	5.4	5.6	5.8	6.0	6.1	6.3	6.4	6.6	6.7	6.8
	0.5	5.1	5.4	5.5	5.7	5.9	6.0	6.1	6.3	6.4	6.5
	0.4	4.9	5.1	5.2	5.4	5.5	5.7	5.8	5.9	6.0	6.1
	0.3	4.5	4.7	4.9	5.0	5.1	5.3	5.4	5.5	5.6	5.7
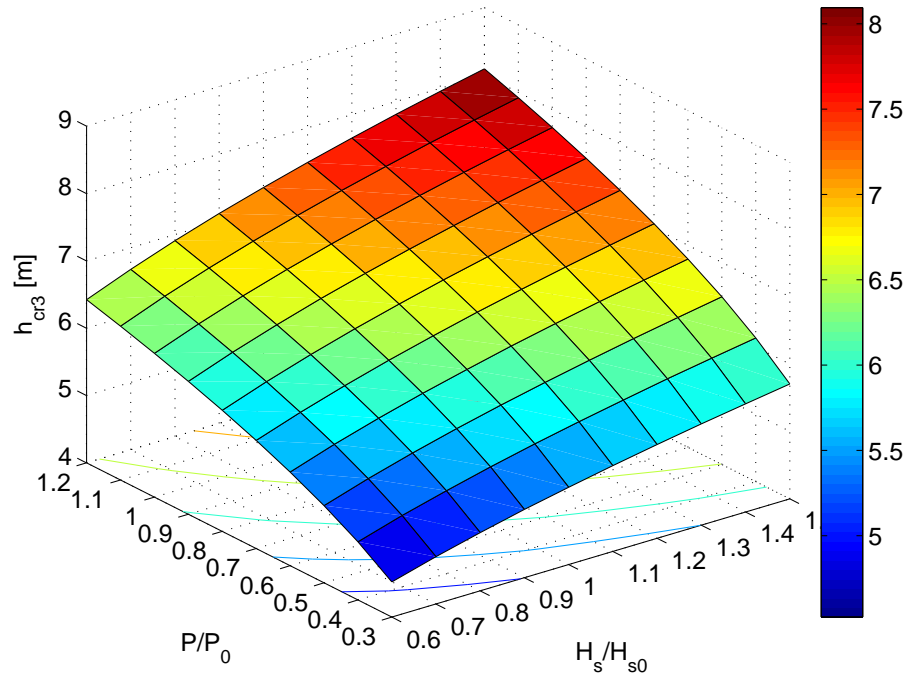
Figure 3.15: Sensitivity analysis of the ebb shoal crest depth, h_{Cr3}, for varying waveheight H_s and tidal prism P.

Equation (2.6) with the revised constants from (Kraus, 2010) is used to calculate the volume of the ebb shoal (see Fig. 3.16). The equation gives the volume as $V_E = 27 \times 10^6$ m^3.
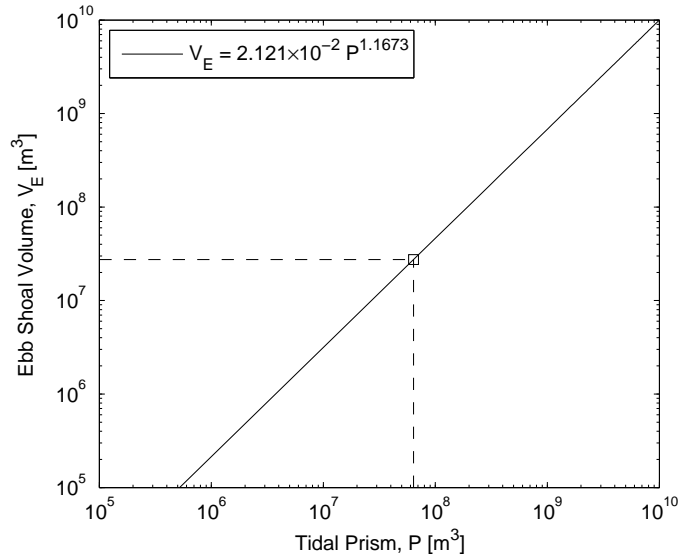
Figure 3.16: Plot of the ebb shoal volume as a function tidal prism. The ebb shoal volume for $P = 64 \times 10^6$ m^3 is shown with dotted lines.

For a relative land rise and therefore decrease in tidal prism the ebb shoal volume equation shows that the volume decreases. The ebb shoal volume for 0.5 m and 1.0 m would decrease to 16.6×10^6 m^3 and 7.8×10^6 m^3 respectively, which is a 39% and 70% decrease respectively.

The water depth and volume analysis in this subsection indicates that the water depth on the ebb shoal is both decreasing and increasing with relative land rise. Calculating ebb shoal water depth at a tidal inlet is difficult and empirical equations are mostly used for that purpose. The equations for both the water depth and volume are such equations. They emphasize on different aspects and were formulated with limited number of tidal inlets. Ebb shoal water depth calculations are not exact science but these calculations show that even though there is a land rise it may not necessarily mean a decrease in ebb shoal water depth.

3.3 Sediment Transport Model Results

3.3.1 Wave modelling

The bathymetry of the area close to and around the tidal inlet is shown in Fig. 3.17. The reefs south of the inlet, Hvanneyjasker, partially shelter the inlet from the waves.
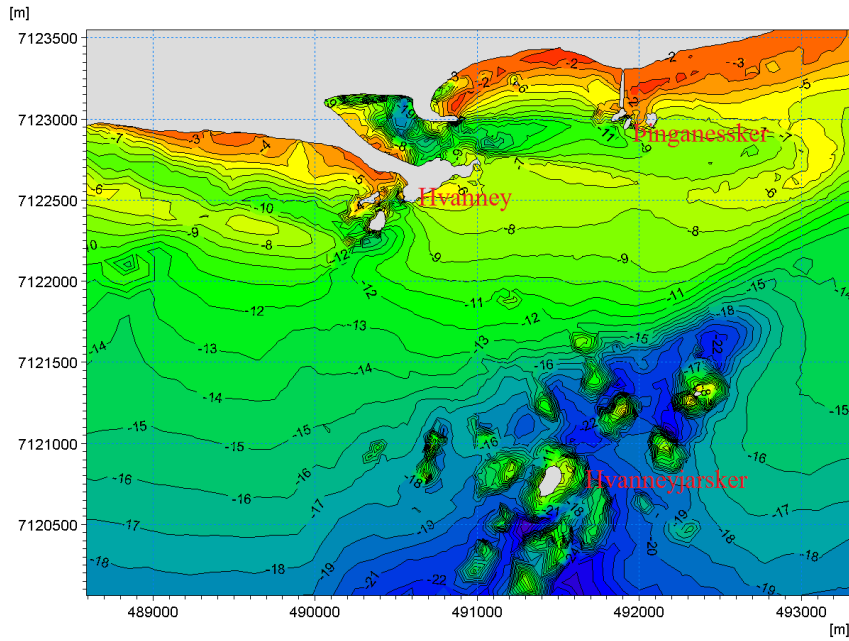
Figure 3.17: Bathymetry of the area close to the tidal inlet.

In *MIKE21 SW* triangle shaped mesh grid was made for the calculation area and the bathymetry is connected to the nodes of each triangle. The mesh grid size ranges from 4 million m^2 at the boundary of the calculation area to 1,600 m^2 closest to the tidal inlet. The side length of the triangles ranges from 2,500 m to 50 m respectively. The mesh grid is shown in Fig. 3.18 and with a close-up of the tidal inlet in Fig. 3.19.
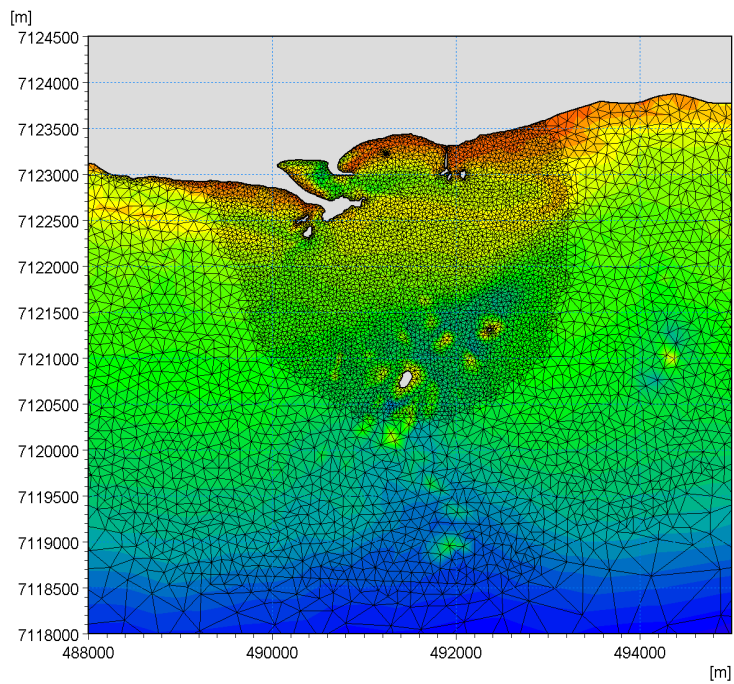
Figure 3.18: Mesh overview, course near the offshore boundary and fine near the inlet entrance.
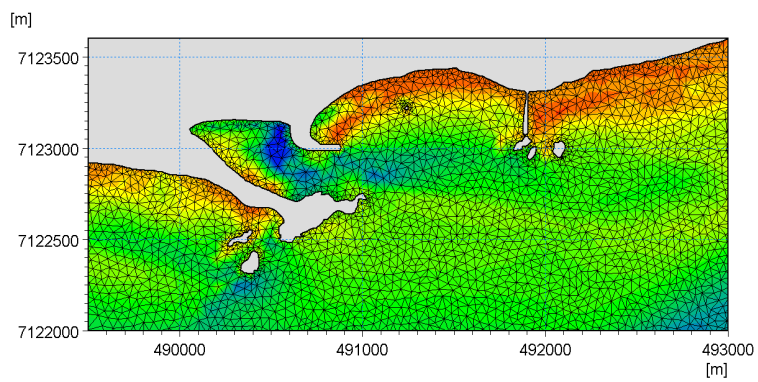
Figure 3.19: Close-up look at the mesh near the inlet entrance.

3.3.2 Littoral Drift

The Basic Profiles

The basic profiles considered in this thesis are 10 in total, 5 on either side of the ebb shoal, with 500 m intervals. Additional three were added at the ebb shoal with 250 m intervals marked with 'G' for Grynnsli. Those profiles are of special interest because of their location and the results from them was examined separately from the others. All profiles are shown in Fig. 3.20 and in enlarged figure in Appendix B.1.
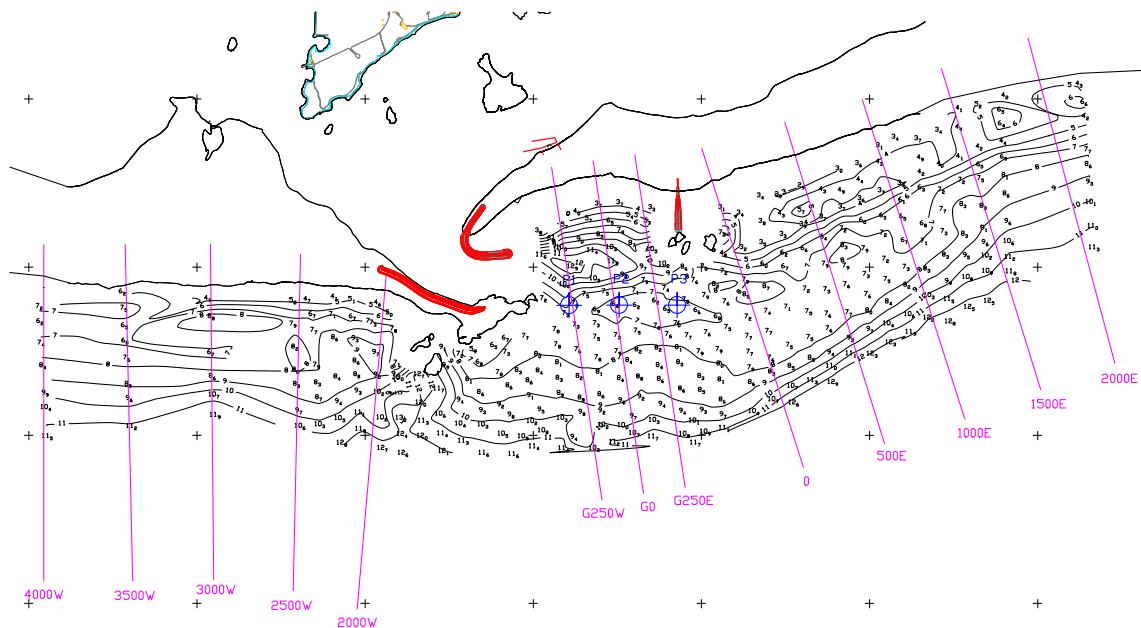
Figure 3.20: Overview of the profiles used in the sediment transport model. Profiles on the ebb shoal are marked with 'G' infront of their names.

The yearly sediment transport capacity for the 10 profiles, excluding the 'G' profiles, are shown in Table 3.4 with positive values indicating westward sediment transport and negative values indicating eastward transport. Net sediment transport capacity from previous research (from Table 1.1) is also shown for available profiles, they were situated at the same location but with slightly different coastline orientation (CO). Often sediment transport calculations are considered for several years like was done in previous study and covered 13 years. In this study however, the period of one year, from September 2013 to August 2014, was chosen because of interesting bathymetric surveys from same period showing unusually large sediment transport on the ebb shoal.

The gross sediment transport west and east of the tidal inlet ranges from approximately 500 thousand m^3 to 1,500 thousand m^3. As the profiles get closer to the ebb shoal the

gross sediment transport decreases, both west and east of the ebb shoal, not including profiles *2000W* and *0* which show abnormal results. The decrease in sediment transport on either side of the ebb shoal indicates that the sediment transport is being affected and sheltering from Hvanneyjarsker is the most probable explanation. In the east profiles the westward sediment transport capacity is approximately the same while the eastward transport capacity grows considerably further east. For a south-east wave direction the sheltering effects from Hvanneyjarsker are minimal and thus the small change in westward sediment transport capacity. However, for south-west wave directions the sheltering effects are noticeable as there is much more sediment transport in profile *2000E* than in profile *500E* where the wave height is smaller because of sheltering.

The areas on either side of the ebb shoal, west of Hvanny and east of Þinganessker, act as buffer zones where sediment aggregates at Hvanney for eastward wave direction and at Þinganessker for westward wave direction. If these areas would be enlarged somehow, e.g. proposal from professors Hans Hanson and Magnus Larsson, then the sediment transport at the ebb shoal due to offshore waves would decrease.

The sediment transport calculations show a rather large net transport towards west in profile *2000W* and is not in accordance to the profiles next to it which have transport of almost the same size in each direction. The eastward transport is around 100 thousand m^3 while the westward is around 500 thousand m^3. The direction of net sediment transport in profile *0* is similarly strange but less extreme. Sediment profiles *2000W* and *0* are shown in Appendix B.2.

The sediment model assumes that the beach is uniform in either direction and that the profile is orthogonal to coast and bathymetry. The deviation in profile *2000W* happened also in the previous study which indicates that the model assumption cannot be applied for that profile and in all likelihood not for profile *0* either. Profile *2000W* is next to the islands west of Hvanney and the bathymetry is non-uniform so it is difficult to locate the profile perpendicularly to coast and bathymetry. Same can be said for profile *0* which was located close to Þinganessker.

Table 3.4: *Yearly sediment transport capacity for the profiles in Fig. 3.20 and from previous research with positive values showing transport towards west and negative values showing transport towards east.*

	Prev. Res.			Sediment transport model			
	CO	Net	CO	Net	Gross	West	East
Profile	[°]	$\times 10^3 [\text{m}^3]$	[°]		$\times 10^3$ [m^3]		
4000W	180	-92	180	94	1436	765	-671
3500W	-	-	179	21	1078	549	-529
3000W	178	-141	179	-17	1034	508	-526
2500W	-	-	181	-2	884	441	-443
2000W	175	244	185	429	621	525	-96
0	164	-332	162	50	480	265	-215
500E	-	-	163	-35	426	196	-230
1000E	167	-93	162	-315	717	201	-516
1500E	-	-	163	-375	839	232	-607
2000E	153	-532	165	-667	1142	238	-904

Four of the profiles were chosen to represent the sediment transport on either side of the tidal inlet and hence the ebb shoal. They were profiles *3000W*, *2500W*, *1000E* and *1500E*, which were estimated far enough away from Hvanney and Þinganssker so that the sediment transport would not be affected. Their sediment distribution are shown in Fig. 3.21 and the wave rose plot for each of them is shown in Fig. 3.22. All sediment transport profiles are shown in Appendix B.2.

Based on these four profiles the gross sediment transport west and east of the tidal inlet was estimated between 700 and 1,000 thousand m^3. West of the inlet the westward and eastward transport was similar in volume while east of the tidal inlet the net transport was towards east and was estimated between 300 to 400 thousand m^3.

Figure 3.21 shows that sediment transport takes place at profile bars and closest to the coast, with the main portion of the transport taking place at low water depth close to the coast. The direction of the transport depends on the wave direction and profile orientation towards the coast.

The wave roses in Figures 3.22a and 3.22b, taken at a reference depth of 10 m, show the largest waves coming from south-west, south and south-east, mainly from south-west. Hence it would be a good guess to estimate the direction of the net transport to be towards east which was the case. Figure 3.22b and 3.22c on the other hand show the largest waves coming from south. In profiles *1000E* and *1500E* the net transport was large and coming from south with the profile orientation around 162° (see Fig. 3.20 and Table 3.4).

The orientation of the profiles in Fig. 3.21a and 3.21b is around 180° towards the coast and so the waves coming from south can result in either eastward or westward sediment transport. The difference between the westward transport and eastward transport was small in profiles *3000W* and *2500W* where the respective net transport was -17,000 m^3 and -2,000 m^3, i.e. towards east. However, further away from the tidal inlet in profiles *3500W* and *4000W* the net transport direction changes from east to west. The sensitivity of the coastal orientation was very high for these profiles, which is shown in Appendix B.3, and a change of -1° to -2° results again in net transport towards east. Wave roses for all profiles are shown in Appendix B.4.
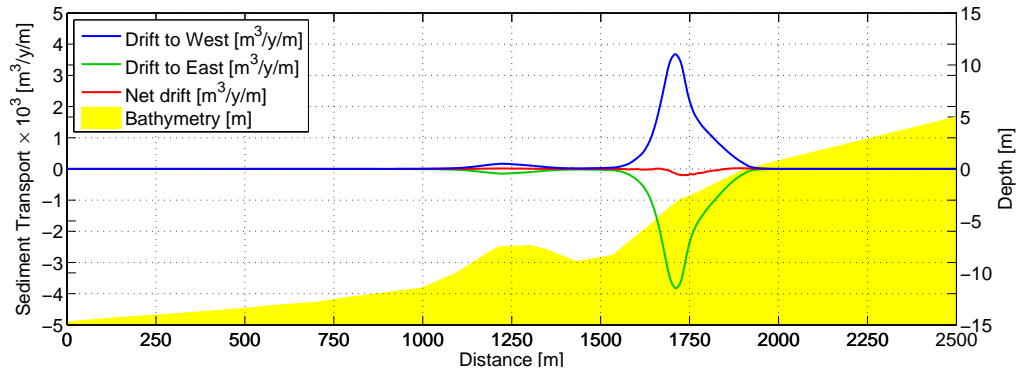
(a) Profile 3000W
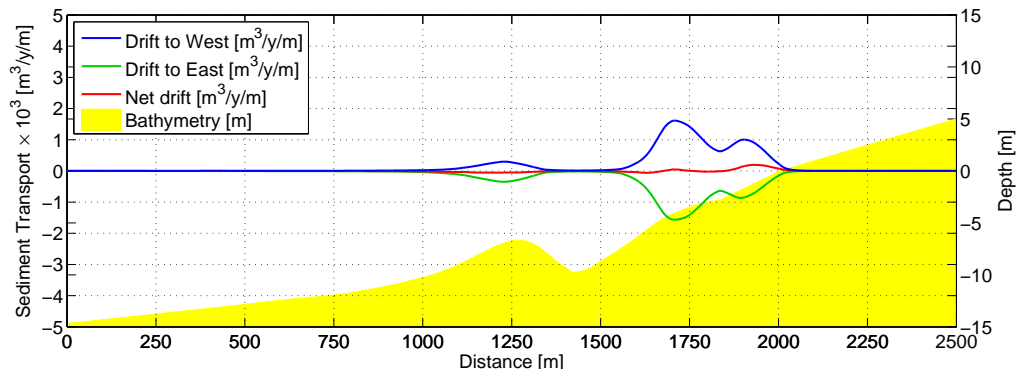
(b) Profile 2500W
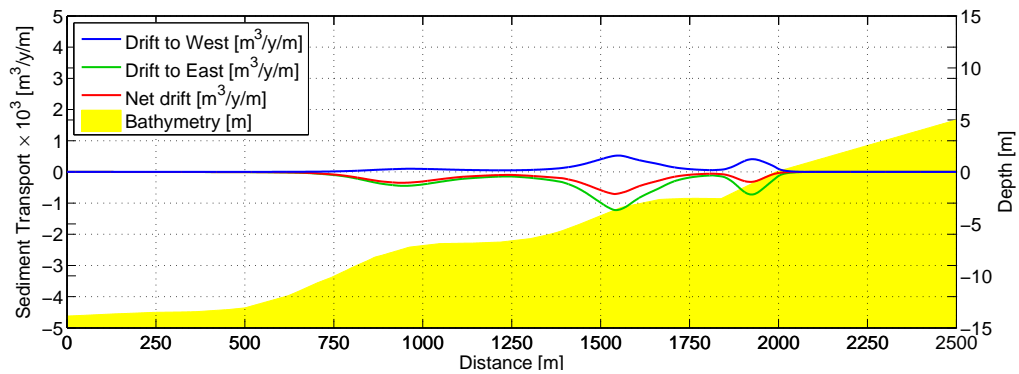
(c) Profile 1000E
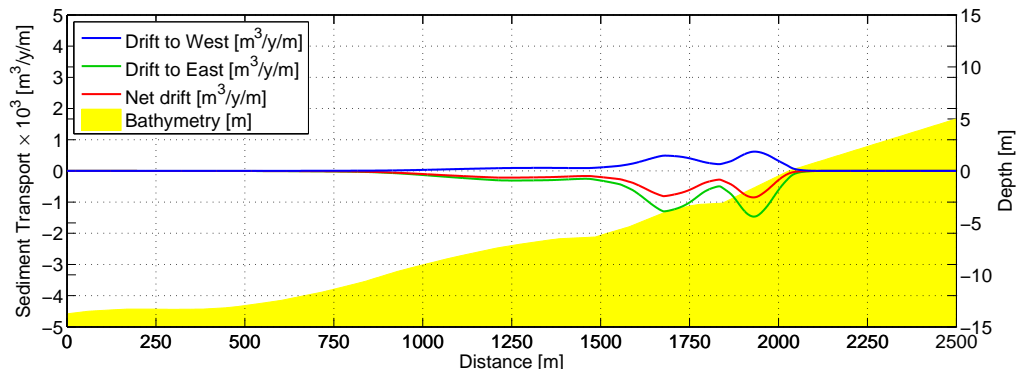
(d) Profile 1500E

Figure 3.21: Sediment transport for four of the profiles shown in Fig. 3.20

(a) Profile 3000W

(b) Profile 2500W

(c) Profile 1000E

(d) Profile 1500E
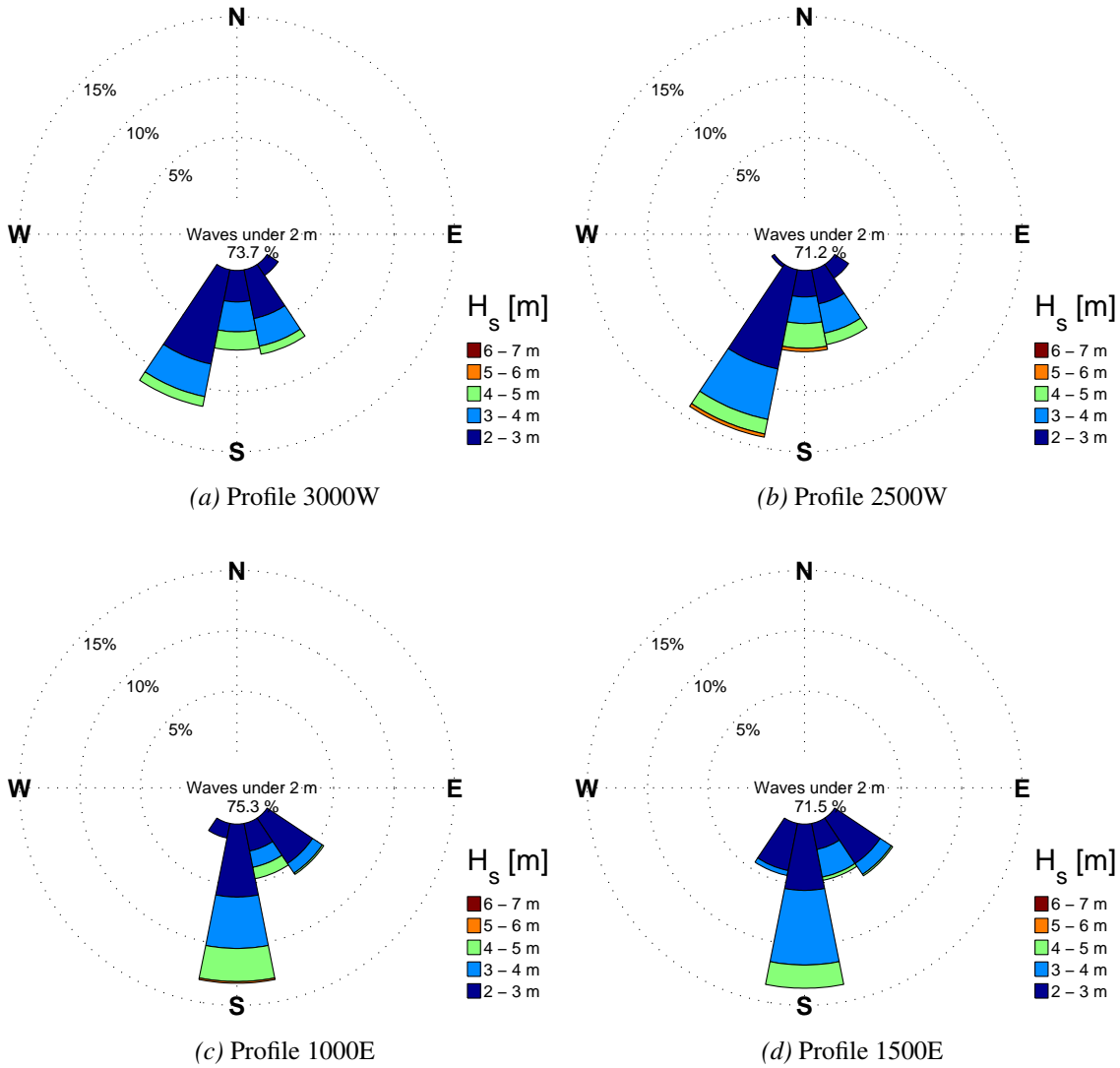
Figure 3.22: Wave roses for four of the profiles shown in Fig. 3.20

The sediment transport for each month was found for the 4 profiles in Fig. 3.23. It shows the westward, eastward and net transport for each month of the period that was considered. Figure 3.23 is based on the sediment transport calculations made with the sediment transport model. The largest transports occur on the period from November to March. In November, December and March the dominant direction of sediment transport is towards east but in January and February the dominant direction is towards west.

In the profiles west of the tidal inlet, *3000W* and *2500W*, the westward transport in January and February is two times larger than in the profiles east of the tidal inlet, *1000E* and *1500E*.

(a) Profile 3000W

(b) Profile 2500W

(c) Profile 1000E

(d) Profile 1500E
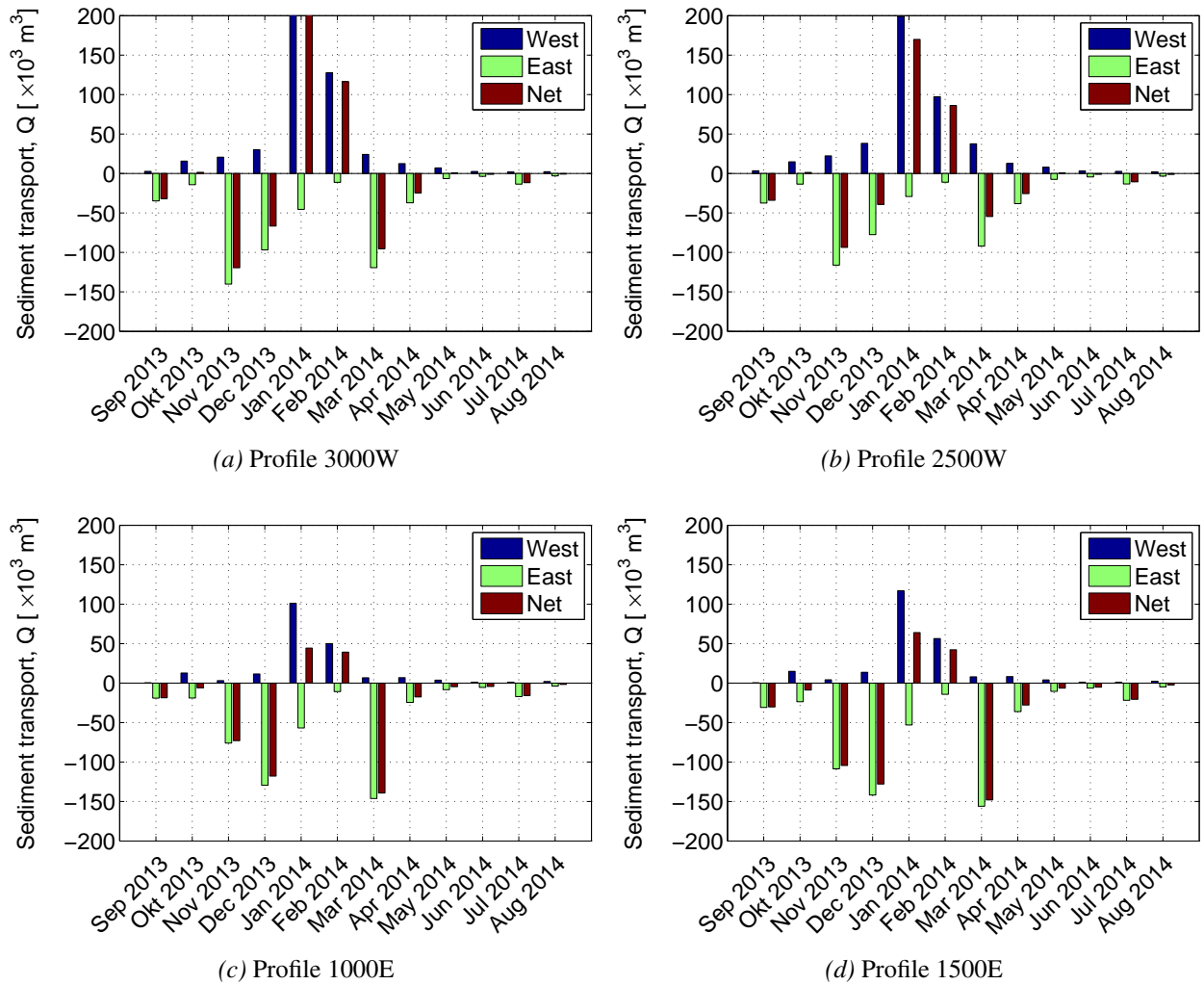
Figure 3.23: Westward, eastward and net sediment transport for each month in four of the profiles shown in Fig. 3.20.

According to Fig. 3.10a, which shows the actual sediment transport from late October to early February, large quantity of sediment aggregated at Þinganessker. This quantity was estimated as 300 thousand m^3 (see Section 3.2.1). The sediment transport calculations show the westward sediment transport capacity east of the tidal inlet (profiles *500E* to *2000E* in Table 3.4) to be between 200 and 240 thousand m^3 which is around 25% less than the actual sediment transport, but still of the same order of magnitude.

In March the south-east waves give way and the tidal flow clears sediment from the ebb jetty and Þinganessker. This is shown in Fig. 3.23c and 3.23d where the westward sediment transport in January and February drop to almost nothing in March and eastward sediment transport starts to dominate again.

Ebb Shoal Profiles

The profiles on the ebb shoal, which are marked with 'G' in their names in Fig. 3.20, are different from the most of the other 10 profiles. The assumption of infinitive coast doesn't apply for them since they are partially sheltered by both Hvanney and Þinganessker.

The model showed significant amount of sediment transported closest to the coast but in fact in this case it is next to nothing because the area closer to the beach is fixed between a jetty on the end of the East barrier and the groyne to Þinganessker.

In order to estimate the sediment transport the distribution in the profiles was cut off in the trough at 1,400 m, indicated by dotted line in Fig. 3.24.

The results from the sediment transport model for the three profiles on the ebb shoal are listed in Table 3.5. The gross sediment transport is around 30 thousand m^3 in all three profiles but the westward and eastward transport varies between them. The wave roses in Fig. 3.25 show the waves coming mostly from south and south-east, mainly south-east, in profiles *G0* and *G250E*. The three profiles are all oriented as 171° towards the coast. The waves in profile *G250W* are more coming from south than in the other two profiles and that explains the eastward direction of the net transport which is towards west in profile *G0* and *G250E*.

The coastline orientation was assumed as 171° and the reference depth was taken at 10 m water depth. The difference in westward and eastward transport probably stems from a combination of actual coastline orientation and reference depth of the profiles. However, all of them show a gross sediment transport around 30 thousand m^3 and this will be considered as the sediment transport on the ebb shoal due to offshore waves.

The dredging in 2005 showed that between 55 to 65 thousand m^3 of sediment transported back to the dredged channel in matter of months. If this amount is assumed to be the total yearly sediment transport at the ebb shoal, both from tidal flow and offshore waves, then the sediment transport that aggregates on the ebb shoal due to tidal flow current is between 25 and 35 thousand m^3.

Table 3.5: Sediment transport results for the ebb shoal profiles in Fig. 3.20 marked with 'G'.

Profile	CO [°]	Net	Gross	West	East
		×10³ [m³]			
G250W	171	-12	31	10	-21
G0	171	4	31	17	-14
G250E	171	18	29	23	-6
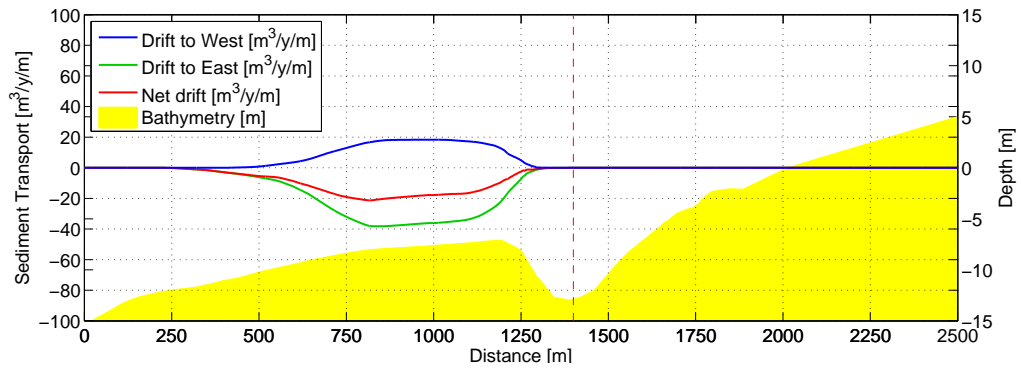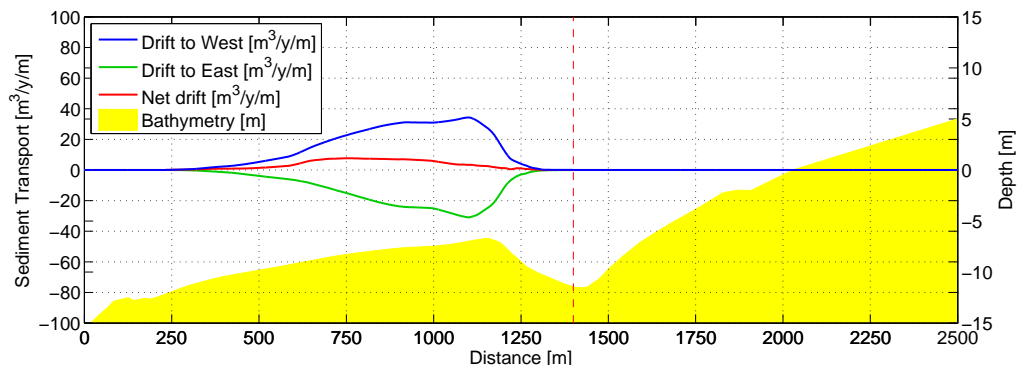
(a) Profile G250W
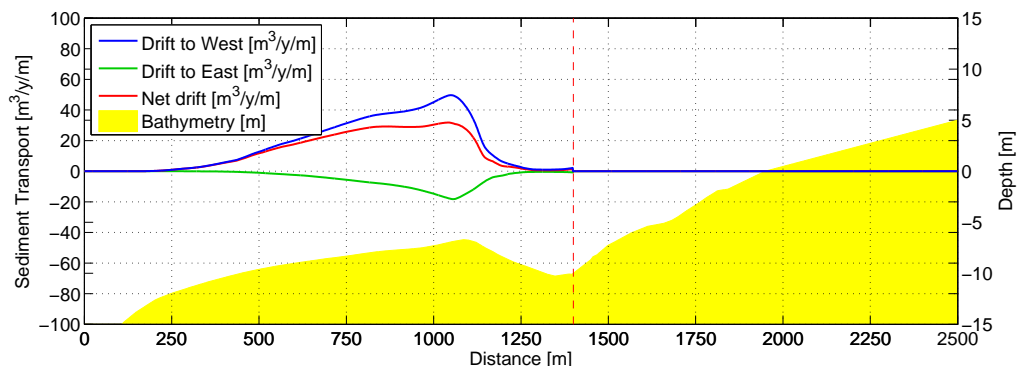
(b) Profile G0

(c) Profile G250E

Figure 3.24: Sediment transport for the profiles at the ebb shoal shown in Fig. 3.20 marked with 'G'.

(a) Profile G250W

(b) Profile G0

(c) Profile G250E
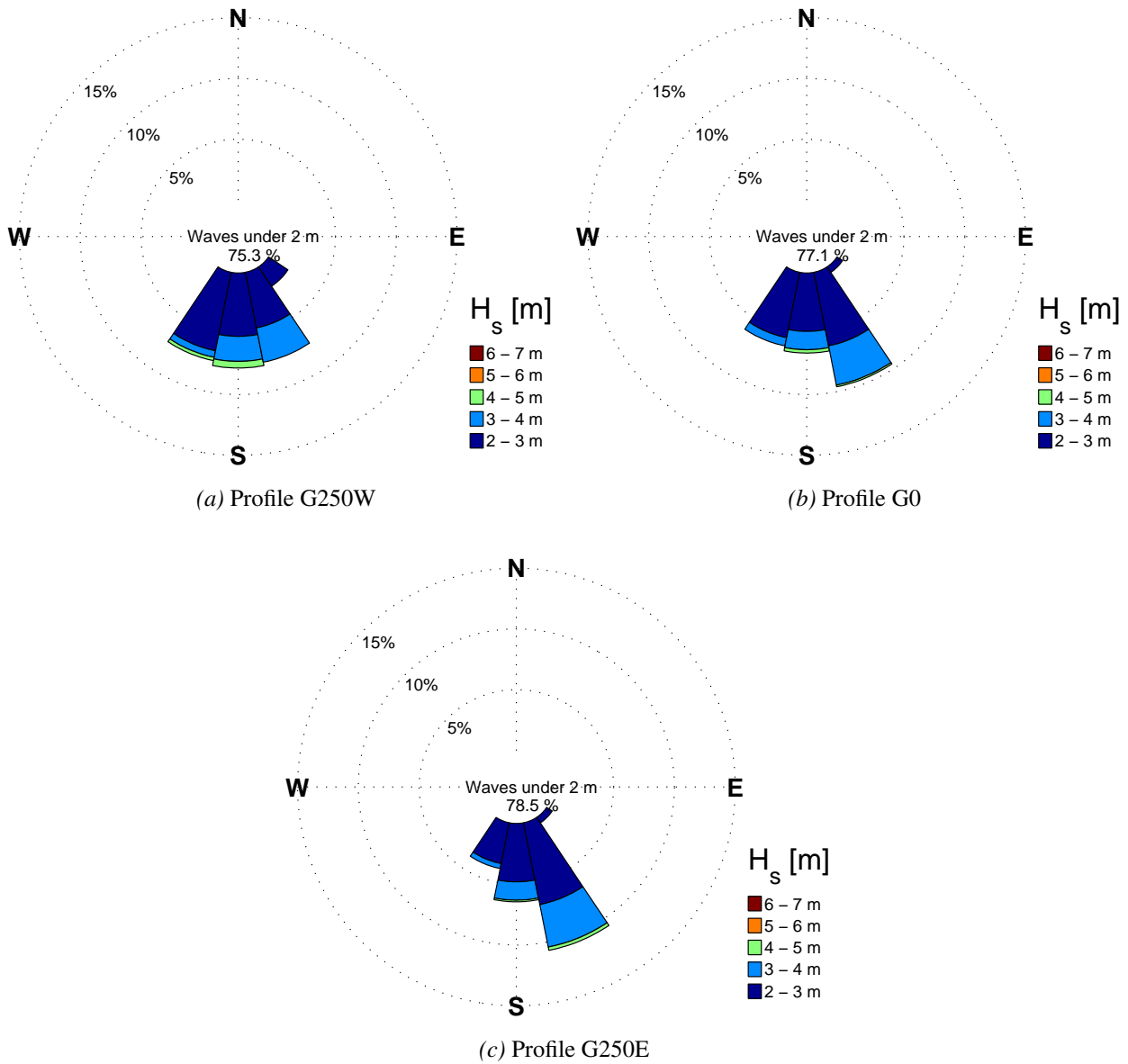
Figure 3.25: Wave roses for the profiles at the ebb shoal shown in Fig. 3.20 marked with 'G'.

Sensitivity Analysis

Some factors which are roughly estimated can change the results from the sediment transport model drastically. Therefore it is necessary to perform sensitivity analysis on factors such as coastline orientation, slope towards coast, mean grain size and reference depth. For this purpose one of the profiles, *1500E*, was chosen as an example.

The profiles in Fig. 3.20 were positioned so they are oriented perpendicularly to the coast. Figure 3.26 and Table 3.6 show the change in sediment transport in profile *1500E* for coastline orientation varying between -10° and +10°. The sediment transport was extremely sensitive to coastline orientation, e.g. a small change in orientation such as ±5° showed between 20 and 30% change for westward and eastward sediment transport in profile *1500E*. Hence it was thought necessary to make a sensitivity analysis of coastline orientation for all the profiles. They are shown in Appendix B.3 both tabulated and as plots.
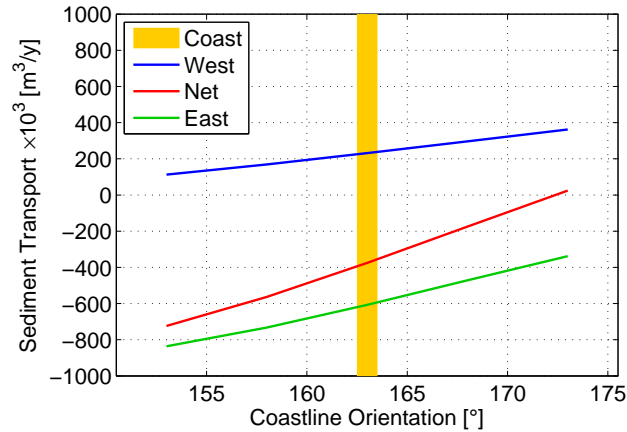

Figure 3.26: Sensitivity analysis plot of coastline orientation (CO) for profile 1500E.

Table 3.6: Tabulated sensitivity analysis of coastline orientation (CO) for profile 1500E.

	1500E				
	Coastline orientation [°]				
	153	158	163	168	173
	Sediment transport				
Gross	113%	107%	100%	92%	83%
West	48%	73%	100%	128%	156%
East	138%	121%	100%	78%	56%

The bathymetric surveys do not cover the area that is closest to the coast, where the water depth is small and actually where most of the sediment transport takes place. The water depth in the profiles where the survey ends varies between profiles from approximately -2 m down to -4 m. A slope up towards the chart datum was assumed in the profiles between 1:50 and 1:60. In Table 3.7 the sediment transport for slopes between 1:10 and 1:100. The steeper the slope the more sediment transport occurs.

According to the coastal profile classification (see Section 1.2.1) the gross sediment transport should not be much larger than 1 million m^3 which excludes slopes steeper than 1:30. There is not great difference in sediment transport between slopes 1:40 to 1:80 so assumed slopes of 1:50 to 1:60 for the profiles seems to be a good estimation for them.

Table 3.7: Sensitivity analysis of coast slope for profile 1500E.

1500E				
	Sediment transport model			
	Net	Gross	West	East
Slope	Change [%]			
1:10	269%	255%	245%	259%
1:15	221%	211%	202%	214%
1:20	179%	172%	166%	174%
1:30	134%	130%	128%	131%
1:40	114%	113%	112%	113%
1:50	105%	105%	104%	105%
1:60	100%	100%	100%	100%
1:80	95%	95%	95%	95%
1:100	92%	92%	93%	92%

A small change in the size of the sediment grains can cause a large change in sediment transport. Most often the mean grains size is considered as 0.25 mm and that size was assumed in the sediment transport model. The sediment coming from the tidal inlet is glacial till and therefore probably larger than 0.25 mm. Table 3.8 shows that if the grain size is increased up to 0.3 mm the gross sediment transport drops 15% (in profile *1500E*). Therefore it is important to have accurate sediment grain size.

Table 3.8: Sensitivity analysis of grain size for profile 1500E.

1500E				
	Sediment transport model			
Grain size	Net	Gross	West	East
[mm]	Change [%]			
0.20	162%	153%	147%	156%
0.25	100%	100%	100%	100%
0.30	83%	86%	88%	85%
0.40	77%	83%	87%	81%

The reference depth is the depth of the location in a profile where data are extracted for wave climate input file for *Litdrift*. The data extracted are applied to the whole profile in reference.

The closure depth, which is the depth where sediment transport starts to take place, was calculated with Eq. (2.35), for $H_{s,12h} = 5.5$ m and $T_s = 9.0$ s, as $d_c = 12.5$ m. Data from the wave buoy south of Hvanneyjarsker were used in finding the $H_{s,12h}$.

Table 3.9 shows sediment transport for varying reference depth. The reference depth of

-15 m is larger than the closure depth which explains the deviation from the other considered reference depths. For a 2 m change in the reference depth the gross sediment transport either decreases or increases of more than 25% (in profile *1500E*). There is minimal change in the westward transport but almost around 40% for the eastward transport, which can be explained by the sheltering effects from Hvanneyjarsker. If there is a large variability in wave height or direction along the profile then the reference depth is important.

The reference depth in profile *1500E* is located approximately in in the center of the profile according to Fig. 3.20 which is a good location to take the reference depth since the data taken from there are distributed over the whole profile. The location of the reference depth is not in the center of all the profiles considered but in the 4 profiles considered before (*3000W*, *2500W*, *1000E* and *1500E*) it is.

Table 3.9: Sensitivity analysis of reference depth for profile 1500E.

1500E				
	Sediment transport model			
Refr. depth	Net	Gross	West	East
[m]	Change [%]			
-8	34%	71%	101%	60%
-10	100%	100%	100%	100%
-12	163%	126%	96%	137%
-15	122%	113%	106%	116%

For the ebb shoal the sensitivity of reference depth location is shown in Tables 3.10 and 3.11. The gross sediment transport decreases about 30% for 2 m decrease in reference depth but increases only about 10% for 2 m increase in reference depth. The eastward transport decreases about 20 to 25% no matter whether there is increase or decrease in reference depth while the westward transport decreases and increases about 40 to 45% for respective changes in reference depth.

Table 3.10: Sensitivity analysis of reference depth for profile G0 *on the ebb shoal.*

G0				
	Sediment transport model			
Refr. depth	Net	Gross	West	East
[m]	$\times 10^3$ [m^3]			
-8	0.3	20.5	10.4	-10.1
-10	3.8	30.8	17.3	-13.5
-12	15.6	34.6	25.1	-9.5

Table 3.11: Sensitivity analysis of reference depth for profile G0 *on the ebb shoal.*

G0				
	Sediment transport model			
Refr. depth	Net	Gross	West	East
[m]	Change [%]			
-8	8%	67%	60%	75%
-10	100%	100%	100%	100%
-12	411%	112%	145%	70%

The sediment transport calculations above show that the sediment transport at the ebb shoal due to offshore waves is around 30 thousand m^3 which is considerably less then in the areas on either side of it (see profiles *3000W*, *2500W*, *1000E* and *1500E*). Sediment aggregation at the ebb shoal due to tidal flow was estimated between 25 and 35 thousand m^3 for the assumption of total sediment transport between 55 and 65 thousand m^3.

Dredging was performed at the ebb shoal in 2005 and filled up in matter of months so it was clear that regular dredging would not be feasible unless the sediment transport could be reduced. Ebb shoal volume calculations indicated that the sediment transport due to tidal flow will decrease with relative land rise and the sediment transport due to offshore waves could be reduced with a jetty from Hvanney to Einholtsklettar (see proposal in Section 1.2.2) making regular dredging a realistic option.

The calculations of sediment transport capacity is an estimation which depends on several uncertain factors such as coastline orientation, coast slope, grain size and location of reference depth. A small change in one of these factors can show from 15% up to 30% change in gross sediment transport capacity, which is well worth to bear in mind.

4 Conclusions

The main objective was to estimate the sediment transport on the ebb shoal of Hornafjörður tidal inlet with regards to water depth on the ebb shoal and relative land rise.

Classification of the tidal inlet yielded contradictory results. It was expected beforehand that the inlet would be wave dominated since that is how the coast of Iceland is commonly classified. The classifications by shape and Hayes method showed the tidal inlet at Hornafjörður to be wave dominated with large tidal energy acting also upon it. The recently developed method by Nielsen & Thuy showed it to be tidal dominated, but as it is fairly recent it has not been used much elsewhere than in Australia. A number of reasons could explain this contradiction, such as difference in sediment type, sheltering from Hvanne-jarsker reefs or simply that the method is biased for smaller tidal forces. It is clear from bathymetric surveys that the wave and tidal forces are both strong at Hornafjörður tidal inlet but that the the wave force is perhaps slightly stronger and hence the classification: "Mixed Energy (wave dominated)".

The bathymetric surveys showed that during summertime the tidal flow clears the tidal inlet ebb jetty of sediments and in contrast during wintertime the strong waves break on the ebb shoal and seek to fill it up again. Seasonal variation of water depth on the ebb shoal was detected, at least in point P1 closest to Hvanney (see Fig. 2.3), which indicates that the wave effects were significant on the ebb shoal.

The ebb shoal water depth was calculated with regards to wave height and tidal prism as 7.0 m, which is a good estimate since the water depth at the ebb shoal is usually between 7.0 and 7.5 m. A relative land rise would cause a decrease in tidal prism, which had been estimated to be a decrease of 35% and 66% for respective 0.5 and 1.0 m land rise. This may possibly cause a 10% and 24% respective decrease in ebb shoal water depth. The decrease in tidal prism also decreases the ebb shoal volume which was calculated about 27 million m^3 and could decreases about 39% and 70% for respective 0.5 and 1.0 m relative land rise. This indicated that there would not necessarily be a water depth decrease on the ebb shoal for a relative land rise.

Sediment transport on the ebb shoal is twofold. There is sediment transport due to the tidal flow and the offshore waves. The tidal flow has been seen to move sediments up to 300 thousand m^3 from the ebb jetty but the sediments that aggregate on the ebb shoal due to the tidal flow is only a fraction of that. Dredging on the ebb shoal performed in 2005

showed that 55 to 65 thousand m^3 of sediment aggregated on the ebb shoal. It would be logical, to assume that to be the total amount of sediment aggregating on the ebb shoal annually.

Professor Hans Hanson and professor Magnus Larsson proposed a jetty from Hvanney towards south-west connecting to Einholtsklettar. This would increase the size of the buffer zone west of the ebb shoal and hence decrease the sediment transport from west towards the ebb shoal where it would settle instead at the new jetty at Hvanney. This decrease in sediment transport would make regular dredging at the ebb shoal a realistic future option, but further research of desired water depth would be required for that decision.

The gross sediment transport on either side of the ebb shoal was estimated between 700 and 1,000 thousand m^3 due to waves. The calculations showed a decrease in transport capacity as the profiles got closer to the ebb shoal, which indicates some sheltering in the transport, most probably due to sheltering from Hvanneyjarsker. The areas on either side of ebb shoal act as buffer zones where the sediment aggregates at Hvanney for eastward wave direction and at Þinganessker for westward wave direction. The sediment transport on the ebb shoal itself was estimated as 30 thousand m^3 per year. The aggregation on the ebb shoal due to tidal flow current would then be between 25 to 35 thousand m^3.

The sediment transport calculations are rather sensitive to various uncertain factors such as coastline orientation, grain size and reference depth. Those factors were estimated to the best of ability, but a slight change can cause a large difference in sediment transport capacity.

References

Andersen, O. H. and Fredsøe, J. (1983). Transport of suspended sediment along the coast. *Progress Repor No. 59, ISVA, Technical University of Denmark*.

Arnason, T. (2015). Thorri Photo/Film. URL: http://www.facebook.com/ThorriPhotoFilm/.

Asgrímsdóttir, S. R., Sigurðarson, S., and Viggósson, G. (2014). Hornafjarðarós: Rannsóknir á Grynnslunum utan við Hornafjarðarós og áhrif á siglingar. Technical report, Icelandic Road and Coastal Administration (Vegagerðin).

Bruun, P. (1967). *Tidal Inlets and Littoral Drift*, volume 2. Universitetsforlaget.

Bruun, P., Viggósson, G., and Sigurðarson, S. (1991). Influence of ice covers, tidal prism of tidal inlets. Hornafjörður, Iceland. *11th International Conference on Port and Ocean Engineering under Arctic Conditions. St. John's, Canada*.

Buonaiuto, F. S. and Kraus, N. C. (2003). Limiting slopes and depths at ebb-tidal shoals. *Coastal Engineering*, 48:51–65.

de Swart, H. E. and Zimmerman, J. T. F. (2009). Morphodynamics of tidal inlet systems. *Annual Review of Fluid Mechanics*, 41:203–229.

de Vriend, H. J., Dronkers, J., Stive, M. J. F., van Dongeren, A., and Wang, Z. B. (1999). Coastal inlets and tidal basins. *Lecture Notes. TU Delft, Delft*.

Deigaard, R., Fredsøe, J., and Hedegaard, I. B. (1986). Mathematical model for littoral drift. *Journal of Waterway, Port, Coastal and Ocean Engineering, ASCE*, 112(3):351–369.

DHI (2011). *LITDRIFT: Longshore Current and Littoral Drift User Guide*. DHI Water and Environment.

DHI-Group (2014). *MIKE 21 SW: Spectral Waves User Guide*. Danmarks Hydrologiska Institut.

ECMWF (2015). European Centre for Medium-Range Weather Forecasts. URL: http://www.ecmwf.int/.

REFERENCES

Engelund, F. and Fredsøe, J. (1976). A sediment transport model for straight alluvial channels. *Nordic Hydrolgy*, 7(5):293–306.

Fenton, J. D. and McKee, W. D. (1991). On calculating the length of water waves. *Coastal Engineering*, 14(6):499–513.

Floyd, C. D. (1968). River mouth training in New Souh Wales, Aust. *Coastal Engineering, ASCE*, 1(11):1267–1281.

Fredsøe, J., Andersen, O. H., and Silberg, S. (1985). Distribution of suspended sediment in large waves. *Journal of Waterway, Port, Coastal and Ocean Engineering, ASCE*, 111(6):1041–1059.

Fredsøe, J. and Deigaard, R. (1992). *Mechanics of Coastal Sediment Transport*, volume 3. World Scientific.

Gunnarsson, H. G. and Pálmarsson, S. (2014). Mat á áhrifum landriss í Hornarfirði á sjávarfallaprisma Hornafjarðaróss. Technical report, Vatnaskil.

Hallermeier, R. J. (1981). A profile zonation for seasonal sand beaches from wave climate. *Coastal Engineering*, 4:253–273.

Hayes, M. O. (1979). Barrier island morphology as a function of tidal and wave regime. In Leatherman, S. P., editor, *Barrier Islands: From the Gulf of St. Lawrence to the Gulf of Mexico*, pages 1–28. Academic Press, New York.

Jóhannesson, T. and Ófeigsson, B. G. (2014). Landris við Höfn í Hornafirði og afstæðar sjávarstöðubreytingar. Technical report, Veðurstofa Íslands.

já.is (2015). Kort. URL: http://www.ja.is/kort/.

Jonsson, I. G. and Carlsen, N. A. (1976). Experimental and theoretical investigations in an oscillatory turbulent boundary layer. *Journal of Hydraulic Research*, 14(1):45–60.

Kraus, N. C. (2010). Engineering of tidal inlets and morphologic consequences. In Kim, Y. C., editor, *Handbook of coastal and ocean engineering*, pages 867–900. World Scientific, Los Angeles, USA.

Madsen, H. (2007). *Time Series Analysis*. Chapman & Hall/CRC.

MATLAB (2013). *MATLAB Toolboxes Release 2013a*. The MathWorks, Inc., Natick, Massachusetts, United States.

MOGT (2015). Veðurupplýsingakerfi - Höfn í Hornafirði. URL: http://www.mogt.is/.

Nielsen, P. (2009). *Coastal and Estuarine Processes*, volume 29. World Scientific.

Nielsen, P., Thuy, V. T. T., and Gallaghan, D. P. (2014). Morphology of coastal lagoon entrances: waves versus tides. *Coastal Engineering*, (34).

O'Brien, M. P. (1969). Equilibrium flow areas of tidal inlets on sandy beaches. *Journal of the Waterways and Harbors Divison, ASCE*, pages 43–52.

PIANC (2014). *Countries in Transition (CiT): Coastal Erosion Mitigation Guidelines*. PIANC, CoCom WG123, Brussels.

Swart, D. H. (1974). *Offshore Sediment Transport and Equilibrium Beach profiles*. Number 131. Delft Hydraulics Laboratory, Delft University, 6th edition.

Tryggvason, G. S. (2015). Úrvinnsla sjávarborðsmælinga frá Hornafiriði, Grindavík og Landeyjahöfn. Technical report, Vegagerðin.

Viggósson, G. and Sigurðarson, S. (2000). Hornafjarðarós: Rannsóknir á Siglingaleið um Hornafjarðarós. Technical report, Icelandic Maritime Administration.

Walton, T. L. and Adams, W. D. (1976). Capacity of inlet outer bars to store sand. *Coastal Engineering, ASCE*, (15):1919–1937.

Wang, Z., Hoekstra, P., Ridderinkhof, H., de Swart, H. E., and Stive, M. (2012). Morphodynamics of the Wadden Sea and its barrier island system. *Ocean and Coastal Management*, 68:39–57.

Wu, C. and Thornton, E. (1986). Wave numbers of linear progressive waves. *Journal of Waterway, Port, Coastal and Ocean Engineering, ASCE*, 112(4):536–540.

Zyserman, J. and Fredsøe, J. (1994). Data analysis of bed concentration of suspended sediment. *Journal of Hydraulics Engineering, ASCE*, 120(9):1021–1042.

A Bathymetry

This Appendix includes 15 bathymetric surveys performed between 2009 and 2014 and 10 various bathymetric difference planes.

A Bathymetry

A.1 Bathymetric Surveys
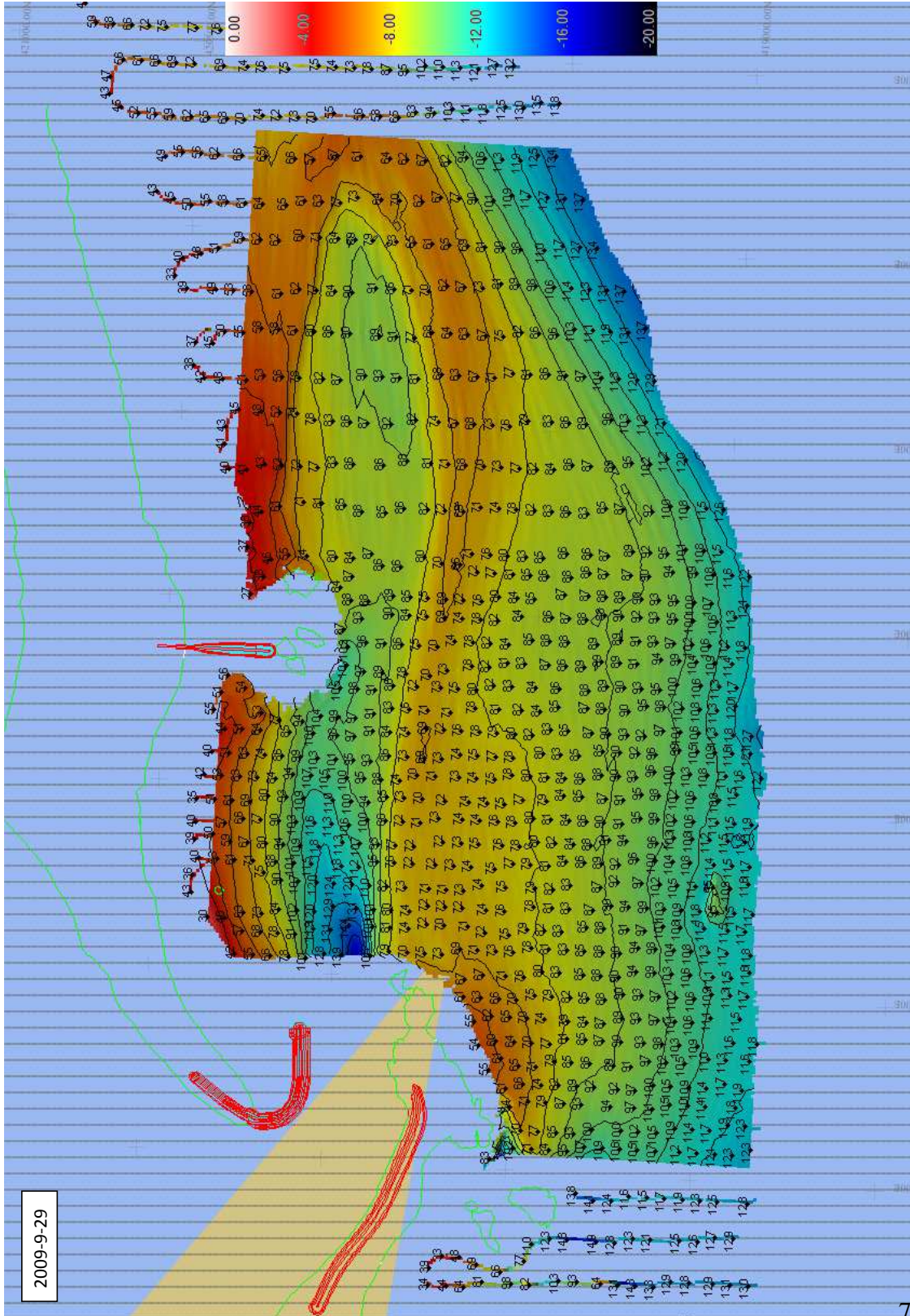
Figure A.1: 2009-09-29
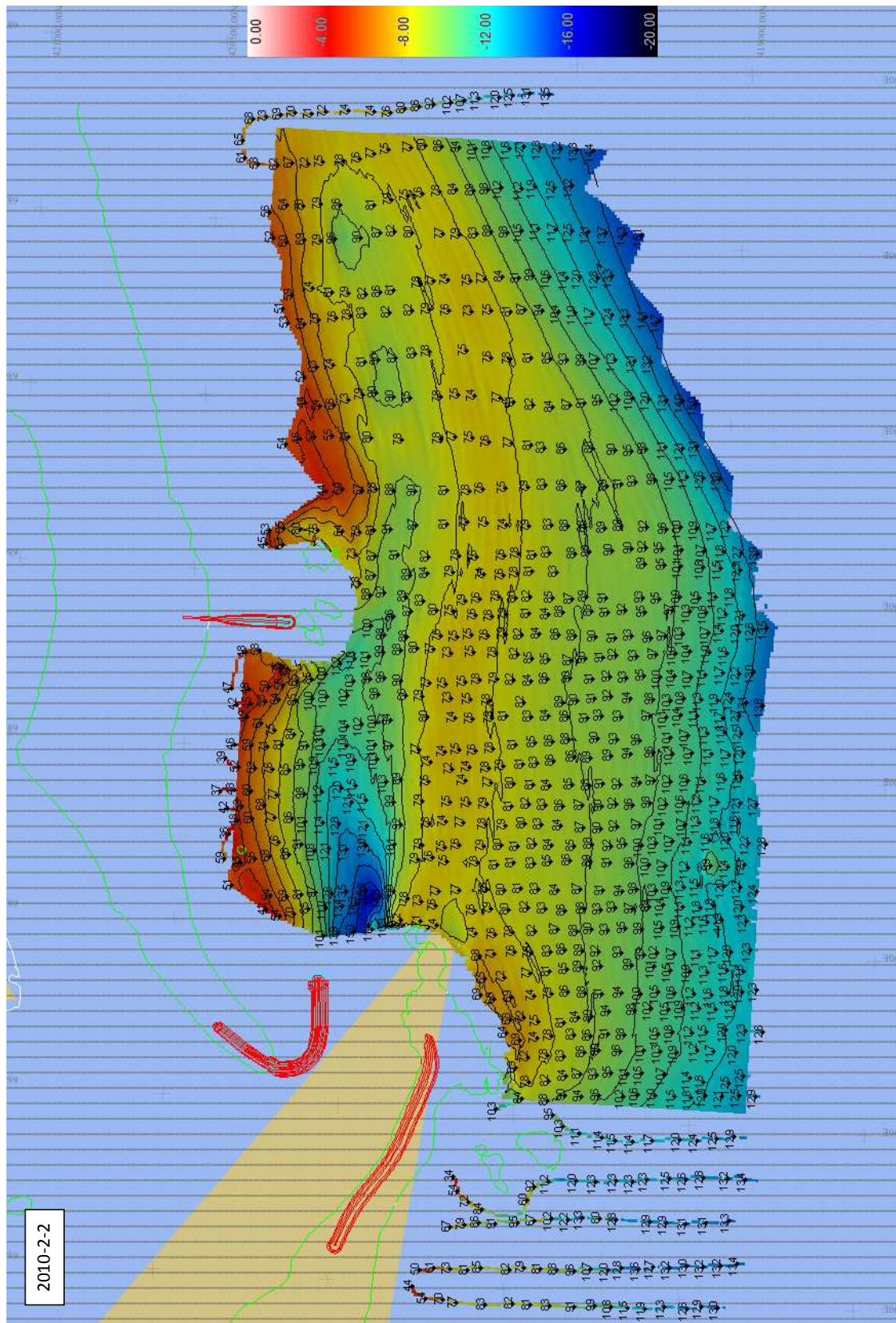
Figure A.2: 2010-02-02
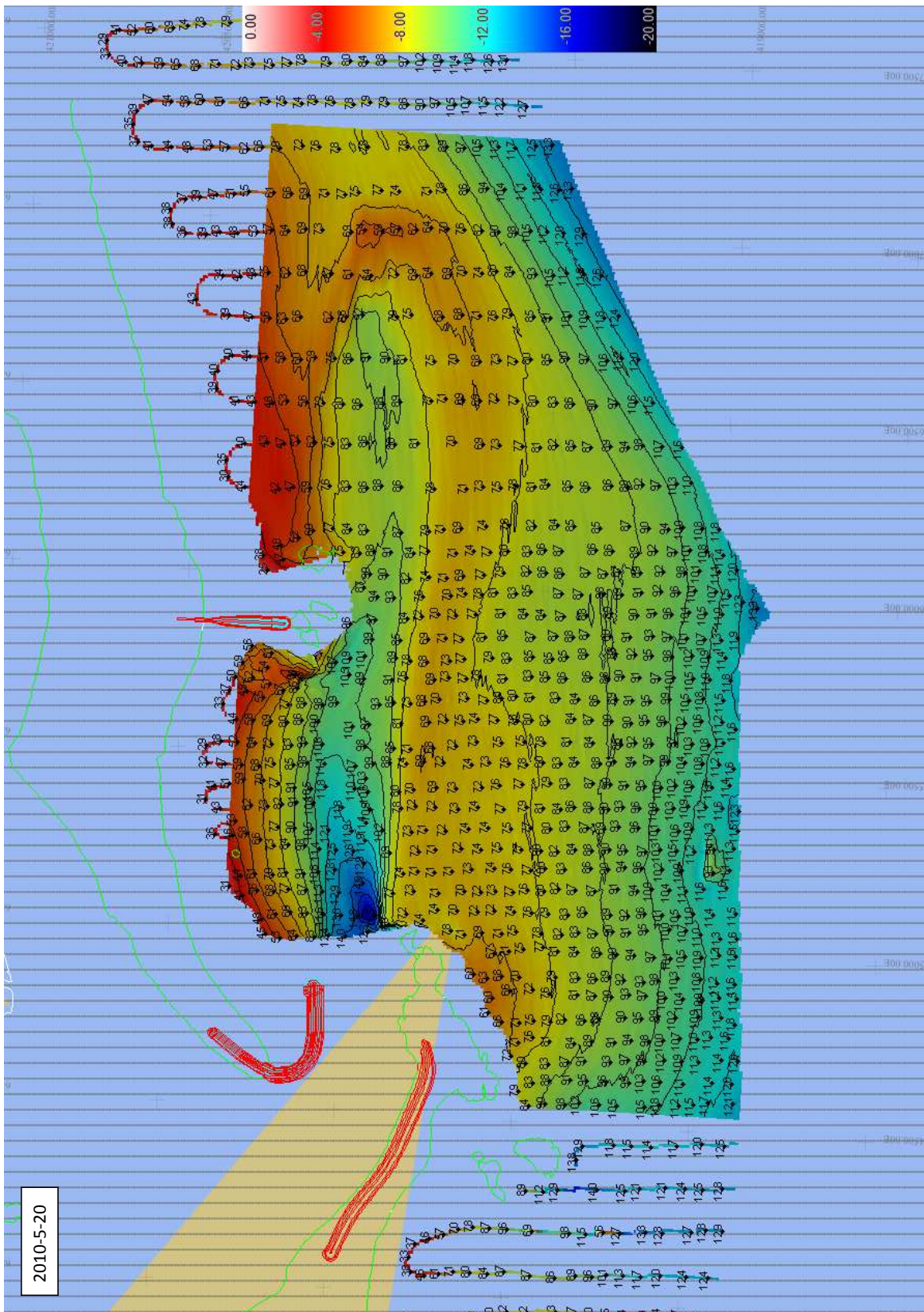
Figure A.3: 2010-05-20
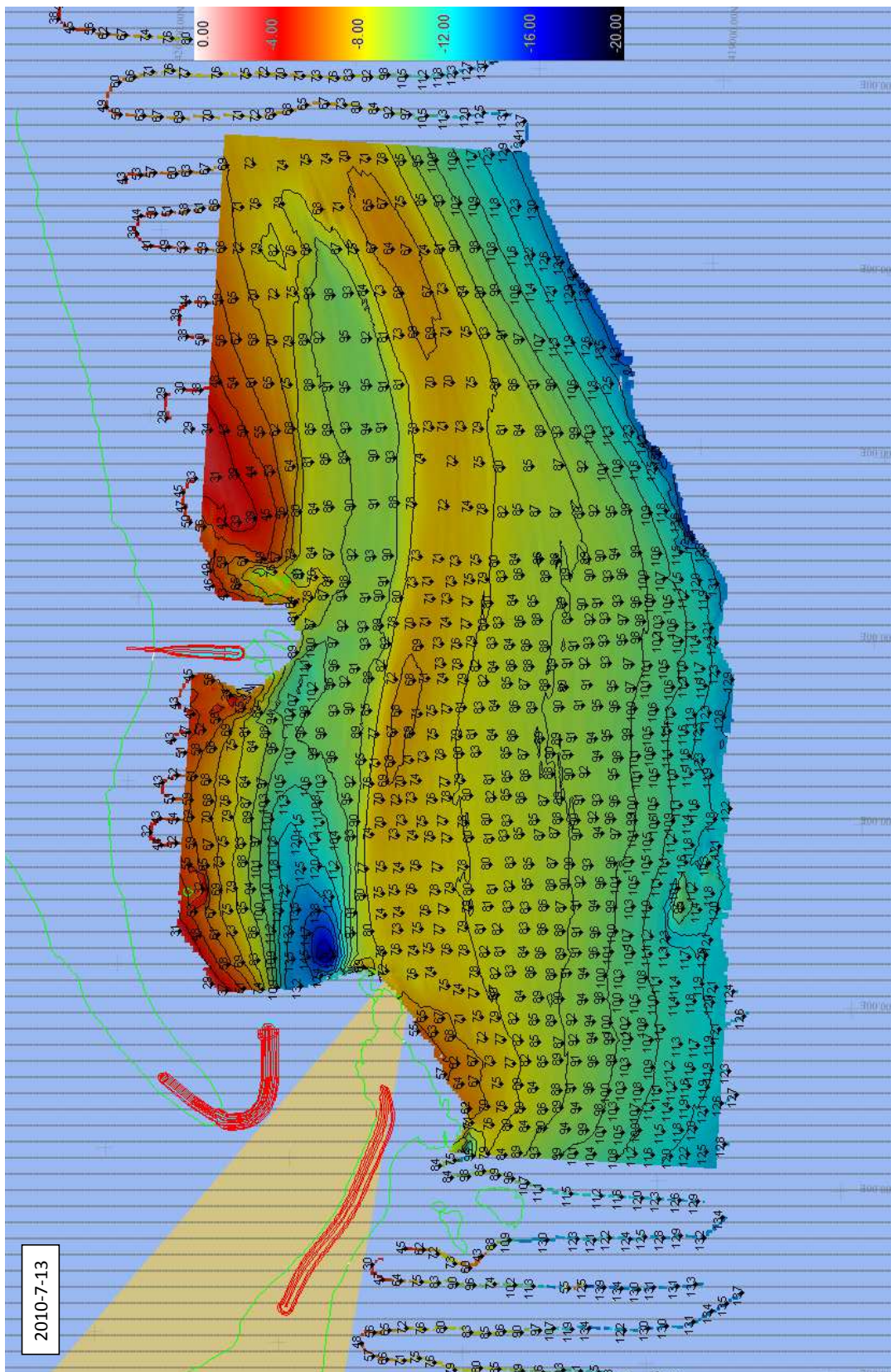
Figure A.4: 2010-07-13
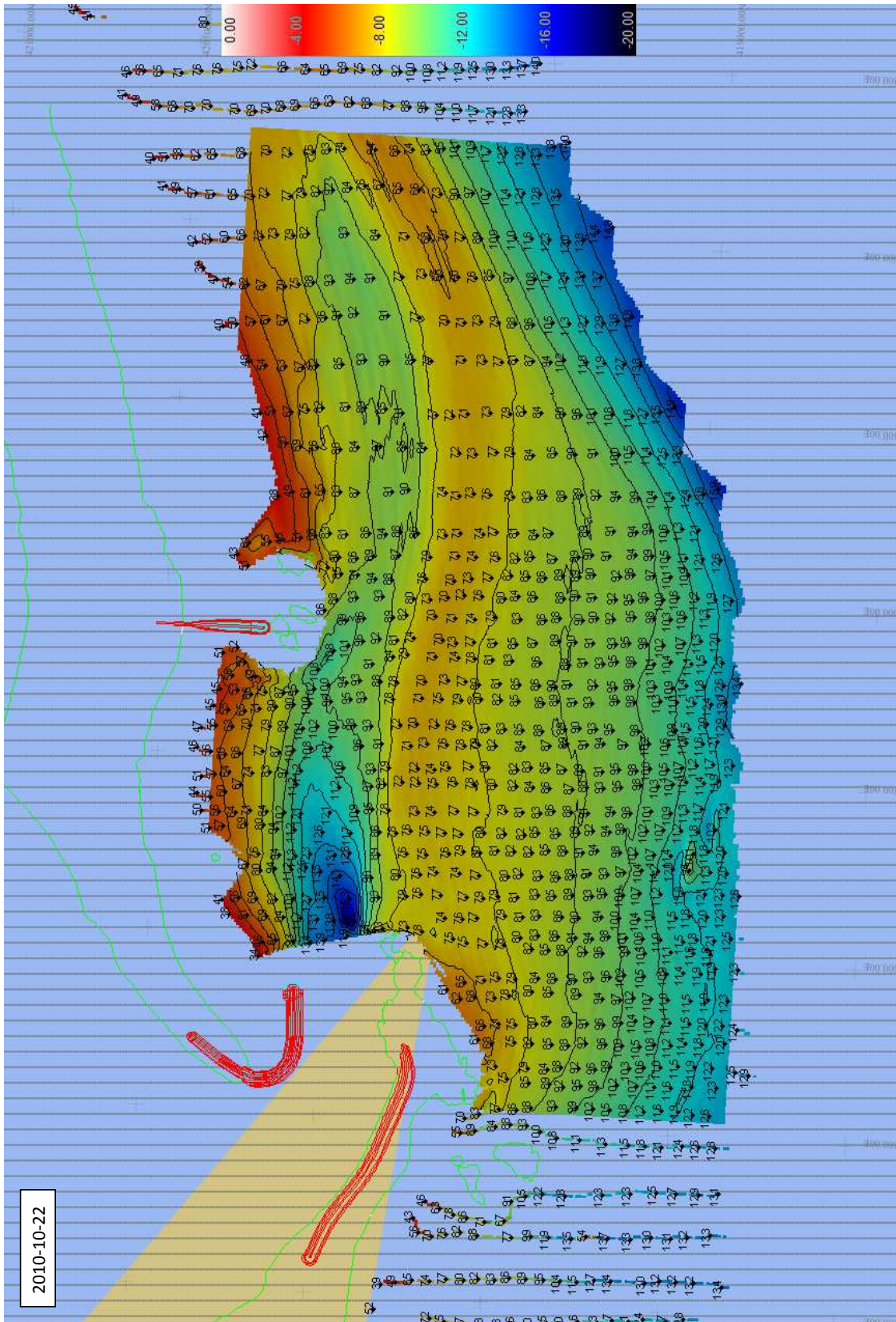
Figure A.5: 2010-10-22

76
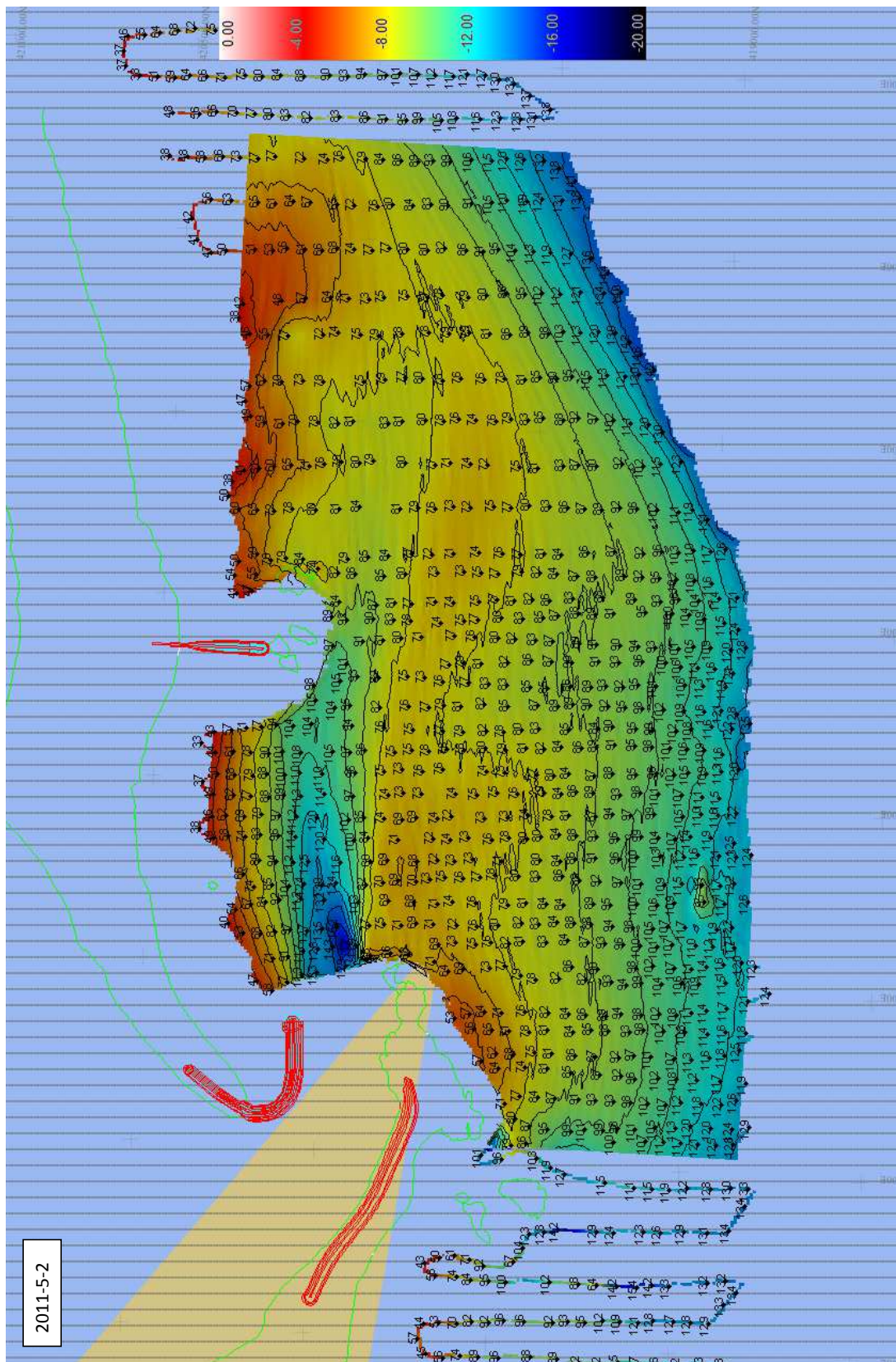
Figure A.6: 2011-05-02
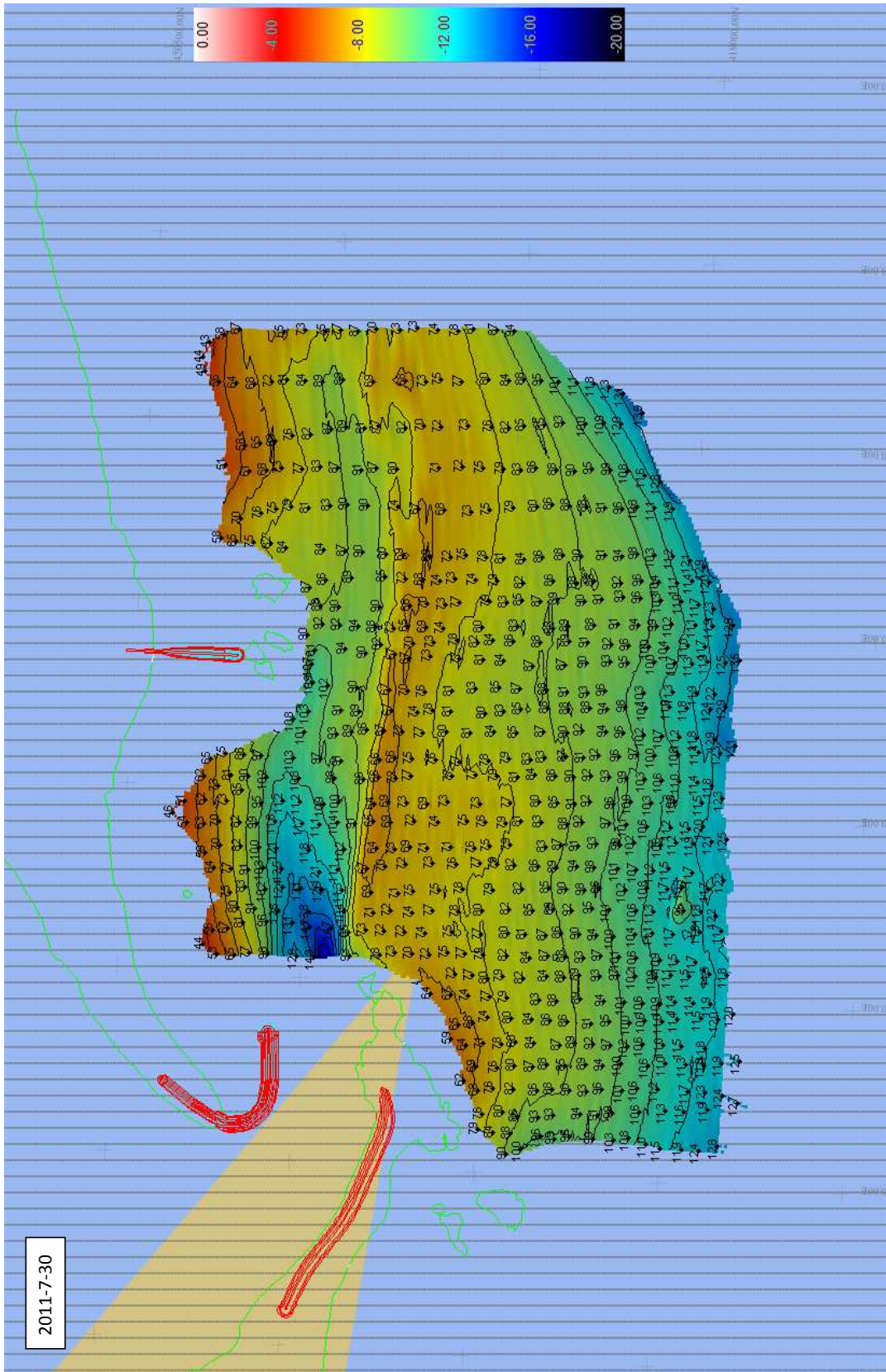
Figure A.7: 2011-07-30
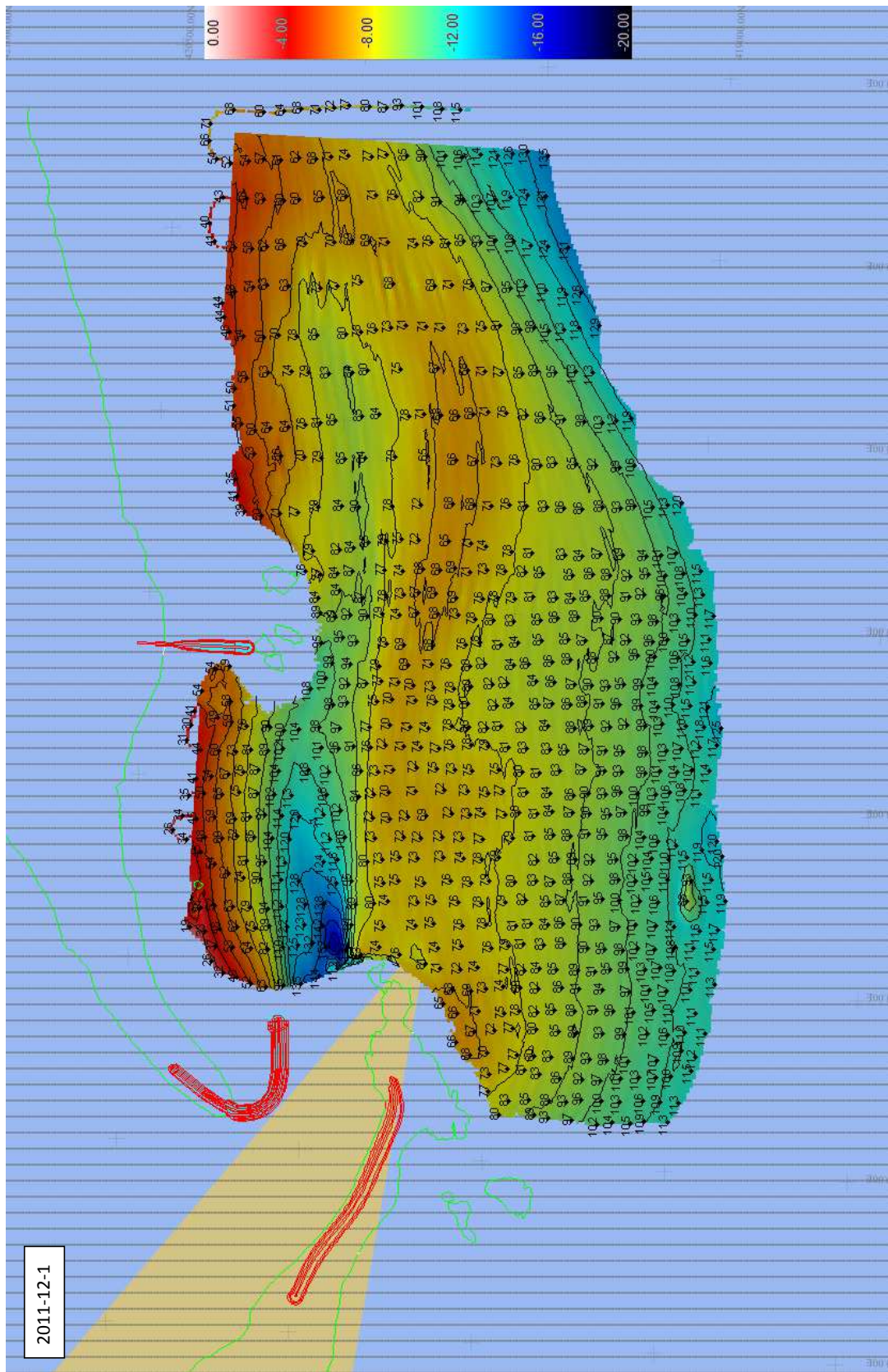
Figure A.8: 2011-12-01
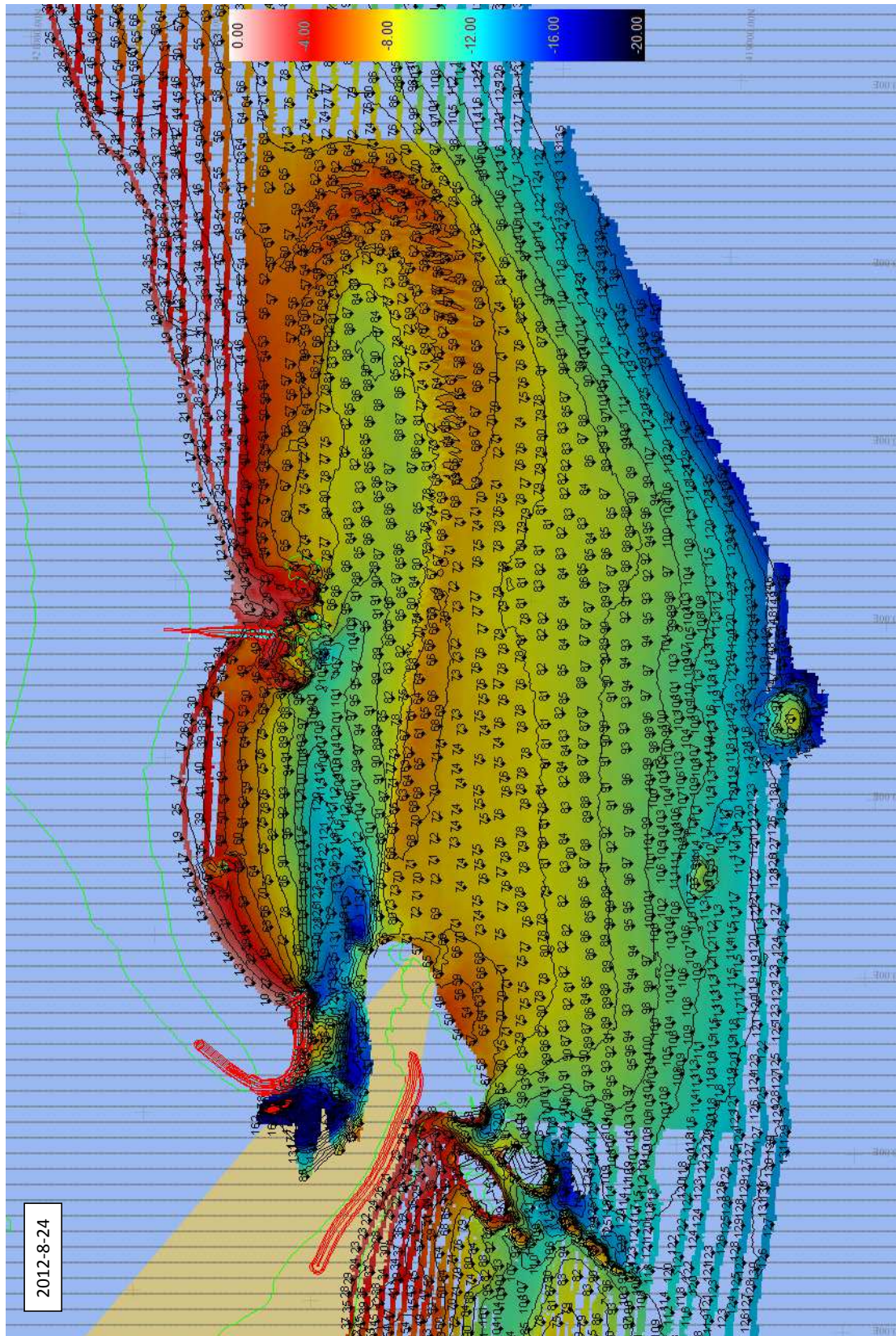
Figure A.9: 2012-08-24

80
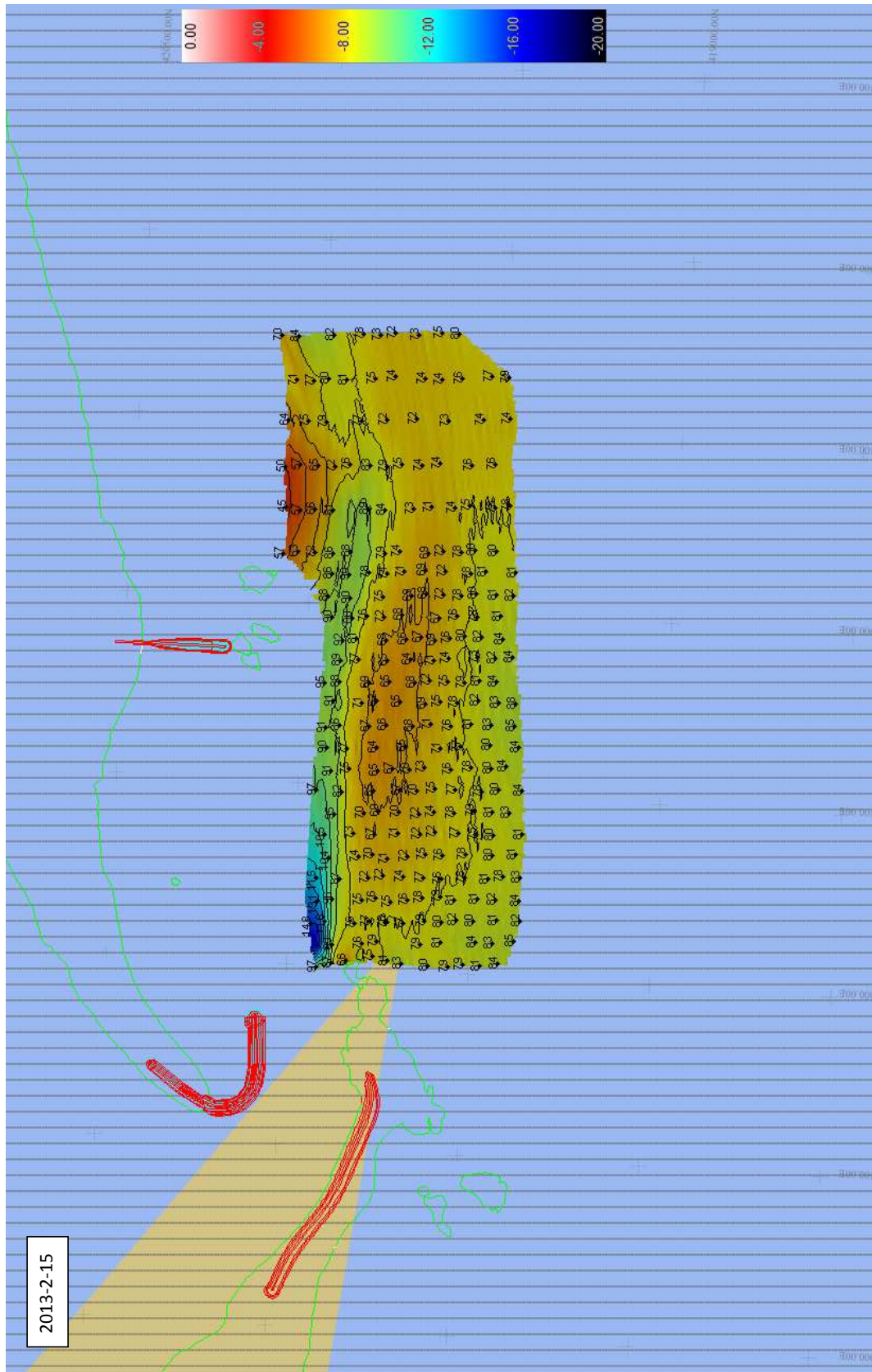
Figure A.10: 2013-02-15
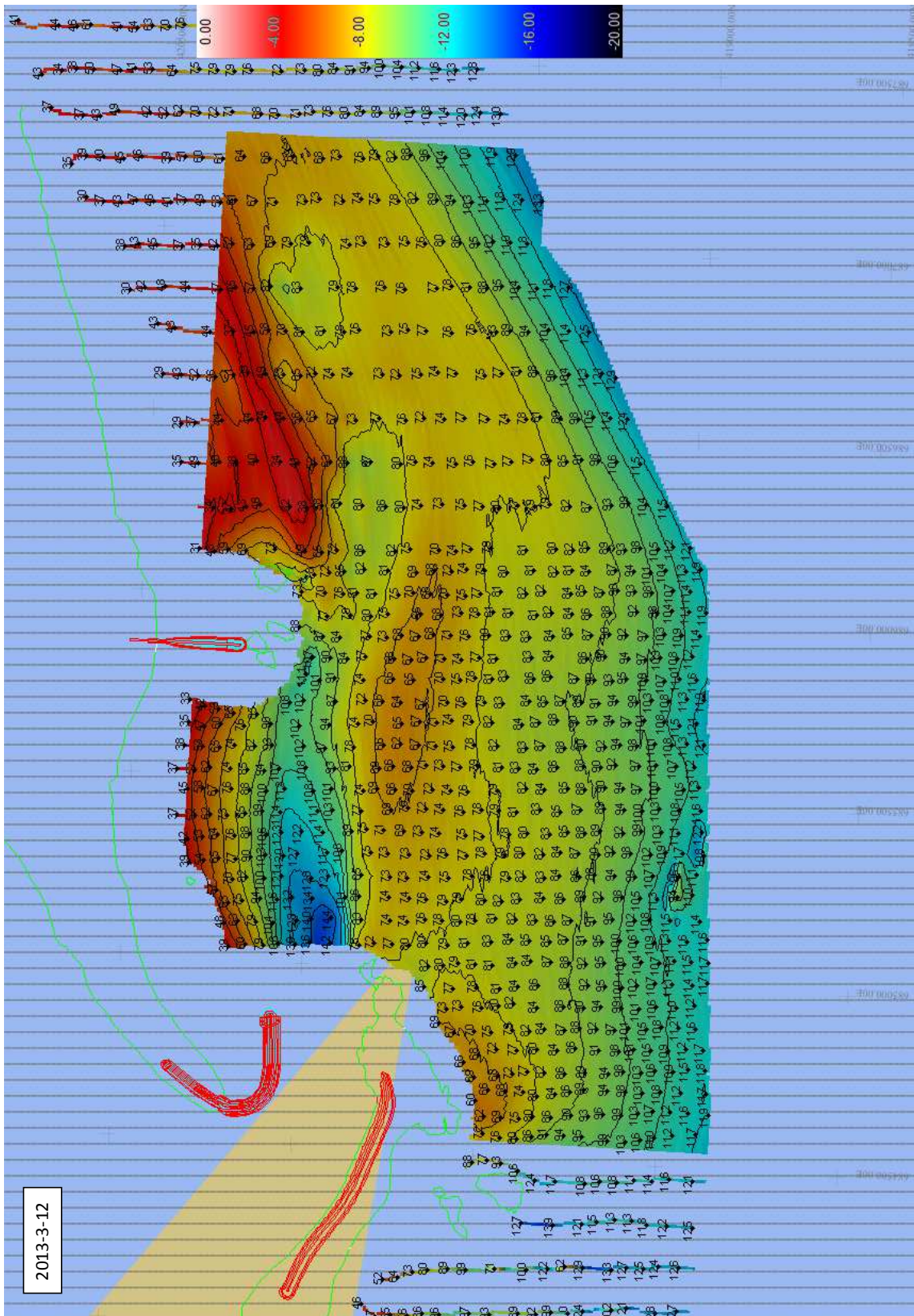
Figure A.11: 2013-03-12

81
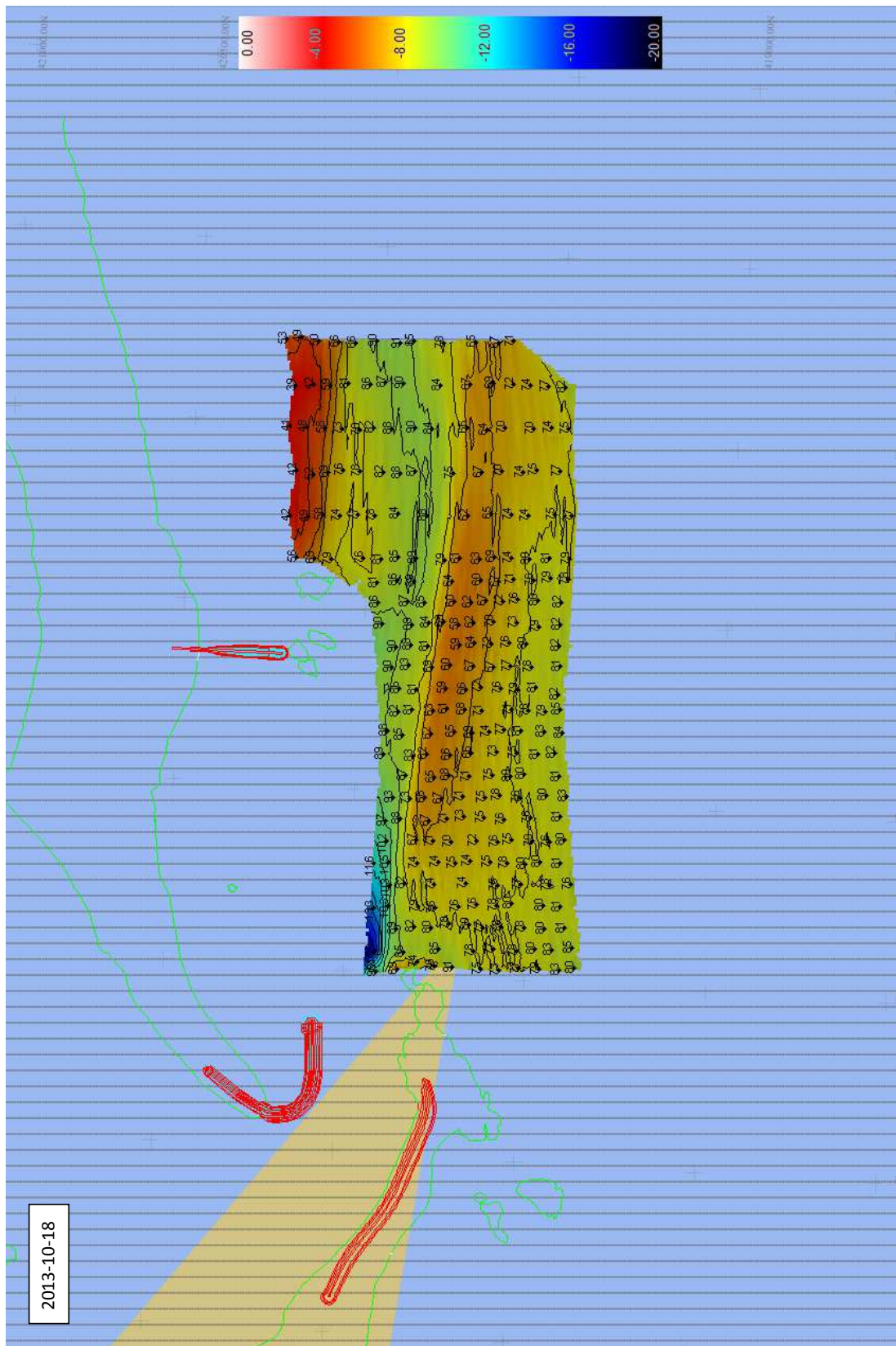
Figure A.12: 2013-10-18
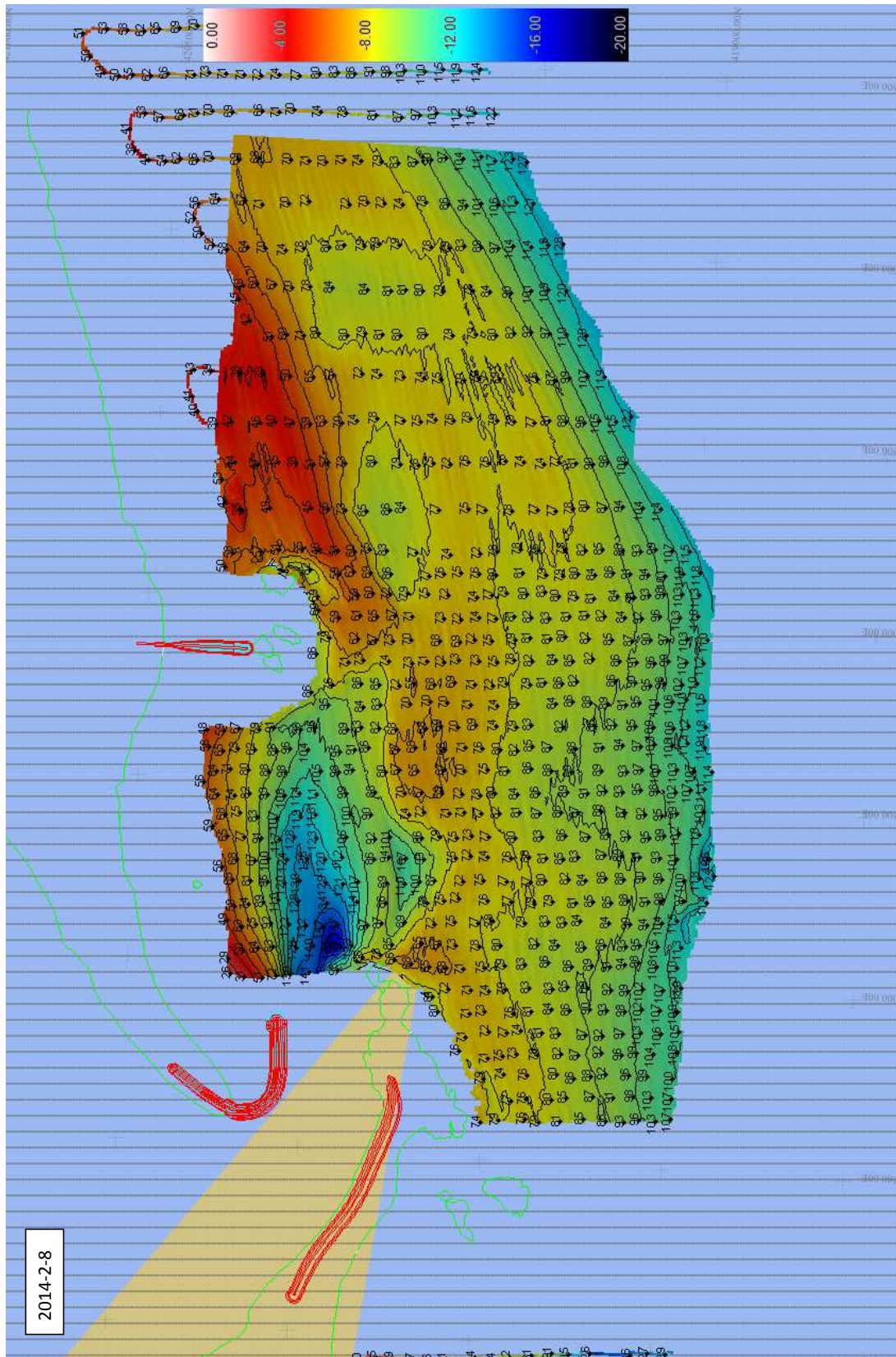
Figure A.13: 2014-02-08

84
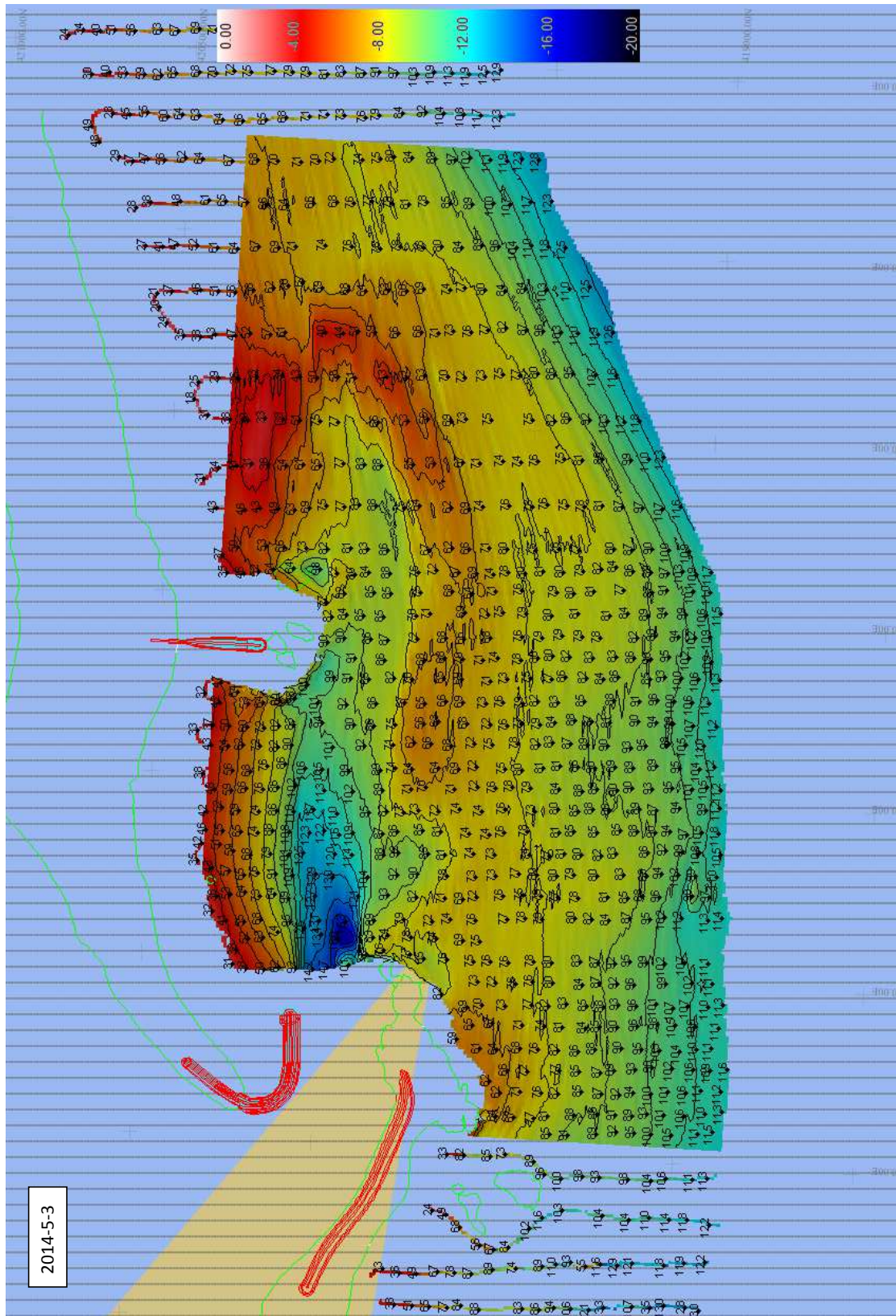
Figure A.14: 2014-05-03

Figure A.15: 2014-07-30

A Bathymetry

A.2 Bathymetric Difference Planes

87
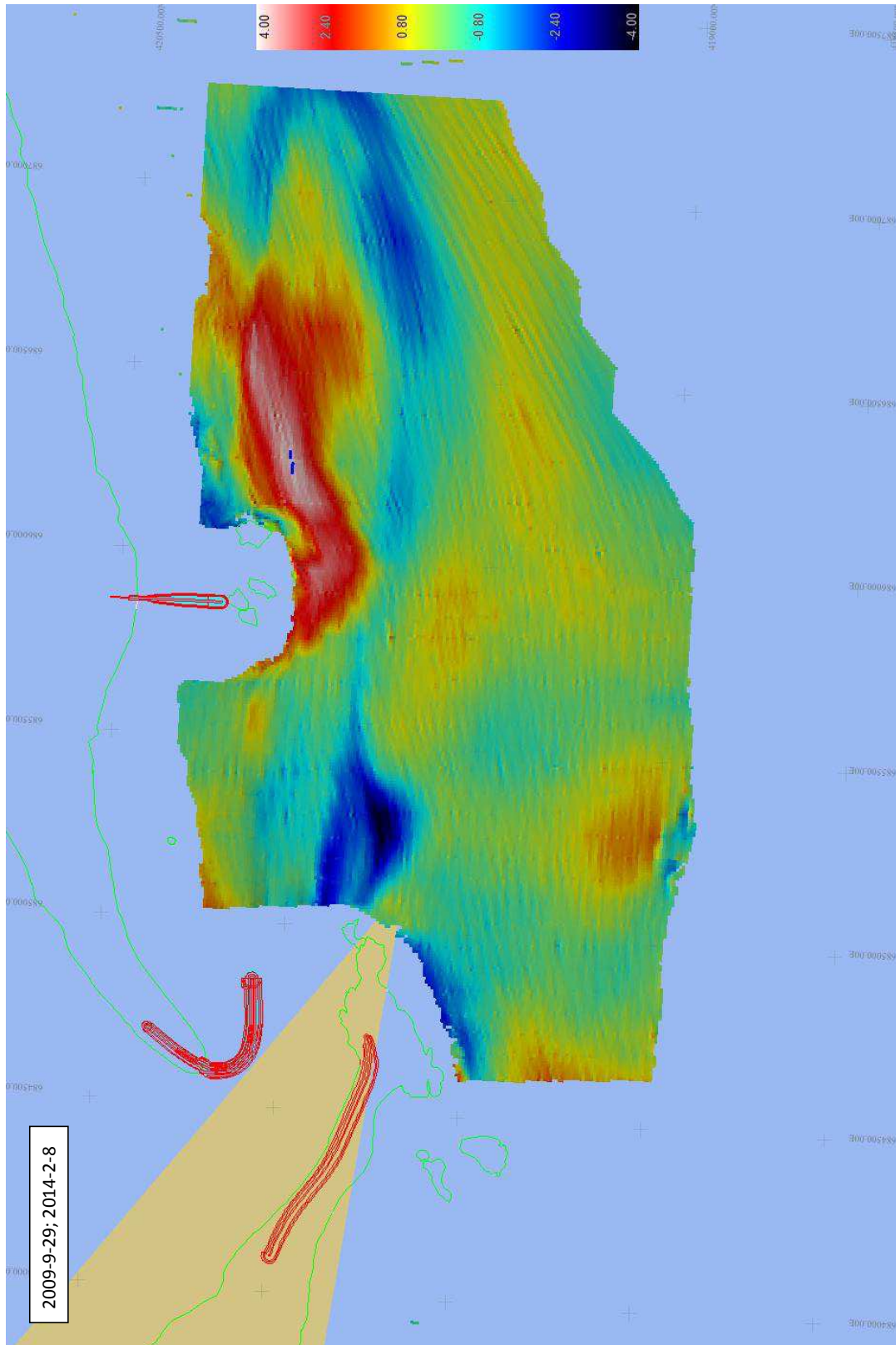
Figure A.16: 2009-09-29 to 2014-02-08
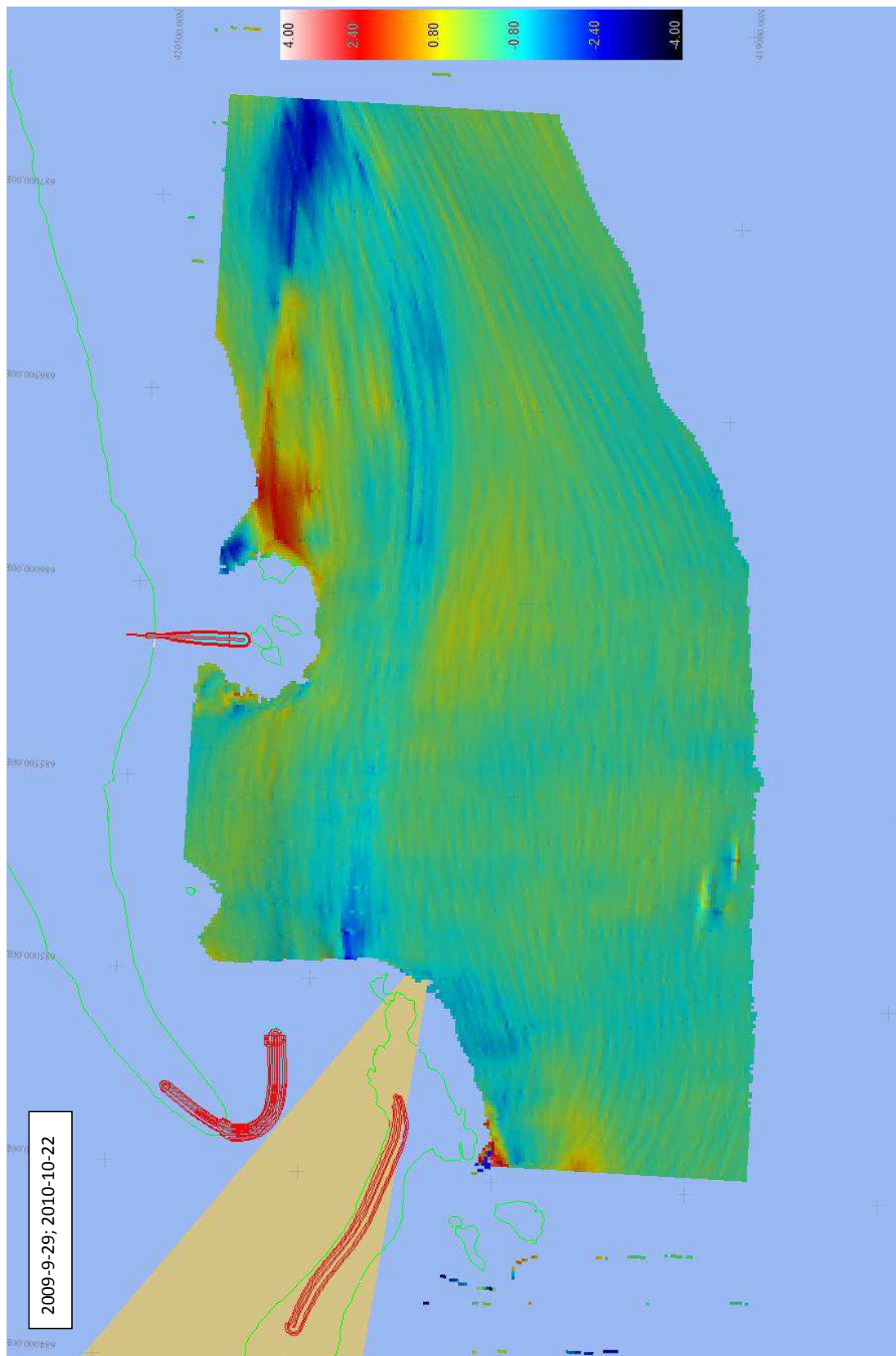
Figure A.17: 2009-09-29 to 2010-10-22
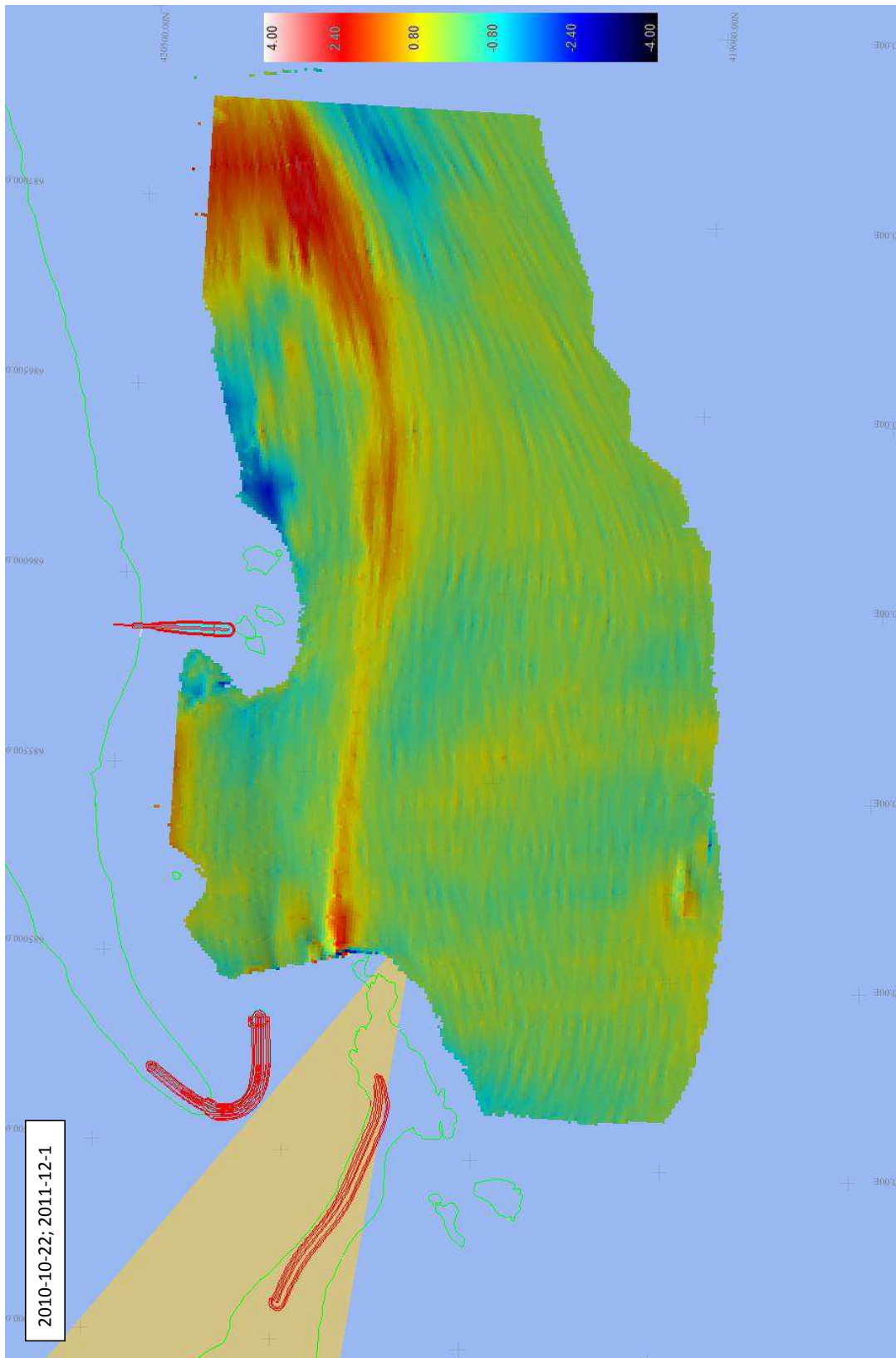
Figure A.18: 2010-10-22 to 2011-12-01
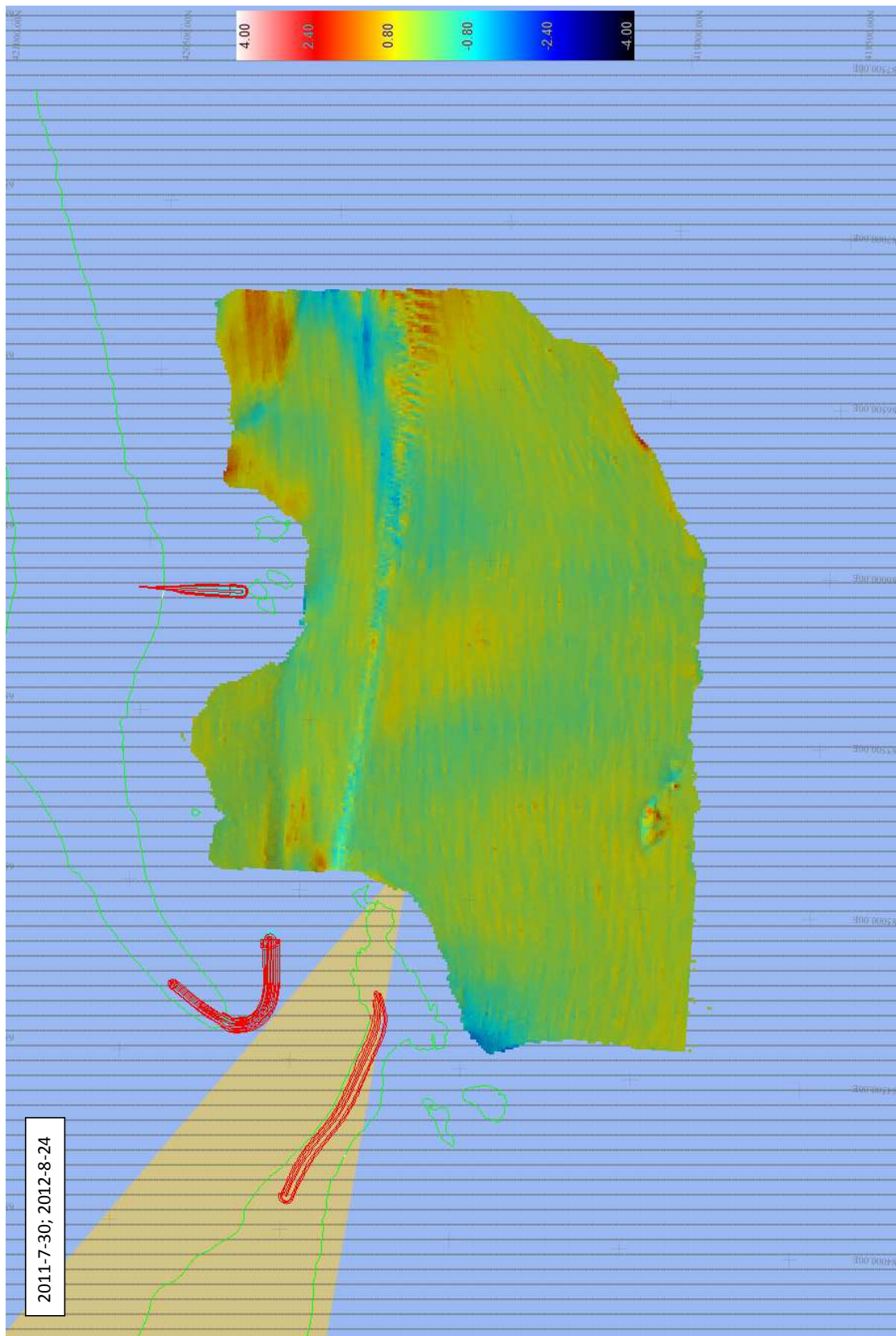
Figure A.19: 2011-07-30 to 2012-08-24

2011-12-1; 2013-2-15

91
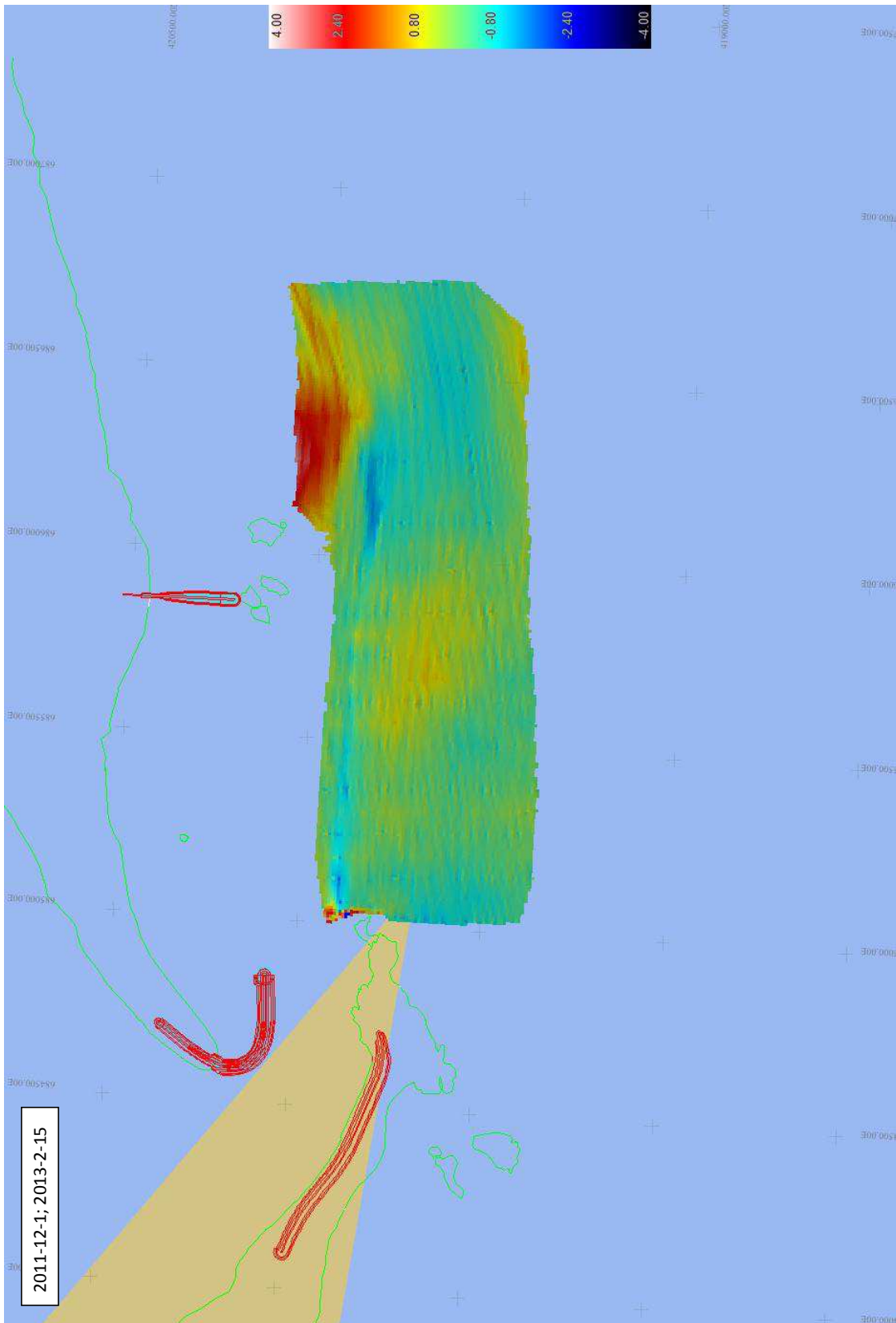
Figure A.20: 2011-12-01 to 2013-02-15
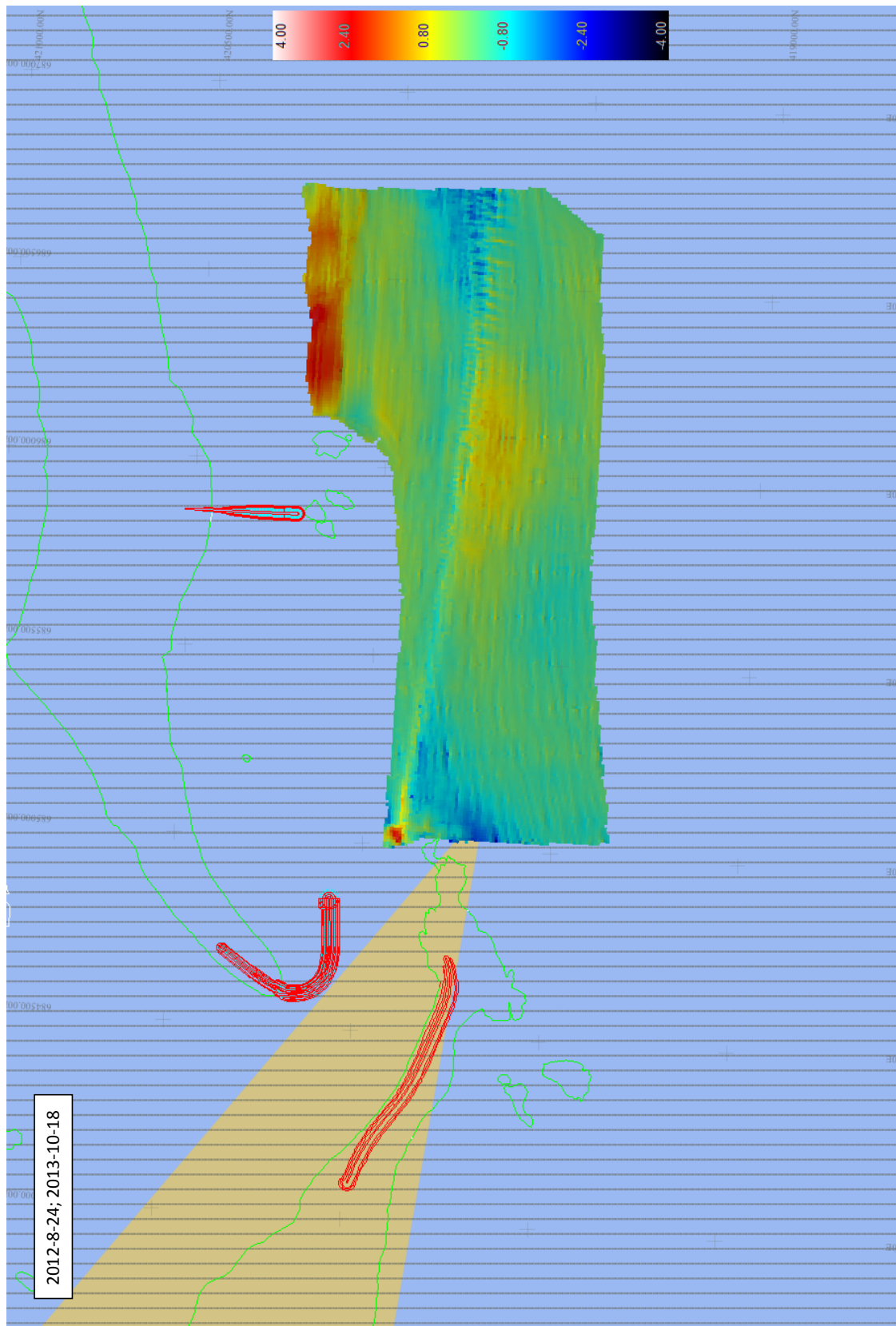
Figure A.21: 2012-08-24 to 2013-10-18
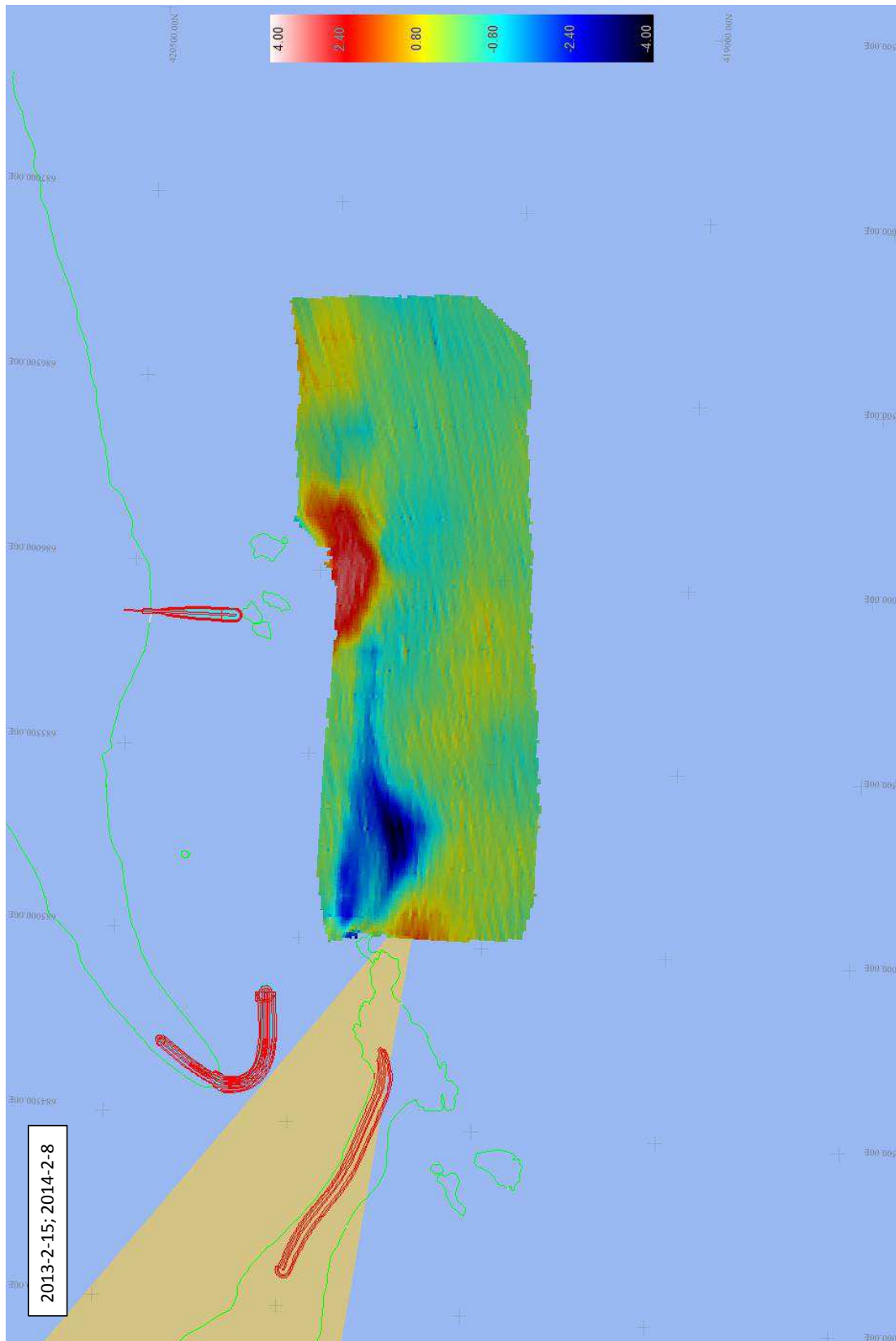
Figure A.22: 2013-02-15 to 2014-02-08

2013-10-18; 2014-2-8
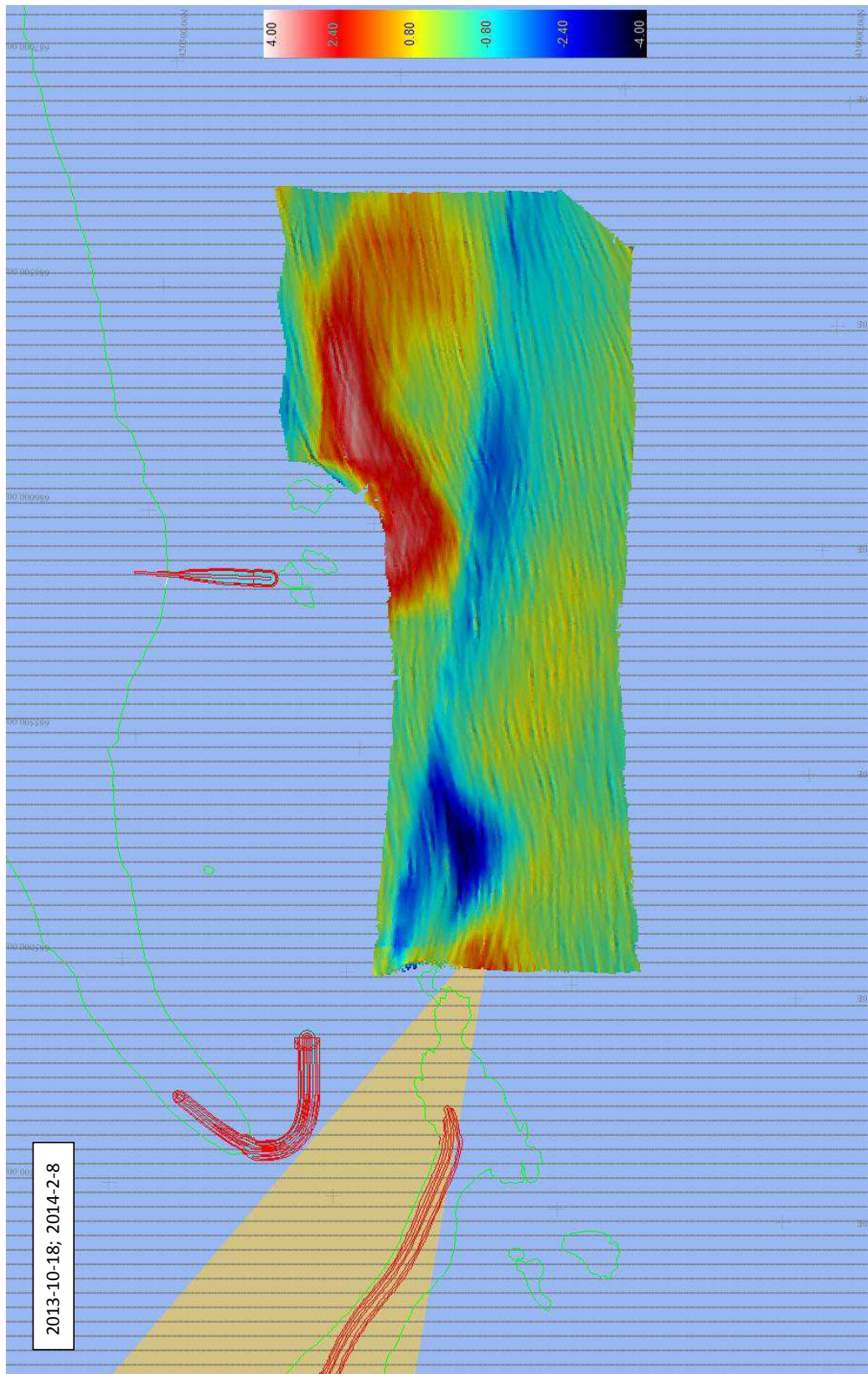
Figure A.23: 2013-10-18 to 2014-02-08
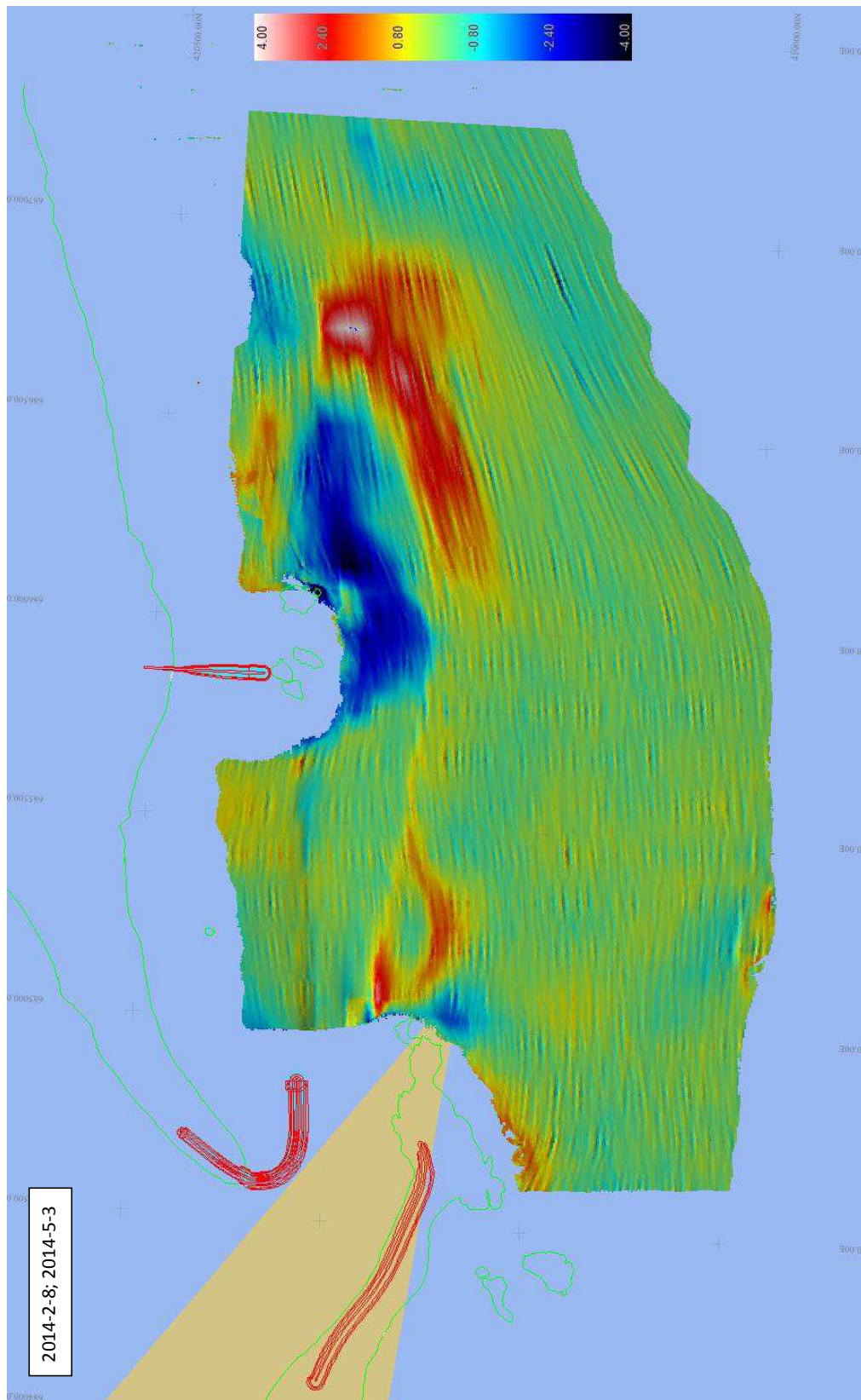
Figure A.24: 2014-02-08 to 2014-05-03

95
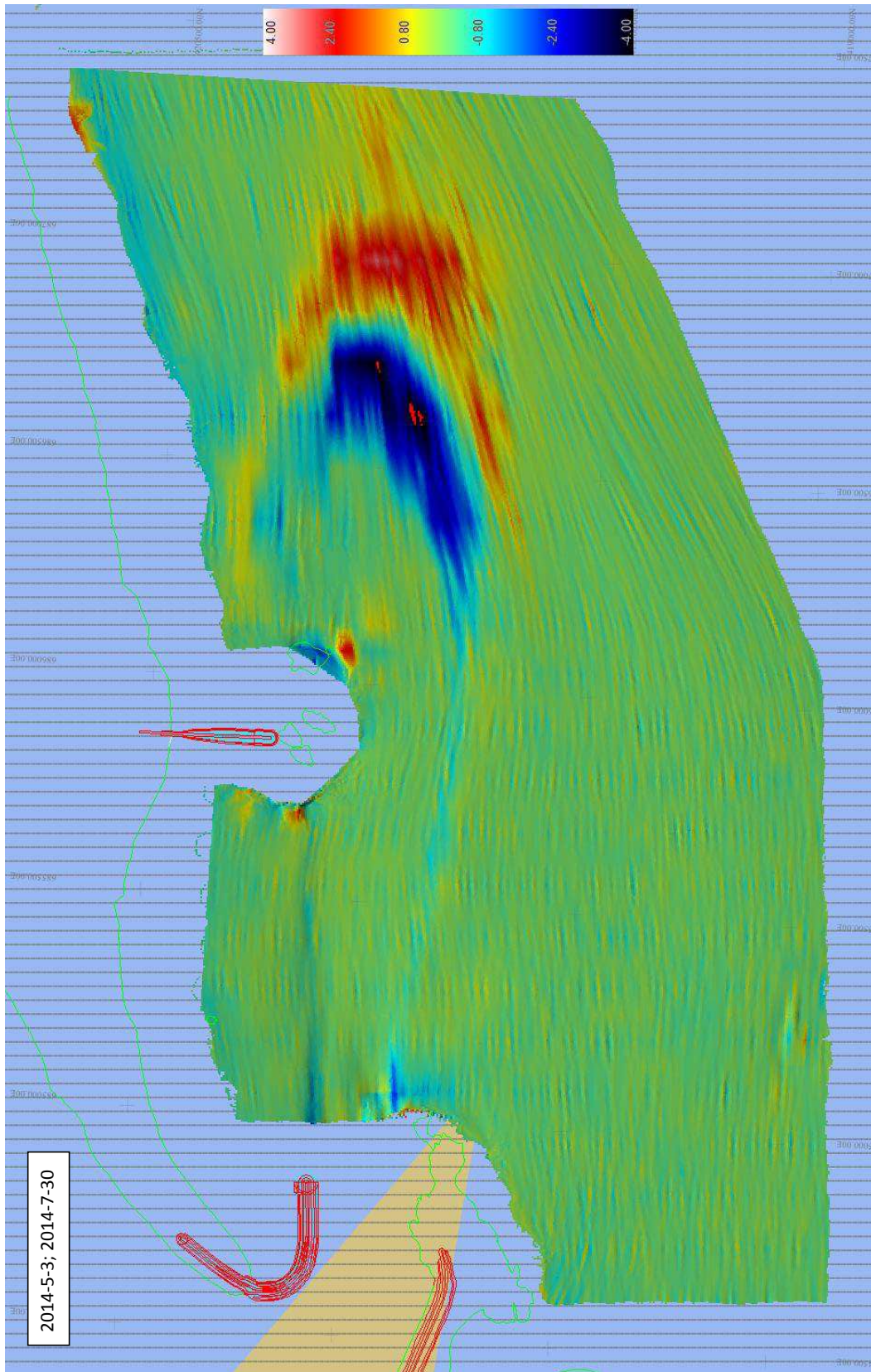
Figure A.25: 2014-05-03 to 2014-07-30

B Sediment Transport

This Appendix includes figures and plots resulting from the sediment transport model.

B.1 Profiles

Figure B.1: Overview of profiles.

B.2 Sediment Transport Distribution in Profiles

(a) Profile 4000W

(b) Profile 3500W
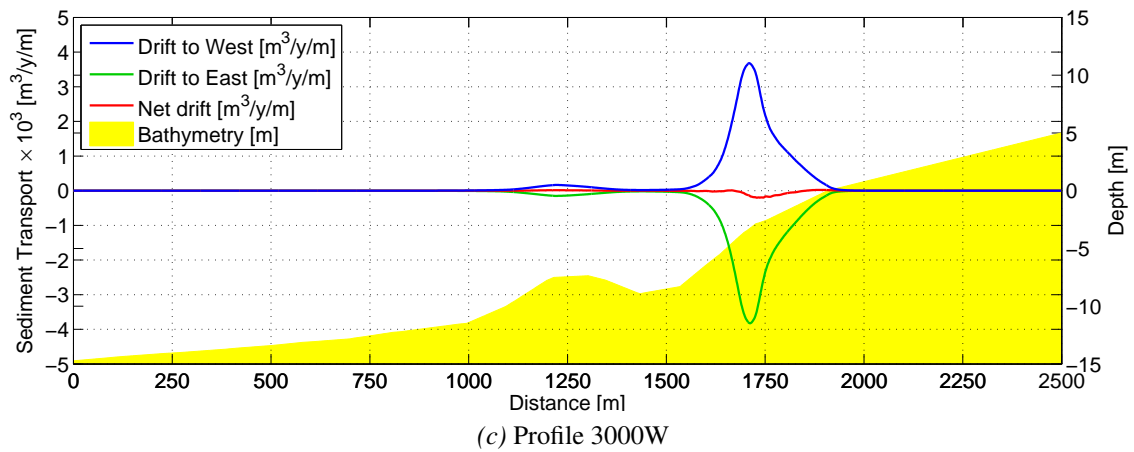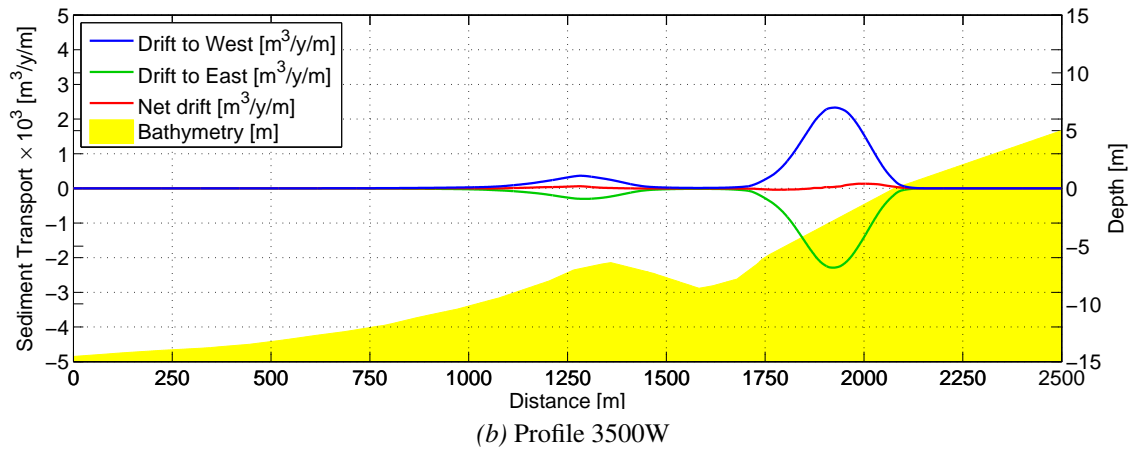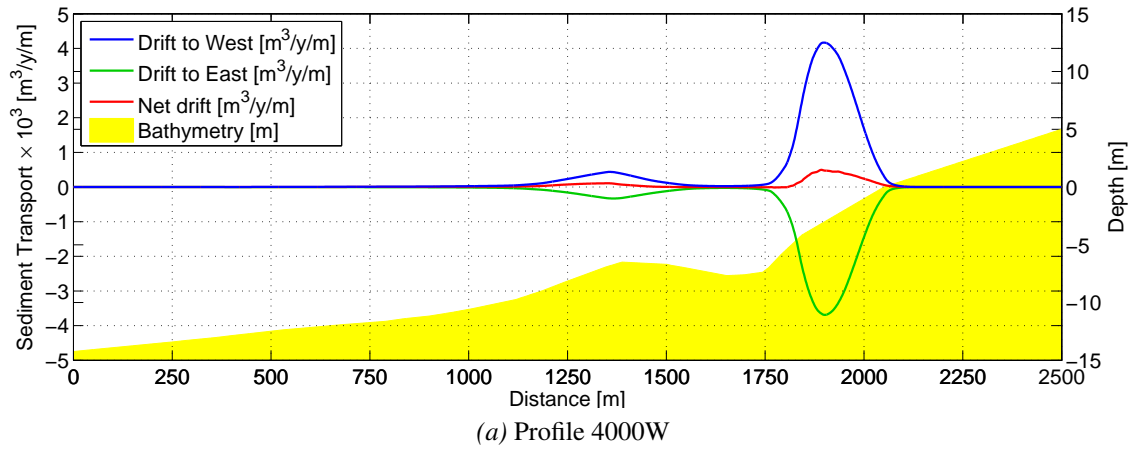
(c) Profile 3000W

Figure B.2: Sediment transport for the profiles shown in Fig. 3.20 (1/5)
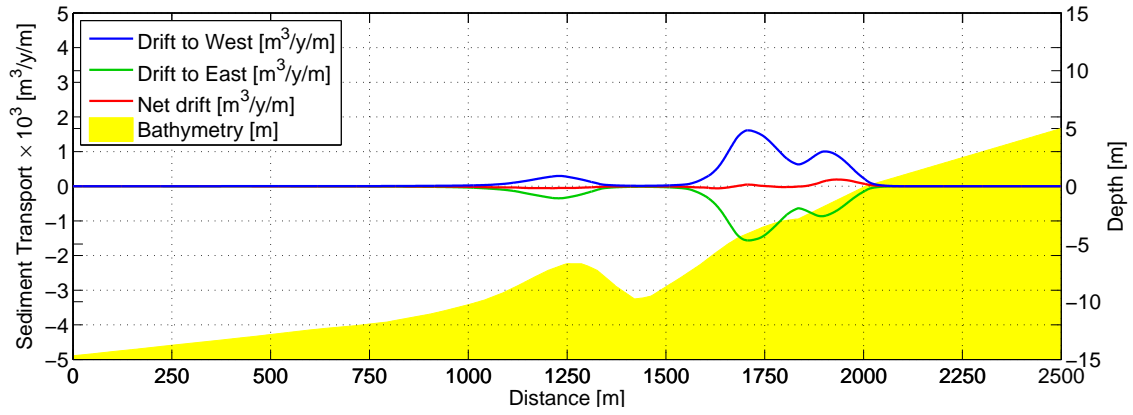
(a) Profile 2500W
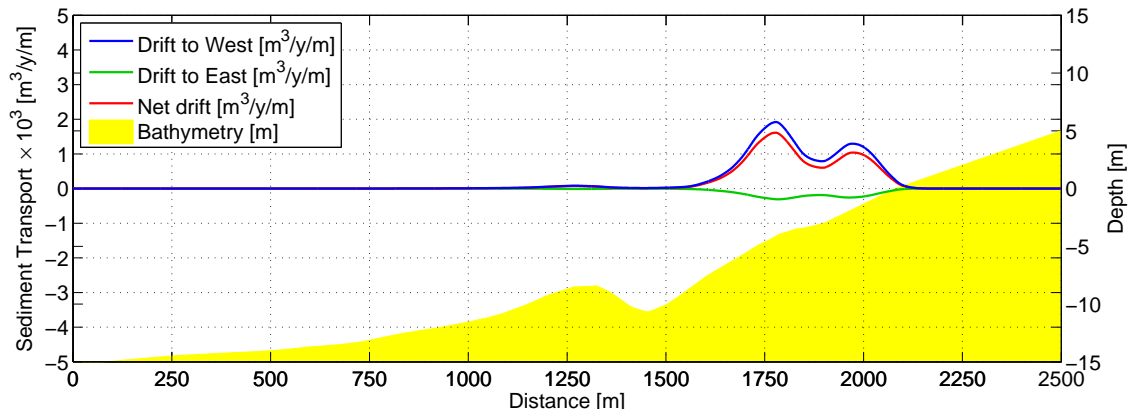
(b) Profile 2000W
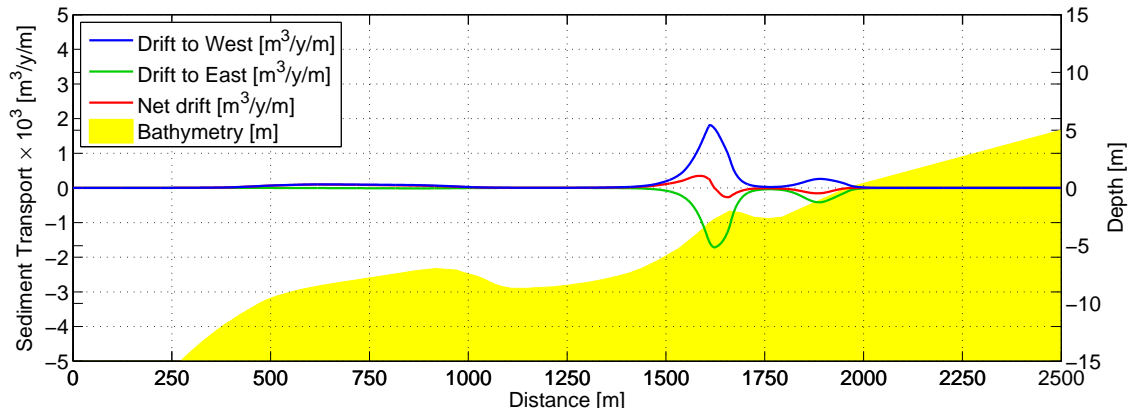
(c) Profile 0

Figure B.3: Sediment transport for the profiles shown in Fig. 3.20 (2/5)

(a) Profile 500E

(b) Profile 1000E

(c) Profile 1500E
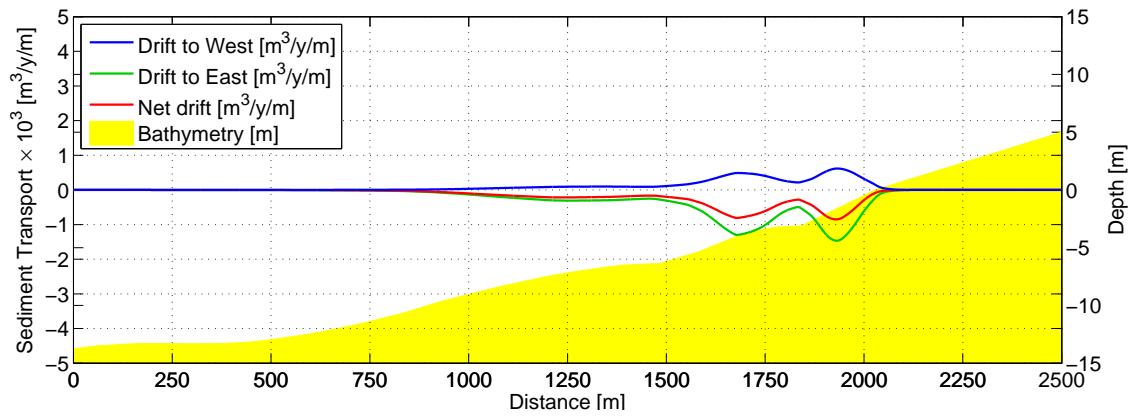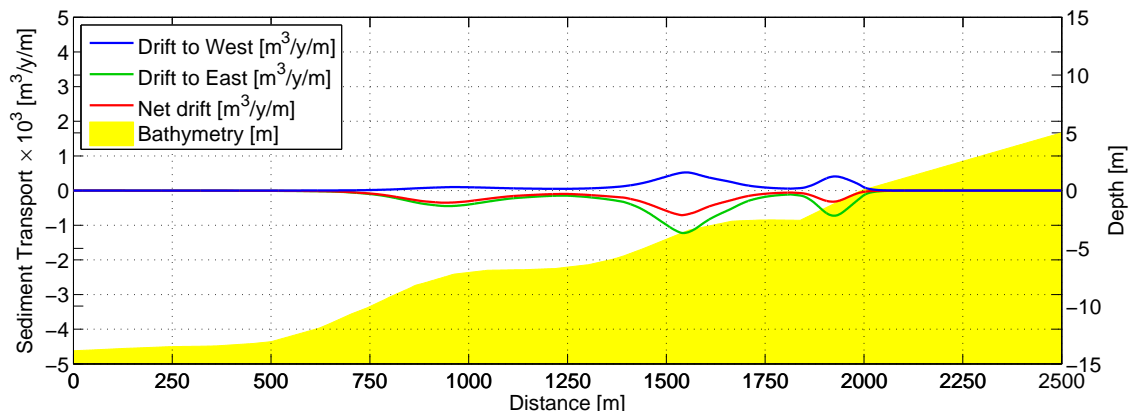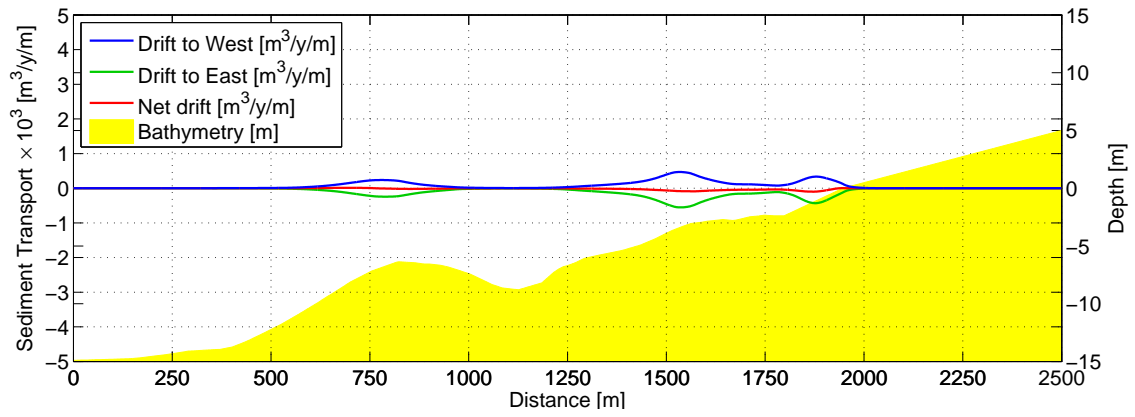
Figure B.4: Sediment transport for the profiles shown in Fig. 3.20 (3/5)
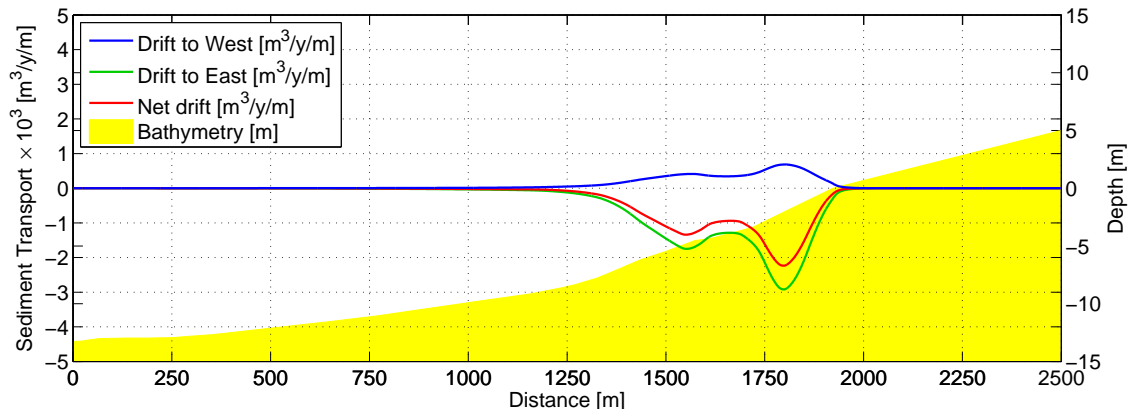
Figure B.5: Sediment transport for the profiles shown in Fig. 3.20 (4/5)

(a) Profile G250W

(b) Profile G0

(c) Profile G250E
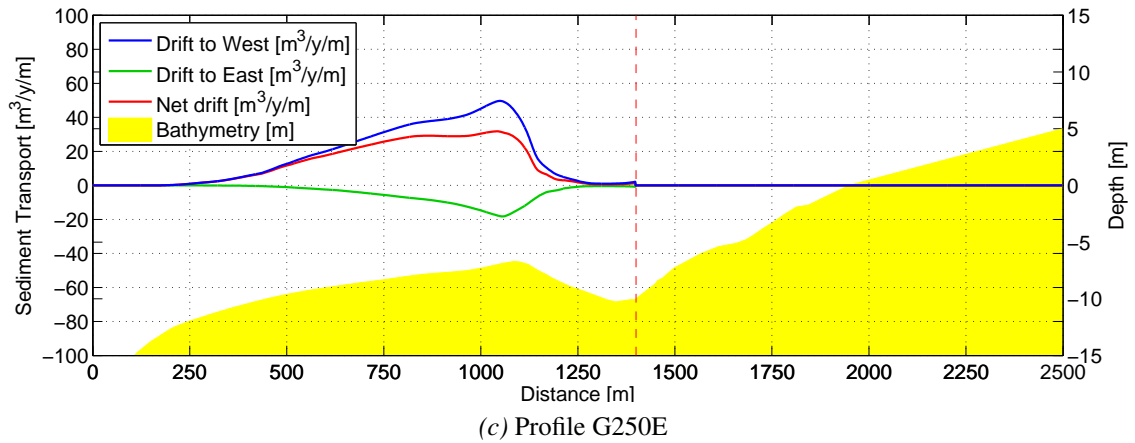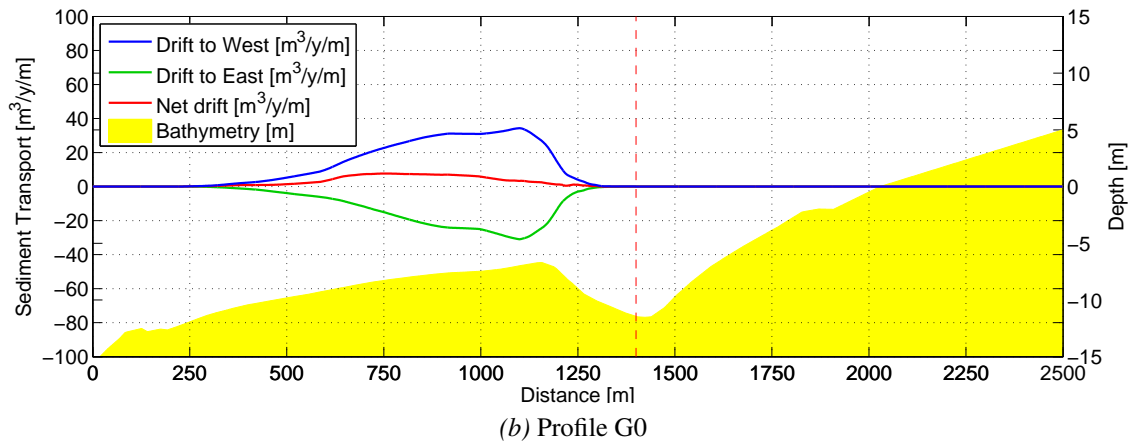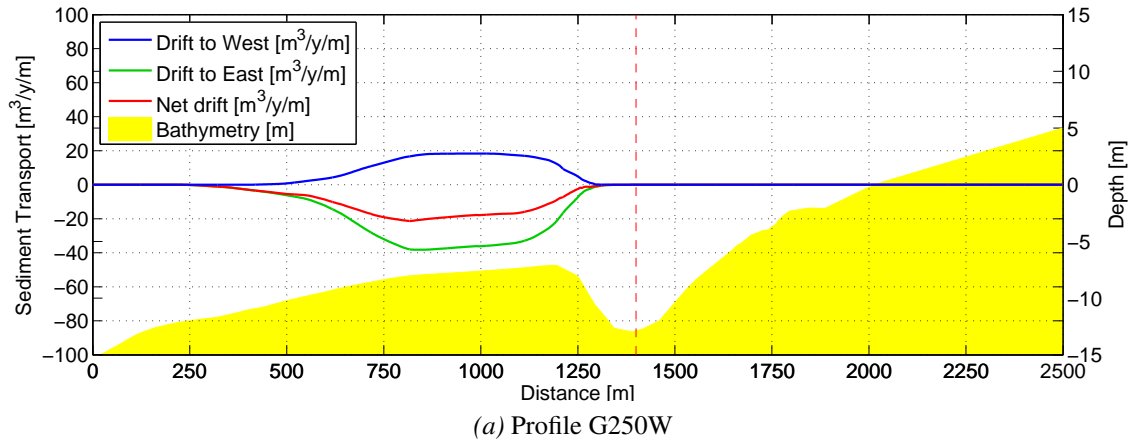
Figure B.6: Sediment transport for the profiles at the ebb shoal shown in Fig. 3.20 marked with 'G' (5/5).

B.3 Sensitivity of Coast Orientation

Table B.1: Coast orientation sensitivity for the profiles shown in Fig. 3.20

4000W						3500W				
Coastline orientation [°]						Coastline orientation [°]				
170	175	180	185	190		169	174	179	184	189
Sediment transport						Sediment transport				
Gross	116%	107%	100%	96%	94%	Gross	117%	107%	100%	96%	94%
West	54%	76%	100%	124%	143%	West	54%	76%	100%	124%	146%
East	188%	142%	100%	65%	38%	East	182%	140%	100%	66%	39%

| 3000W						2500W				
Coastline orientation [°]						Coastline orientation [°]				
169	174	179	184	189		171	176	181	186	191
Sediment transport						Sediment transport				
Gross	130%	111%	100%	99%	106%	Gross	122%	109%	100%	94%	93%
West	41%	67%	100%	140%	183%	West	55%	76%	100%	124%	149%
East	217%	154%	100%	60%	32%	East	188%	142%	100%	64%	37%

2000W						0				
Coastline orientation [°]						Coastline orientation [°]				
175	180	185	190	195		152	157	162	167	172
Sediment transport						Sediment transport				
Gross	104%	97%	100%	115%	135%	Gross	92%	90%	100%	122%	155%
West	60%	78%	100%	129%	158%	West	26%	56%	100%	161%	237%
East	347%	201%	100%	43%	13%	East	172%	132%	100%	74%	53%

500E						1000E				
Coastline orientation [°]						Coastline orientation [°]				
153	158	163	168	173		152	157	162	167	172
Sediment transport						Sediment transport				
Gross	122%	107%	100%	101%	114%	Gross	119%	111%	100%	90%	81%
West	41%	66%	100%	144%	201%	West	52%	75%	100%	127%	157%
East	192%	142%	100%	65%	40%	East	146%	125%	100%	75%	52%

1500E						2000E				
Coastline orientation [°]						Coastline orientation [°]				
153	158	163	168	173		155	160	165	170	175
Sediment transport						Sediment transport				
Gross	113%	107%	100%	92%	83%	Gross	104%	103%	100%	95%	90%
West	48%	73%	100%	128%	156%	West	39%	66%	100%	138%	180%
East	138%	121%	100%	78%	56%	East	121%	113%	100%	84%	66%

(a) Profile 4000W

(b) Profile 3500W

(c) Profile 3000W

(d) Profile 2500W

(e) Profile 2000W

(f) Profile 0

Figure B.7: Coast orientation sensitivity for the profiles shown in Fig. 3.20 (1/3)

(a) Profile 500E

(b) Profile 1000E

(c) Profile 1500E

(d) Profile 2000E

Figure B.8: Coast orientation sensitivity for the profiles shown in Fig. 3.20 (2/3)
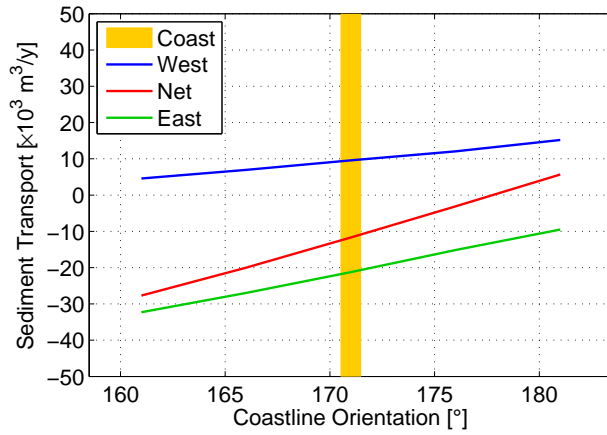
(a) Profile G250W

	G250W				
	Coastline orientation [°]				
	161	166	171	176	181
	Sediment transport				
Gross	120%	110%	100%	89%	80%
West	48%	73%	100%	126%	158%
East	152%	127%	100%	72%	45%
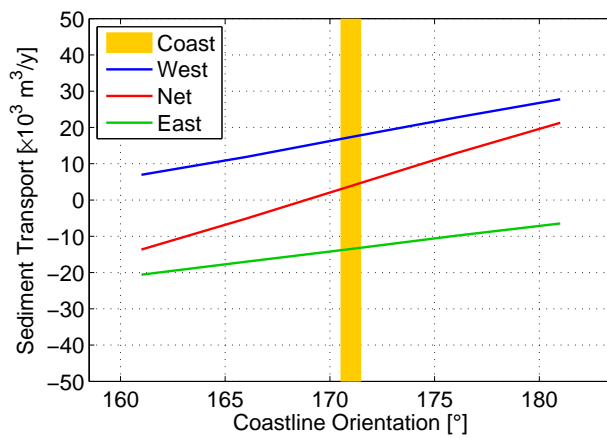
(c) Profile G0

	G0				
	Coastline orientation [°]				
	161	166	171	176	181
	Sediment transport				
Gross	90%	94%	100%	106%	111%
West	40%	69%	100%	131%	161%
East	153%	126%	100%	73%	48%
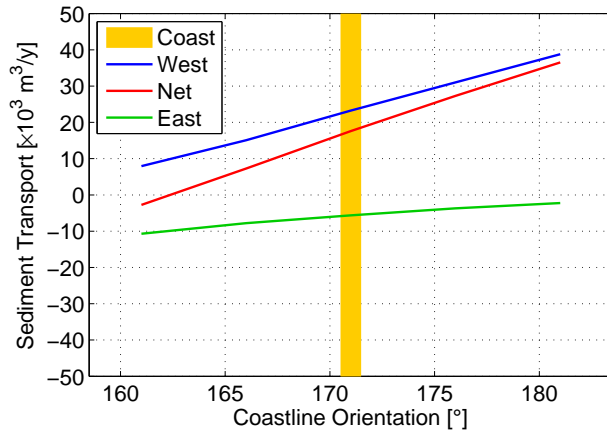
(e) Profile G250E

	G250E				
	Coastline orientation [°]				
	161	166	171	176	181
	Sediment transport				
Gross	65%	80%	100%	120%	142%
West	34%	65%	100%	134%	167%
East	191%	139%	100%	66%	39%

Figure B.9: Coast orientations sensitivity for the profiles at the ebb shoal shown in Fig. 3.20 marked with 'G' (3/3).

B.4 Wave Roses

(a) Profile 4000W

(b) Profile 3500W

(c) Profile 3000W

(d) Profile 2500W

(e) Profile 2000W
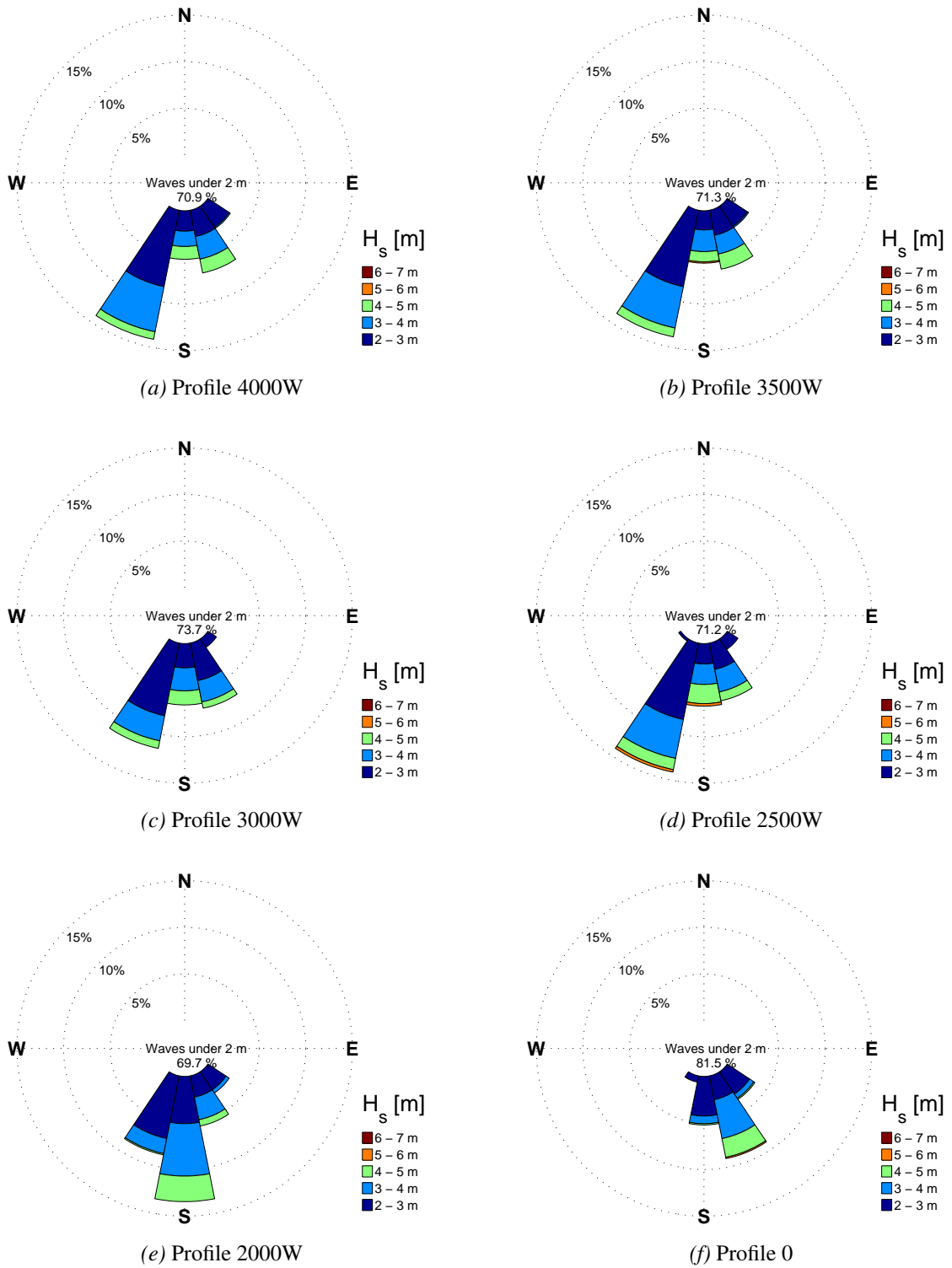
(f) Profile 0

Figure B.10: Wave roses for the profiles shown in Fig. 3.20 (1/2)

(a) Profile 500E

(b) Profile 1000E

(c) Profile 1500E

(d) Profile 2000E
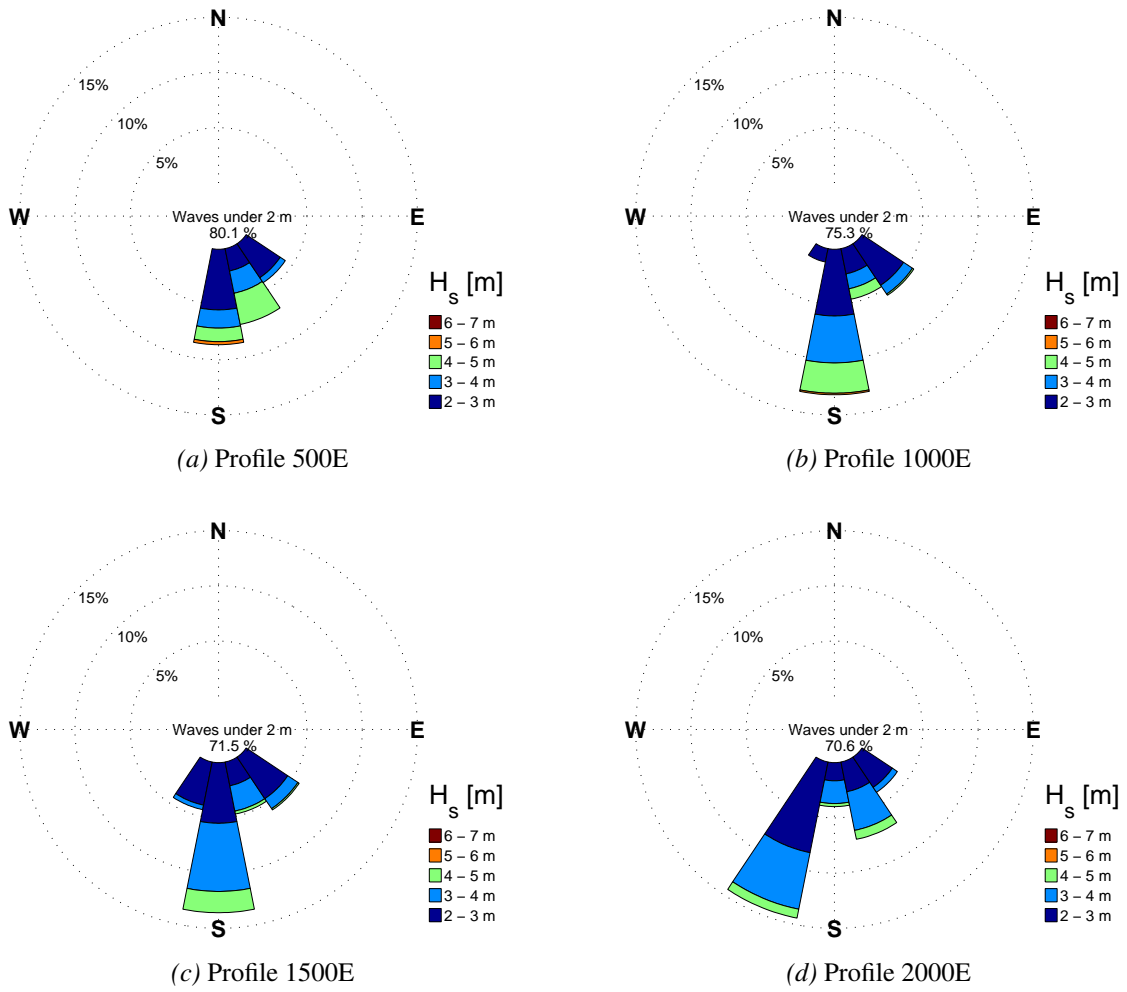
Figure B.11: Wave roses for the profiles shown in Fig. 3.20 (2/2)

C Matlab Codes

This Appendix includes MATLAB codes used for calculation and making plots and figures.

C.1 Hayes.m

```matlab
% Hayes Classification
% Bjarki Omarsson, 2015

clear all
close all
clc

MTR = 1.98;      % Mean tidal range, [m]
load Hs_P123     % From "Hs_Grynnslin.xlsx"

Hs_P1=sort(Hs_P1,'descend');
Hs_P2=sort(Hs_P2,'descend');
Hs_P3=sort(Hs_P3,'descend');

Hsmean_P1 = mean(Hs_P1);
Hsmean_P2 = mean(Hs_P2);
Hsmean_P3 = mean(Hs_P3);

Hs_mean = mean(mean([Hs_P1 Hs_P2 Hs_P3]));
```

C.2 NielsenThuy.m

```matlab
% Nielsen & Thuy classification
% Bjarki Omarsson, 2015

clear all
close all
clc

%% INPUT PARAMETERS

Qh_tide = 4420; % Peak tidal discharge, m3/s
Q_f = 100;      % Fresh water discharge, m3/s
g = 9.81;       % m/s2


%% WAVE HEIGHT, Hs

% Data from wave buoy
data = xlsread('dufl_2000_2009.xlsx','dufl_2000-2009','b2:b87673');

Hs1 = data;
t1 = find(isnan(Hs1)==1);
t2 = find(Hs1<0);

Hs1([t1; t2])=[];
Hs1 = sort(Hs1,'descend');
Hs2 = mean(Hs1(1:(ceil(length(Hs1)/3))));

% Average offshore sign. wave height:
Hs_mean = mean(Hs1);


%% THUY & NIELSEN

% y-axis:
R_TW = Qh_tide/sqrt(g*Hs_mean^5);
% x-axis:
R_f = Q_f/sqrt(g*Hs_mean^5);

% Plot settings
fs = 12;
set(0,'DefaultAxesFontSize',fs)
set(0,'DefaultTextFontSize',fs)

loglog([0.001 100],[75 75],'k')
hold on
loglog([2 2],[0.01 1000],'k')
loglog(R_f,R_TW,'rp','markersize',12,'markeredgecolor','k',...
    'markerfacecolor','r')
hold off
```

```matlab
ylim([0.01 1000])
xlim([0.001 100])

text(0.003,31,'\downarrow','fontsize',30)
text(0.003,12,'Wave dominated')
text(2,2,'\rightarrow','fontsize',30)
text(10,400,'Tidal dominated')
text(30,130,'\uparrow','fontsize',30)
text(3,0.8,'River dominated')
xlabel('R_f','fontsize',fs)
ylabel('R_{TW}','fontsize',fs)
set(gca,'xtick',[0.001 0.01 0.1 1 10 100])
set(gca,'xticklabel',{'0.001','0.01','0.1','1','10','100'})
set(gca,'yticklabel',{'0.01','0.1','1','10','100','1000'})

set(gcf, 'PaperUnits', 'centimeters');
x_width=12.5 ;y_width=10;
set(gcf, 'PaperPosition', [1 3 x_width y_width]);
```

C.3 EbbShoalSeasonVar.m

```matlab
% EbbShoalSeasonVar
% Bjarki Omarsson, 2015

clear all
close all
clc

data = xlsread('DyptP1P2P3.xlsx','Heild','a2:d202');
date = data(:,1)+693960;
P1 = data(:,2);
P2 = data(:,3);
P3 = data(:,4);
save('grynndepth.mat','date','P1','P2','P3')
load grynndepth

ind = ~isnan(P1);
date = date(ind);
P1 = P1(ind);
P2 = P2(ind);
P3 = P3(ind);

fs = 12;
set(0,'DefaultAxesFontSize',fs)
set(0,'DefaultTextFontSize',fs)
```

C Matlab Codes

```matlab
% P1
figure
plot(date,P1)
hold on
plot(date,P1,'o')
ylim([6 8.5])
xlim([729770 735795])
set(gca,'Xtick',linspace(729770,735795,17))
datetick('x','yyyy','keepticks')
xticklabel_rotate([],45,[])
ylabel('Depth (m)','fontsize',fs)
% title('Timeserie for P1','fontsize',fs+2)
set(gca,'FontSize',fs)
set(gcf, 'PaperUnits', 'centimeters');
x_width=25 ;y_width=7.5;
set(gcf, 'PaperPosition', [1 3 x_width y_width]);
grid on

figure
subplot(1,2,1), pburg(P1,7)
ylabel('Power/frequency (dB/rad/sample)','fontsize',fs)
xlabel('Normalized frequency (\times pi rad/sample)','fontsize',fs)
% title('Burg Power Spectral Density Estimate','fontsize',fs+2)
title(' ')
set(gca,'FontSize',fs)

subplot(1,2,2),autocorr(P1,40)
ylabel('Sample Autocorrelation','fontsize',fs)
xlabel('Lag','fontsize',fs)
% title('Autocorrelation Function','fontsize',fs+2)
title(' ')
set(gca,'FontSize',fs)

set(gcf, 'PaperUnits', 'centimeters');
x_width=25 ;y_width=7.5;
set(gcf, 'PaperPosition', [1 3 x_width y_width]);


% P2
figure
plot(date,P2,'r')
hold on
plot(date,P2,'ro')
ylim([6 8.5])
xlim([729770 735795])
set(gca,'Xtick',linspace(729770,735795,17))
datetick('x','yyyy','keepticks')
xticklabel_rotate([],45,[])
ylabel('Depth (m)','fontsize',fs)
% title('Timeserie for P2','fontsize',fs+2)
set(gca,'FontSize',fs)
set(gcf, 'PaperUnits', 'centimeters');
```

```matlab
x_width=25 ;y_width=7.5;
set(gcf, 'PaperPosition', [1 3 x_width y_width]); %
grid on

figure
subplot(1,2,1), pburg(P2,7)
ylabel('Power/frequency (dB/rad/sample)','fontsize',fs)
xlabel('Normalized frequency (\times pi rad/sample)','fontsize',fs)
% title('Burg Power Spectral Density Estimate','fontsize',fs+2)
title(' ')
set(gca,'FontSize',fs)

subplot(1,2,2),autocorr(P2,40)
ylabel('Sample Autocorrelation','fontsize',fs)
xlabel('Lag','fontsize',fs)
% title('Autocorrelation Function','fontsize',fs+2)
title(' ')
set(gca,'FontSize',fs)

set(gcf, 'PaperUnits', 'centimeters');
x_width=25 ;y_width=7.5;
set(gcf, 'PaperPosition', [1 3 x_width y_width]);


% P3
figure
plot(date,P3,'g')
hold on
plot(date,P3,'go')
ylim([6 8.5])
xlim([729770 735795])
set(gca,'Xtick',linspace(729770,735795,17))
datetick('x','yyyy','keepticks')
xticklabel_rotate([],45,[])
ylabel('Depth (m)','fontsize',fs)
% title('Timeserie for P3','fontsize',fs+2)
set(gca,'FontSize',fs)
set(gcf, 'PaperUnits', 'centimeters');
x_width=25 ;y_width=7.5;
set(gcf, 'PaperPosition', [1 3 x_width y_width]); %
grid on

figure
subplot(1,2,1), pburg(P3,7)
ylabel('Power/frequency (dB/rad/sample)','fontsize',fs)
xlabel('Normalized frequency (\times pi rad/sample)','fontsize',fs)
% title('Burg Power Spectral Density Estimate','fontsize',fs+2)
title(' ')
set(gca,'FontSize',fs)

subplot(1,2,2),autocorr(P3,40)
ylabel('Sample Autocorrelation','fontsize',fs)
```

117

```matlab
xlabel('Lag','fontsize',fs)
% title('Autocorrelation Function','fontsize',fs+2)
title(' ')
set(gca,'FontSize',fs)

set(gcf, 'PaperUnits', 'centimeters');
x_width=25 ;y_width=7.5;
set(gcf, 'PaperPosition', [1 3 x_width y_width]);
```

C.4 EbbShoalDepth.m

```matlab
% Ebb Shoal Depth Calculations
% Bjarki Omarsson, 2015

clear all
close all
clc

%% INPUT PARAMETERS

P = 64e6;          % Tidal prism (m3), 64 GL
Hs = 8.6;          % Average annual sign. wave height, [m]

h_Cr1 = 0.27 + 3.6*Hs;
h_Cr2 = 0.0063*P^0.35;
h_Cr3 = -0.066 + 0.045*(Hs*P)^0.25;

% 0.5m land rise: -35% change in tidal prism
P05 = (1-0.35)*P;
h_Cr3_05 = -0.066 + 0.045*(Hs*P05)^0.25;
% 1.0m land rise: -66% change in tidal prism
P10 = (1-0.66)*P;
h_Cr3_10 = -0.066 + 0.045*(Hs*P10)^0.25;

HsP14 = (Hs*P)^0.25
h_Cr3

% Sensitvity analysis
Hs_S = [8.0 8.25 8.5 8.6 8.75 9.0 9.25 9.5 9.75 10];
hl = [1.2 1.1 1 0.9 0.8 0.7 0.6 0.5 0.4 0.3];
P_S = 64e6 *hl;

for i = 1:length(Hs_S)
    for j = 1:length(P_S)
        hCr_S(j+1,i+1) = -0.066 + 0.045*(Hs_S(i)*P_S(j))^0.25;
    end
end
```

```
hCr_S(1,2:end) = Hs_S;
hCr_S(2:end,1) = hl';
```

C.5 EbbShoalVol.m

```matlab
% Ebb Shoal Volume Calculations
% Bjarki Omarsson, 2015

clear all
close all
clc

C_E1 = 2.21e-2;
P_E = 64e6;
V_E1 = C_E1*P_E^1.23;

C_E2 = 2.121e-2;
V_E2 = C_E2*P_E^1.1673;

P = linspace(1e5, 1e10, 100);
V1 = C_E1*P.^1.23;
V2 = C_E2*P.^1.1673;

loglog(P,V1)
hold on
loglog(P,V2,'color',[0 0.5 0])
loglog(P_E, V_E1, 'rs')
loglog(P_E, V_E2, 'rs')
loglog([P_E P_E],[10^4 V_E1],'r--')
loglog([10^5 P_E],[V_E1 V_E1],'r--')
loglog([10^5 P_E],[V_E2 V_E2],'r--')
legend('V_E = 2.21\times10^{-2} P^{1.23}',...
    'V_E = 2.121\times10^{-2} P^{1.1673}','location','northwest')
xlabel('Tidal Prism, P [m^3]');
ylabel('Ebb Shoal Volume, V_E [m^3]');

xlim([10^5 10^10]);
ylim([10^5 10^10]);

set(gca,'xtick',[10^5 10^6 10^7 10^8 10^9 10^10], 'ytick',...
    [10^5 10^6 10^7 10^8 10^9 10^10]);

V_E1
V_E2

% Plot settings
fs = 12;
```

```matlab
set(0,'DefaultAxesFontSize',fs)
set(0,'DefaultTextFontSize',fs)

set(gcf, 'PaperUnits', 'centimeters');
x_width=12.5 ;y_width=10;
set(gcf, 'PaperPosition', [1 3 x_width y_width]);
```

C.6 ClosureDepth.m

```matlab
% Closure Depth Calculations
% Bjarki Omarsson, 2015

clear all
close all
clc

data = xlsread('dufl_2000_2009.xlsx','','a2:c87650');
Hs = data(:,1);
Tz = data(:,2);
dbeg = datenum(2000,1,1,0,0,0);
dend = datenum(2009,12,31,0,0,0);
int = datenum(2000,1,1,1,0,0)-datenum(2000,1,1,0,0,0);
date = dbeg:int:dend;
date = date';
save('closuredepthdata.mat','Hs','Tz','date')

load closuredepthdata

% Get rid of -1 and NaN values
NaNg = find(Hs<0 | isnan(Hs)== 1);
Hs(NaNg) = [];
Tz(NaNg) = [];

% 12hr value
int2 = 1:12:length(Hs);
for i = 1:length(int2)-1
    Hs_n(i,1) = mean(Hs(int2(i):int2(i+1)));
    Ts_n(i,1) = mean(Tz(int2(i):int2(i+1)));
end

[H_1yr] = WEIB_Hs1yr(Hs_n,0.25,2000,2009);
```